GEOLOGY AND U-Pb GEOCHRONOLOGY OF THE ROCKS OF THE EOKUK UPLIFT, NORTHWESTERN SLAVE PROVINCE, NUNAVUT, CANADA

KELLIE A. EMON

Canadä

Geology and U-Pb Geochronology of the Rocks of the Eokuk Uplift, Northwestern

Slave Province, Nunavut, Canada

by

© **Kellie A. Emon (B.Sc. Hons.)**

A thesis submitted to the School of Graduate Studies in partial fulfillment of the

requirements for the degree of

Master of Science

Department of Earth Sciences

Memorial University of Newfoundland

December 1998

St. John's   Newfoundland

Abstract

Rocks of the Eokuk Uplift have been mapped in detail along the coast of Coronation Gulf and 10 key units have been dated by both conventional Thermal Ionization Mass Spectrometry (TIMS) and Laser Ablation Microprobe Inductively Coupled Plasma Mass Spectrometry (LAM-ICP-MS) U-Pb analysis. Zircon, monazite, and titanite from the various units were dated and the combined data indicate that this inlier of the Slave province has a >3.2 Ga crustal component, evidence of a granulite grade orogenic event pre-dating 2.8 Ga (possibly ca. 2.9 Ga) and a lack of evidence for any significant orogenic activity corresponding with the 2.7-2.6 Ga events common in the rest of the Slave Province. The oldest rocks in the study area are a succession of granitoid and supracrustal gneisses that have been metamorphosed to upper amphibolite to granulite facies. From field relationships, the oldest unit is a granodiorite to tonalite orthogneiss, with a zircon crystallization age of 3254 +13/-6 Ma. A granite gneiss, which may be a small felsic intrusion or an anatectic melt of the tonalite gneiss, yields a zircon age of 3216 +14/-13 Ma. A K-feldspar megacrystic monzogranite gneiss contains old, discordant, possibly inherited zircons with $^{207}Pb/^{206}Pb$ ages ranging from 3039-3103 Ma, together with coexisting 2879 +/-3 Ma zircon and monazite. These high-grade gneisses are intruded by two megacrystic granite plutons, dated at 2887 +/-2 and 2881+4/-3 Ma. LAM-ICP-MS analyses of zoned zircons from the 2887 Ma granite reveal the presence of xenocrystic zircon with ages of 3165 +57/-34 and 3363 +68/-53 Ma. This implies that the older granites were intruded into, and possibly derived from, still older crust. The absence of extensive recrystallization and complex structures in these plutons indicates

that this igneous event post-dated the high-grade metamorphism. An amphibolite-grade synplutonic metamorphic event is dated at ~2880 Ma by metamorphic monazite in the older gneiss units. A series of variably deformed mafic to felsic dykes and pegmatites intrude both the granites and gneisses and constrain the end of penetrative deformation in the area to ca. 2850 Ma. This contrasts with data from the rest of the Slave Province, where the main phases of deformation, metamorphism and synmetamorphic plutonism have been dated at ca. 2.62-2.59 Ga. Metamorphic titanite ages from the diorite and granodiorite dykes indicate two lower amphibolite to greenschist-grade metamorphic events: one at ca. 2705 Ma and one at ca. 2646 Ma. The youngest Archean magmatic event in the area is represented by granite intrusion at 2594 +3/-2 Ma, coeval with crystallization of titanite at greenschist-grade conditions in some of the older gneissic and intrusive rocks.

Acknowledgements

Table of Contents

List of Figures

List of Tables

Chapter 1:Introduction to the Geology of the Slave Province and Eokuk Uplift

1.1 Introduction

The Slave Province is an Archean age granite-greenstone terrane located in the northwest part of the Canadian Shield (Figure 1.1). It extends over an area of 190,000 square kilometres between Great Slave Lake in the south and Coronation Gulf in the north. It is bounded to the east by the Thelon Orogen (2.0-1.9 Ga) and to the west by the Wopmay Orogen (1.9-1.8 Ga) (Card and King, 1992). The Eokuk Uplift is an inlier of granitoid, gneissic and supracrustal rocks separated from the western part of the Slave Province by the Proterozoic sedimentary rocks of the Coronation Supergroup (see Figure 1.1). In recent years, geochronological studies have allowed the subdivision of rocks in the Slave Province into three broad lithological groups, including an older package of pre-2.8 Ga supracrustal, gneissic and granitoid rocks (Easton, 1985; Frith et al., 1986; Bowring et al., 1989; Villeneuve et al, 1993; Gebert, 1994; Relf, 1995; Bleeker and Stern, 1997). However, until the present study, there were no radiometric age data on the rocks of the Eokuk Uplift. The current study is part of a five-year project undertaken by the

Indian and Northern Affairs Canada (INAC) in 1991 to map the northwestern margin of the Slave Province, including the Eokuk Uplift. The purpose of this thesis is threefold. First, to use U-Pb dating methods to determine whether the rocks of the Eokuk Uplift are Archean and to ascertain whether they are part of the basement (i.e. pre-2.8 Ga) lithologic sequence which appears to occur to the west of 112^0 W longitude. Second, to provide constraints on the timing of formation, metamorphism and deformation of rocks in the study area. Finally, to attempt to relate the ages of the rocks in the Uplift to tectonic magmatic and metamorphic events elsewhere in the Slave Province.

The thesis area is located in the Kikerk Lake map sheet (NTS 86P #9-10) between 67^0 42' N, 112^0 21' W and 67^0 40' N, 112^0 38' W (Figure 1.1). It is roughly 600 km north of Yellowknife and 110 km east of Kugluktuk (formerly Coppermine), along the Coronation Gulf coast. Access to the area is by float or ski-equipped aircraft or helicopter from Yellowknife or Kugluktuk. Access by float plane is limited to the summer months when the ocean is ice-free (July-early Oct.).

Detailed geological mapping of a twelve kilometer long section of the Eokuk Uplift coast at Coronation Gulf was carried out over two weeks in the summer of 1994 and 5 days in the summer of 1995, using 1:15,000 scale air photos. The coastal outcrops along the eastern side of the Uplift were deemed most suitable for mapping since they are free of lichen, Quaternary sediments and beach deposits and show the widest variety of lithologies and their contact relationships. Map data was later transferred to a digital base map using the FIELDLOG mapping program developed at the Geological Survey of Canada and AutoCAD.

Representative samples of the main lithologies and intrusive suites were collected over both summers and approximately 70 normal and polished thin sections were used for petrographic and electron microprobe analysis. As well, 10-30 kg samples of the ten major lithologies were collected for U-Pb geochronology. Sample preparation and heavy mineral separation were done according to the methods outlined in Appendix I. Techniques used for mineral dissolution, chemistry and mass spectrometry are described in Chapter 4 and Appendix I. Techniques used for Laser Ablation Inductively Coupled Plasma Mass Spectrometry are given in Chapter 5 and Appendix II. Abbreviations of mineral names used in this text are after Kretz (1983).

1.2 Geology of the Slave Structural Province

Based on isotopic age and lithologic association, the rocks of the Slave province have been divided into three main assemblages. The oldest are granitoid plutonic, gneissic and associated supracrustal rocks greater than 2.8 Ga old. The pre-2.8 Ga rocks are confined to the western part of the Slave province (Card and King, 1992) and have been considered to form a single block, the Anton terrane (Kusky, 1989; 1990) which is thought to underlie much of the Slave Province west of 112^0 W longitude. Significant occurrences of basement gneissic rocks are present in the Acasta River, Point Lake, Beniah Lake, Winter Lake, Napaktulik Lake, the Sleepy Dragon complex and Arcadia Bay. These basement gneisses tend to be predominantly tonalite, with minor granodiorite to granite, and are polydeformed and strongly metamorphosed to migmatitic. The supracrustal rocks of this older assemblage appear to have a fairly uniform character throughout the southern
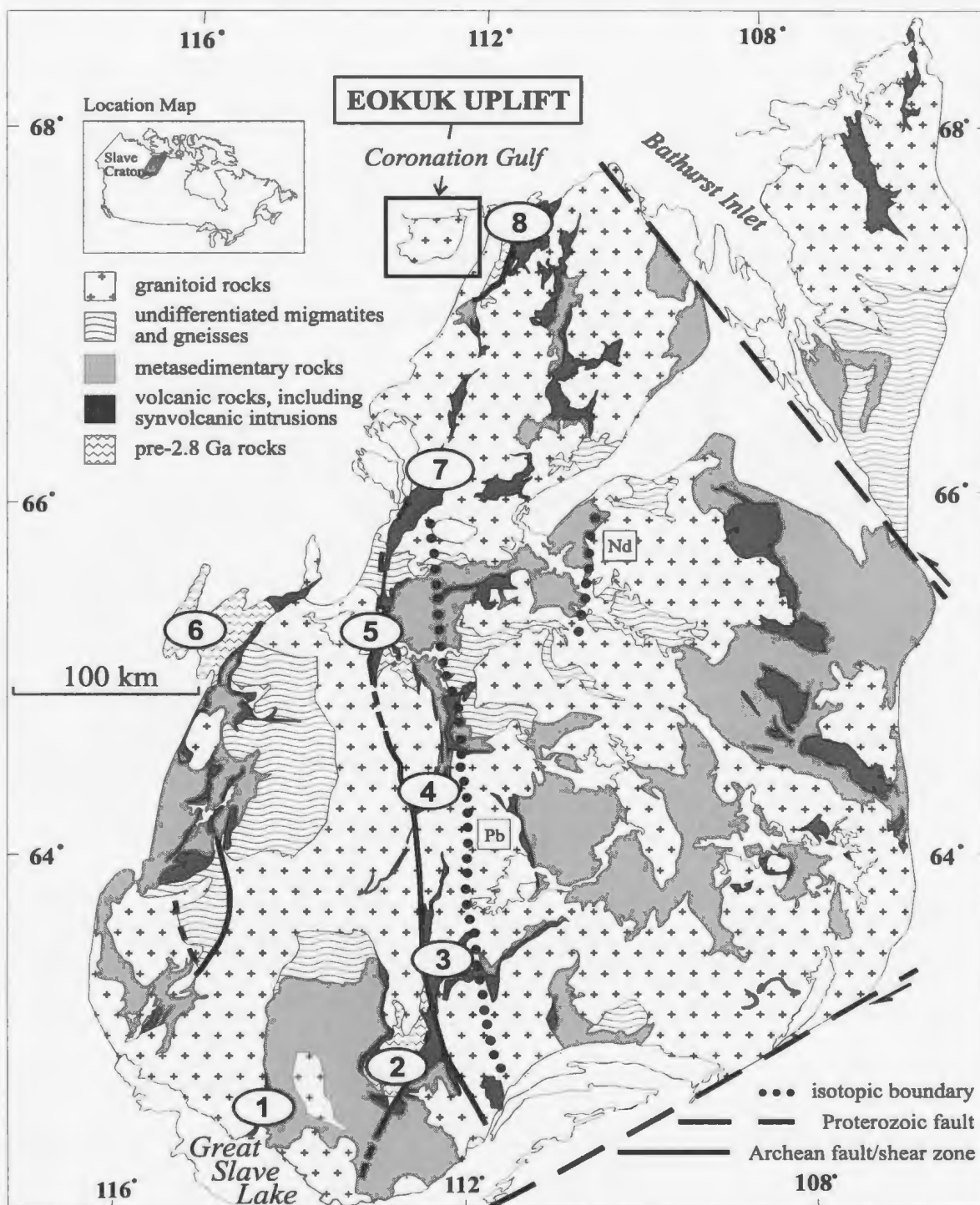
Figure 1.1: Geology map of the Slave Structural Province showing the location of the Eokuk Uplift. Pre-2.8 Ga rocks are shown in zig-zag pattern. Isotopic age boundaries for Nd and Pb are shown with black dots (Nd: Davis and Hegner, 1992; Pb: Thorpe et al., 1992). Numbered ovals show locations discussed in the text: (1) Yellowknife; (2) Sleepy Dragon Complex; (3) Beniah Lake; (4) Winter Lake; (5) Point Lake; (6) Acasta River; (7) Napaktulik Lake; (8) Anialik River.

portion of the Slave Province. They consist of a sequence of quartz arenite, rhyolite, iron formation, and related sedimentary rocks along with mafic to ultramafic dykes that are interpreted to form locally preserved autochthonous cover sequence on basement gneisses from Yellowknife to north of Winter Lake (Covello et al., 1988; Roscoe et al., 1989; Bleeker and Ketchum, 1998). Bleeker and Ketchum (1998) have grouped this supracrustal sequence into a single lithostratigraphic unit called the Central Slave Cover Group. U-Pb ages from detrital zircons from this sequence indicate these supracrustals are younger than ca. 2924 Ma but older than the subsequent 2.72-2.65 Ga old Yellowknife Supergroup supracrustal rocks (Isachsen and Bowring, 1997).

The second assemblage consists of sedimentary, volcanic and associated plutonic rocks of the ca. 2.72-2.65 Ga volcanic-turbidite sequence of Yellowknife Supergroup (YKS) (Henderson, 1981). Metagreywackes, with minor amounts of quartzite and conglomerate, make up approximately 80% of the supracrustal sequence in the YKS, while the less abundant volcanic rocks tend to be intermediate to felsic in the eastern part of the Province and predominantly mafic in the central and western parts (Henderson, 1981). Early U-Pb age data from felsic volcanic rocks of the YKS suggested that volcanic activity may have occurred as two episodes, from 2698-2687 Ma and from 2671-2663 Ma (Mortensen et al., 1988). More recent work suggests that volcanic activity was fairly constant over the whole of the Slave Province from 2720-2660 Ma, with only the Yellowknife greenstone belt displaying a hiatus in volcanism from 2700-2685 Ma (Villeneuve et al., 1997). The age of metaturbiditic rocks of the YKS appears to be roughly coeval with that of the volcanic sequences (Mortensen et al., 1988; van Breemen et al., 1992).

The period from 2640-2625 Ma represents a Slave Province-wide hiatus in magmatism and signals a change from the volcanic activity and minor associated plutonism characteristic of the Yellowknife Supergroup to a period of extensive granitoid plutonism with only minor volcanic activity (Villeneuve et al., 1997).

The youngest rocks in the Slave consist of these granitoid plutons and minor volumes of supracrustal rocks deposited during or after an episode of regional polyphase deformation from 2.62-2.59 Ga. Plutons of this package consist of syn-tectonic (2.62-2.61 Ga.) and late- to post-tectonic (2.59-2.58 Ga) granitoid rocks (van Breemen et al., 1992). Detailed studies of plutonic rocks from the central Slave province have shown that the syn-tectonic granitoids tend to be dioritic to granodioritic in composition, while those that are post-tectonic are characterized by K-feldspar megacrystic biotite granite to granodiorite and two-mica granite (van Breemen et al., 1992). The geochemical compositions of these plutons show an evolution in time from metaluminous to peraluminous (Davis et al., 1994). Synchronous with plutonism and deformation was the deposition of supracrustal rocks, characterized by polymictic conglomerate and minor turbidites younger than 2.6 Ga (Card and King, 1992). Of particular note is the sedimentary sequence present in the Hood River supracrustal belt in the northeastern Slave Province. An angular unconformity exists between turbidites with a minimum age of 2668 +/-4 Ma (van Breemen et al., 1994) and an overlying sequence of conglomerate, arenite, greywacke and volcanic flows and tuffs. A rhyolite clast from the conglomerate has an age of 2605 +2/-3, providing a maximum age for this unit (van Breemen et al., 1994). A similar situation exists in the Anialik greenstone belt, where a syenogranite boulder from a polymictic conglomerate yielded a U-Pb zircon age of 2590 +/-10 Ma and

is therefore thought to lie unconformably on top of the volcanic rocks in the belt (Relf, 1995).

Regional polyphase deformation in the Slave province took place from ca. 2.62-2.59 Ga, synchronous with the emplacement of the syn- to late-tectonic granitoid plutons. Volcanic belts have been deformed into narrow, steeply dipping, homoclinal panels within or marginal to the supracrustal domains. Metasedimentary rocks are polydeformed and exhibit complex folds, cleavages and schistosities (Fyson and Helmstaedt, 1988). Within the sediments, a structural progression exists from large, premetamorphic folds to smaller isoclinal folds and several generations of foliations. Structures appear to flatten in orientation and be deflected around syndeformational granitoid plutons. The same structures are truncated by late to post-deformational plutons (Padgham and Fyson, 1992). A series of north-striking, crustal-scale faults and shear zones can be traced intermittently across the Slave Province between approximately 112-114^0 W, which may be the surface expression of a major tectonic boundary (Figure 1.1; King et al., 1994; Relf, 1995).

The cause and timing of deformation in the northern and central parts of the Slave Province has been the subject of several studies. Of greatest interest to the present study is the work done by Relf (1995) in the Kangguyak gneiss belt and the Anialik River volcanic belt to the east of the Eokuk Uplift (Figure 1.1). The volcanic and gneiss belts display significant differences in lithology, age and structure and were interpreted to represent two distinct geological terranes (Relf, 1995). The Anialik River volcanic belt consists of mafic to felsic volcanic and volcaniclastic rocks with minor sediments. Metamorphic grade ranges from greenschist to upper amphibolite facies. In contrast, the

Kangguyak gneiss belt is composed of polydeformed orthogneiss and paragneiss that have been metamorphosed to amphibolite facies. Relf (1995) proposed the Kangguyak gneisses were part of a pre-2.8 Ga continental margin. In contrast, ca. 2.70-2.68 Ga basalts in the volcanic belt have oceanic island arc geochemical signatures (Relf, 1995). The two terranes were juxtaposed across the Tokhokatak fault during a transpressive collisional event between 2.65-2.64 Ga (Relf, 1995). This resulted in crustal thickening and heating, culminating in mid-amphibolite facies metamorphic conditions. A period of extension followed, between 2.64-2.61 Ga, marked by alkaline intrusions and the deposition of conglomerates in the northern part of the belt. Regional east-southeast/west-southwest shortening occurred syn- to post-2.60 Ga, coincident with granite intrusion along the eastern side of the volcanic belt. The granite intrusion also produced high-temperature/low-pressure metamorphic mineral assemblages in the volcanic belt (Relf, 1995).

This differs from collisional models for the central Slave Province, where collision is not thought to have occurred until ca. 2.62 Ga (Relf, 1992; King et al., 1992). Field and geochronologic data from a transect across the north central Slave province, from Point Lake to Contwoyto Lake (Figure 1.1), suggest that deformation occurred during two distinct episodes of crustal shortening (Relf, 1992). An early episode at ca. 2650-2630 Ma produced a fold and thrust belt at Keskarrah Bay and eastern Point Lake. The later episode at ca. 2620-2600 Ma was responsible for the bulk of shortening east of Point Lake and was synchronous with peak metamorphism (Relf, 1992). The early deformation episode appears to have occurred over an east-dipping subduction zone (King et al, 1992; Relf, 1992).

The thermal peak of metamorphism in the Slave Province appears to have been synchronous with ca. 2.62-2.59 Ga deformation. Supracrustal rocks contain mineral assemblages consistent with regional low-pressure, high-temperature metamorphic conditions, and typically range from greenschist to upper amphibolite facies (Thompson, 1978; 1989). Granulite facies rocks have been found in only four localities in the southwestern part of the Slave Province. The distribution of the various metamorphic grades does not coincide with regional structures, implying that peak P-T conditions were achieved after regional deformation (Thompson, 1978; Card and King, 1992). Following the peak of deformation and metamorphism and the emplacement of post-tectonic plutons, the province appears to have undergone a period of slow cooling and/or uplift, based on young K-Ar ages (Thompson, 1989).

Two isotopic boundaries have been identified which follow the general trend of 112^0 W longitude, one defined by common lead isotopic signatures from volcanogenic massive sulphide showings, the other from ε_{Nd} values from late Archean granite plutons (Figure 1.1). $^{207}Pb/^{204}Pb$ ratios are low in the northern and eastern part of the Slave province and high in the south and west. The high $^{207}Pb/^{204}Pb$ ratios are thought to reflect magmas derived from an older crustal source, while the low values are more consistent with juvenile material from a mantle source (Thorpe, et al., 1992). This is supported by ε_{Nd} values which are negative (-0.2 to -5.3) from granites west of 112^0 W, suggesting contamination from older crust. Granites in the eastern Slave Province are positive (+0.6 to +3.7), consistent with derivation from juvenile mantle sources (Davis and Hegner,

1992). This isotope data is supported by U-Pb age data from the Slave Province. Rocks with pre-2.8 Ga U-Pb ages have not been found in the eastern part of the Slave Province.

Theories concerning the tectonic evolution of the Slave Province are broadly divisible into two models. The first model interpreted the supracrustal rocks of the greenstone belts as basin fill sequences caused by ensialic rifting of older basement, with subsequent compressional deformation and plutonism upon basin closure (Henderson, 1981; Easton, 1985). The second model involves several variations on the accretion of oceanic or arc terranes onto older basement blocks. Hoffman (1986) interpreted the greenstone belts as being parts of prograding arc-trench system(s), in which sea floor bathymetric highs were incorporated into an accretionary prism, with the whole assemblage subsequently intruded by arc magmatic plutons. Kusky (1989, 1990) proposed that the mafic greenstone belts in the western Slave Province were old oceanic crust and that the felsic dominated belts in the east (Hackett River arc) were parts of a volcanic arc formed over an east-dipping subduction zone. East to west shortening and collision resulted in the obduction of ophiolites, arc volcanic rocks and accretionary prism sediments onto an older basement microcontinent (Anton Terrane). Fyson and Helmstaedt (1988) proposed a hybrid model whereby the greenstone belts formed in marginal basins during the rifting and closure of continental margin arcs.

1.3 Regional Geology of the Eokuk Uplift

1.3.1 Introduction

The Eokuk uplift is a 1300 km^2 inlier of Archean rocks exposed to the west of the main body of the Slave craton along the Coronation Gulf coast (Figure 1.2). It is surrounded to the southeast and west by the Proterozoic sedimentary rocks of the Coronation Supergroup. In the north, it is partially overlain by the Mesoproterozoic Rae Group and 723 Ma Franklin diabase sills. Craig et al. (1960) of the Geological Survey of Canada first mapped the Eokuk Uplift, at a scale of one inch to eight miles. The Uplift was mapped as undifferentiated granitoid and granitoid gneissic rocks with a minor occurrence of greenschist facies supracrustal rocks in the south-central segment. Both gneisses and supracrustal rocks were assumed to be of Archean age. The Proterozoic sedimentary rocks surrounding the Uplift, as well as the Uplift margins, were mapped by Hoffman et al. (1984), who also interpreted the Uplift as an Archean structure.

Previous mapping within the study area is limited to the granulite facies mafic gneiss. Silver (Ag), hosted in anastamosing, quartz-carbonate veins, is present the largest block of the mafic gneiss unit within the study area. Informally named the 'Nerak showing', it was the subject of small-scale mapping and drilling by Westsun Petroleum and Minerals Ltd. (Kelly, 1984) and Echo Bay Mines (Vogg, 1984). Both studies concluded that the mafic unit was a Proterozoic layered mafic intrusion, possibly related to the Muskox intrusion near Coppermine, resting on Archean basement.

The following description of the general geology of the Eokuk Uplift is summarized from Jackson (1996).
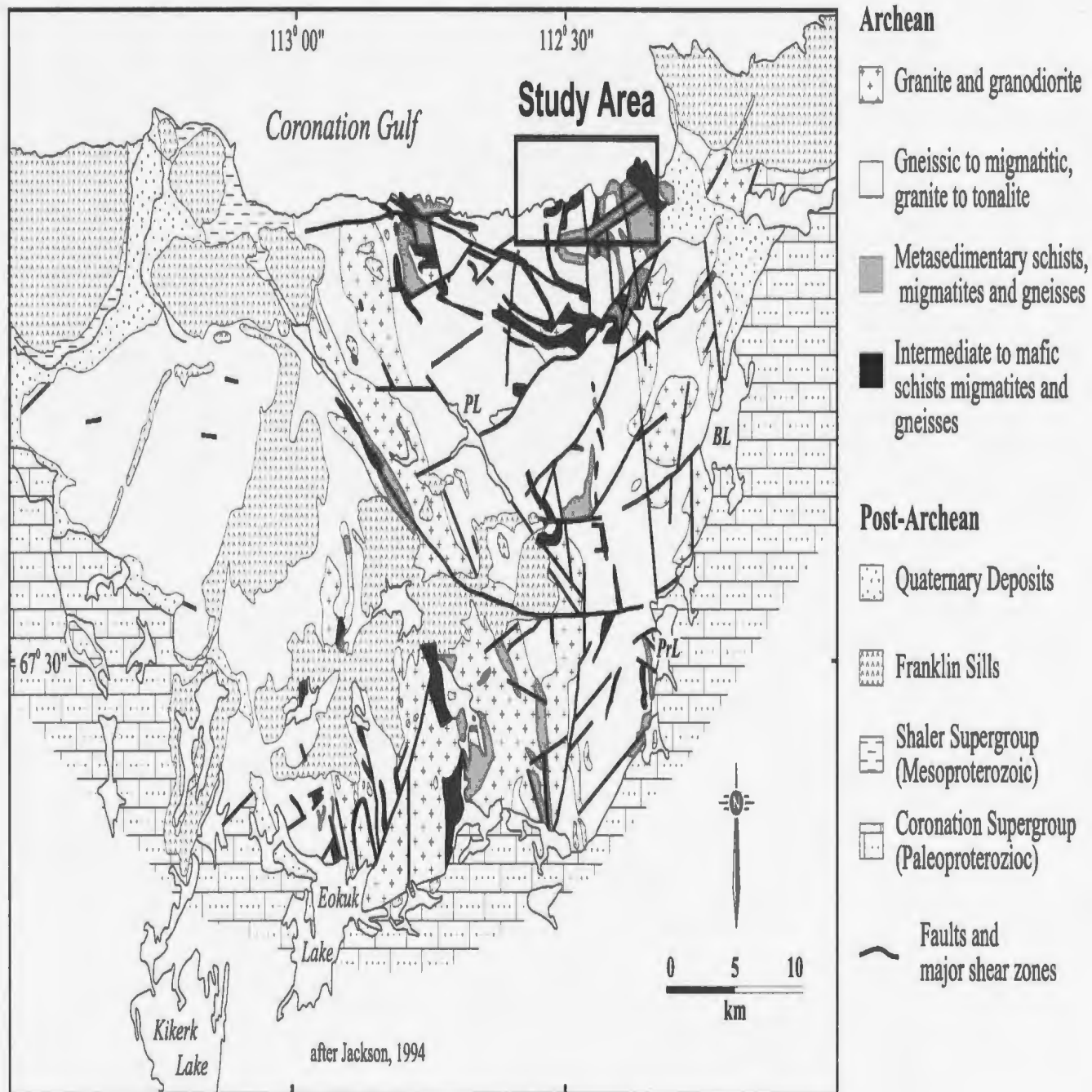
Figure 1.2: Geological map of the Eokuk Uplift. Study area is shown in the box at right. *PL*, 'Purina lake'; *PrL*, 'Profile lake'; *BL*, 'Beaver lake' (informal names). The star west of 'Beaver lake' shows the location of U-Pb sample 94VJ254. Modified after Jackson 1994.

1.3.2 Archean rocks

Variably deformed granite to granodiorite plutons and granitoid migmatite and gneiss are volumetrically the most abundant rocks in the Uplift. Gneissic rocks can be subdivided into two units. The oldest is a tonalite to granodiorite gneiss. This unit is white to grey weathering and consists of a tonalitic leucosome alternating with a biotite +/- hornblende melanosome. In biotite-rich phases of this gneiss, plagioclase and quartz commonly appear as recrystallized, lensoid segregations surrounded by thin layers of biotite. Rafts or screens of the tonalite gneiss are preserved within cross cutting, more abundant, granite to granodiorite gneiss to migmatite. This unit is white to pink weathering and fine- to coarse-grained. K-feldspar megacrysts up to 10 cm long are present locally. Layering, consisting of alternating feldspar/quartz-rich and biotite +/- hornblende-rich layers, is poorly defined.

Later intrusive rocks are defined primarily on the basis of their lower strain state in comparison with the gneisses. They consist of biotite-bearing granodiorite to granite with locally developed hornblende of muscovite. These rocks are heterogeneous and can be leucocratic to mesocratic, fine- to coarse-grained and include equigranular, seriate or feldspar porphyritic phases. These plutons display a variety of strain states and may be massive to foliated to lineated. Many intrusions are in gradational contact with surrounding migmatitic and gneissic rocks, and may be derived either from the migmatitic gneisses or represent less deformed phases of the granitoid gneisses. Massive to weakly deformed, equigranular to weakly feldspar phyric, biotite monzo- to syenogranite intrusions in the 'Beaver lake' area (Figure 1.2) have sharp and discordant

contacts with the host gneisses. These appear to represent the youngest intrusions in the Uplift.

Metasedimentary rocks include siliciclastic-derived schist, migmatite, and gneiss, as well as minor iron formation, marble layers or pods and conglomerate. At lower grade (lower to mid-amphibolite facies) the metasediments are typically schistose and are composed of two possibly gradational sequences. The first is an iron-rich, garnet-biotite schist, interbedded with quartz-rich, biotite-muscovite +/- garnet schist. The second is an interlayered and locally graded sequence of biotite-muscovite (cordierite, andalusite, sillimanite +/-garnet) pelite and psammite. Primary sedimentary structures and detrital quartz and plagioclase grains are locally preserved in both these sequences.

Higher-grade metasedimentary migmatite and gneiss are granoblastic quartzofeldspathic rocks that are commonly garnetiferous and contain one or more of the following metamorphic minerals: biotite, muscovite, sillimanite, cordierite and hornblende. No primary textures or detrital grains are preserved in these rocks.

Conglomerate is found in two locations, near 'Profile lake' in the southern part of the Uplift and southeast of 'Purina lake'. The 'Purina lake' conglomerate is matrix-supported and polymictic, with granite, amphibolite and quartz-rich clasts in a matrix of biotite, hornblende, plagioclase and quartz. The 'Profile lake' conglomerate consists of a garnetiferous, quartz-rich matrix with recrystallized quartz lenses. Isolated lenses have been interpreted as quartz clasts in a quartz pebble conglomerate. There are, however, connected lenses that appear to cut the regional foliation and are interpreted as boudinaged quartz veins.

Iron formation is found in both mafic units and metasedimentary units as layers less than 10 metres thick. It is finely layered to laminated and consists of alternating layers of quartz +/- amphibole +/- garnet and magnetite (oxide-facies) or pyrite (sulphide-facies).

Mafic to intermediate supracrustal rocks include metavolcanic schists and amphibolite to granulite facies gneisses and migmatites. At lower amphibolite facies, schistose metavolcanic units are predominantly fine grained, layered to laminated volcaniclastic rocks with lesser amounts of pillowed to massive flows and coarse-grained gabbroic units. Rare, plagioclase and quartz phyric intermediate to felsic volcaniclastic rocks are also present. In addition to hornblende and plagioclase, epidote is also present in rocks of this grade. At upper amphibolite facies, mafic to intermediate rocks are dominantly medium- to coarse-grained, black weathering amphibolites. These amphibolites are finely to coarsely layered to massive and may be locally gneissic or agmatitic. The typical mineral assemblage is hornblende-plagioclase +/- quartz.

Along the Coronation Gulf coast are mafic to ultramafic, black to brown weathering, hornblende-plagioclase-orthopyroxene +/- clinopyroxene-bearing, granulite facies gneisses. Screens of this gneiss form elongated blocks up to 750 m long, parallel to the regional structural grain. Fine to coarse compositional layering is locally cut by plagioclase-pyroxene (+/- hornblende +/- magnetite) veins. The veins, which are irregular in outline, have diffuse boundaries with the host rocks and are interpreted as a locally derived melt phase. Layering is locally folded and /or boudinaged, with leucosome concentrated in the necks of boudins.

Within the lower amphibolite facies supracrustal rocks of the Eokuk Uplift, metavolcanic rocks structurally overlie metasedimentary rocks, but the lack of facing

directions prevents determination of stratigraphic relations. Within the migmatite and gneiss units, which generally lack primary textures, are rocks that have been interpreted as higher-grade equivalents of the supracrustal rocks, based on their bulk rock composition as estimated from metamorphic assemblages. Correlations between the lower- and higher-grade supracrustal rocks outside and within the gneiss belts respectively, are equivocal because of intervening granitoid rocks. However, at all metamorphic grades the supracrustal rocks have similar lithologic associations and apparent bulk compositions and it is possible that they represent the remnants of a formerly continuous package.

Mafic and (less commonly) ultramafic enclaves are also found within the granitoid rocks, where they are typically aligned within the main foliation. These enclaves can be interpreted to be either part of the supracrustal sequence, exotic blocks or dykes that may have been feeders to some of the metavolcanic rocks.

Numerous, metre-wide dykes of syenogranite pegmatite to aplite, granite to granodiorite, tonalite-diorite and amphibolite are present throughout the Uplift. These dykes document complex age relations that could not be directly related to the major granitoid units in the field.

1.3.3 Proterozoic Rocks

The south and west parts of the Eokuk Uplift are overlain by the Paleoproterozoic sedimentary rocks of the Coronation Supergroup. These are continental-margin clastic and carbonate sediments deposited at approximately 1.9 Ga, during the early rifting

phases of the Wopmay Orogen (Hoffman and Bowring, 1984). They were subsequently detached from the Archean basement, thickened and thrust eastward over the western edge of the Slave Province proper (Hoffman et al, 1984; Hoffman and Bowring, 1984).

All of the Archean rocks and the Coronation Supergroup rocks are cut by northwest-striking diabase dykes of the 1267 Ma old Mackenzie dyke swarm. These dykes have a brownish weathered surface, ophitic texture and strong aeromagnetic signatures (LeCheminant and Heaman, 1989).

In the north, the Uplift is overlain by argillite and sandstone of the Mesoproterozoic Rae Group, part of the Shaler Supergroup (Rainbird and Jefferson, 1993). Detrital zircon grains from these rocks have minimum ages of 1077 Ma (*ibid.*). The Rae Group is intruded and overlain by shallowly dipping to subhorizontal, 723 Ma Franklin diabase sills, which provide a minimum age for the Rae Group sedimentary rocks (Heaman et al., 1992).

Chapter 2: Lithological Units and Contact Relationships

2.1 Introduction

This section provides a description of the major rock units in the study area, including the modal mineralogy of each unit, the nature of the contacts and the relative timing of emplacement of the various units. As mentioned in Chapter 1, rocks of the study area are mainly granitoid plutons and granitoid gneissic rocks interlayered with significant amounts of supracrustal rocks. The rocks have been subdivided into 10 units (Figure 2.1), based on composition, texture and contact relationships. These 10 units can be grouped into two broad subdivisions based on metamorphic grade and degree of deformation. The first is an older subdivision of structurally complex tonalite gneiss, granite gneiss, paragneiss and mafic gneiss whose protoliths have undergone upper amphibolite to granulite facies metamorphism. The second consists of less deformed megacrystic granite plutons, diorite dykes, granodiorite dykes, syenogranite pegmatite and mafic dykes which show no evidence of severe deformation or recrystallization. Of

Coronation Gulf

Figure 2.1: Geological map of the study area showing geochronology sample locations described in text (marked with stars and station numbers). Uncoloured areas represent beach or Quaternary sediments.
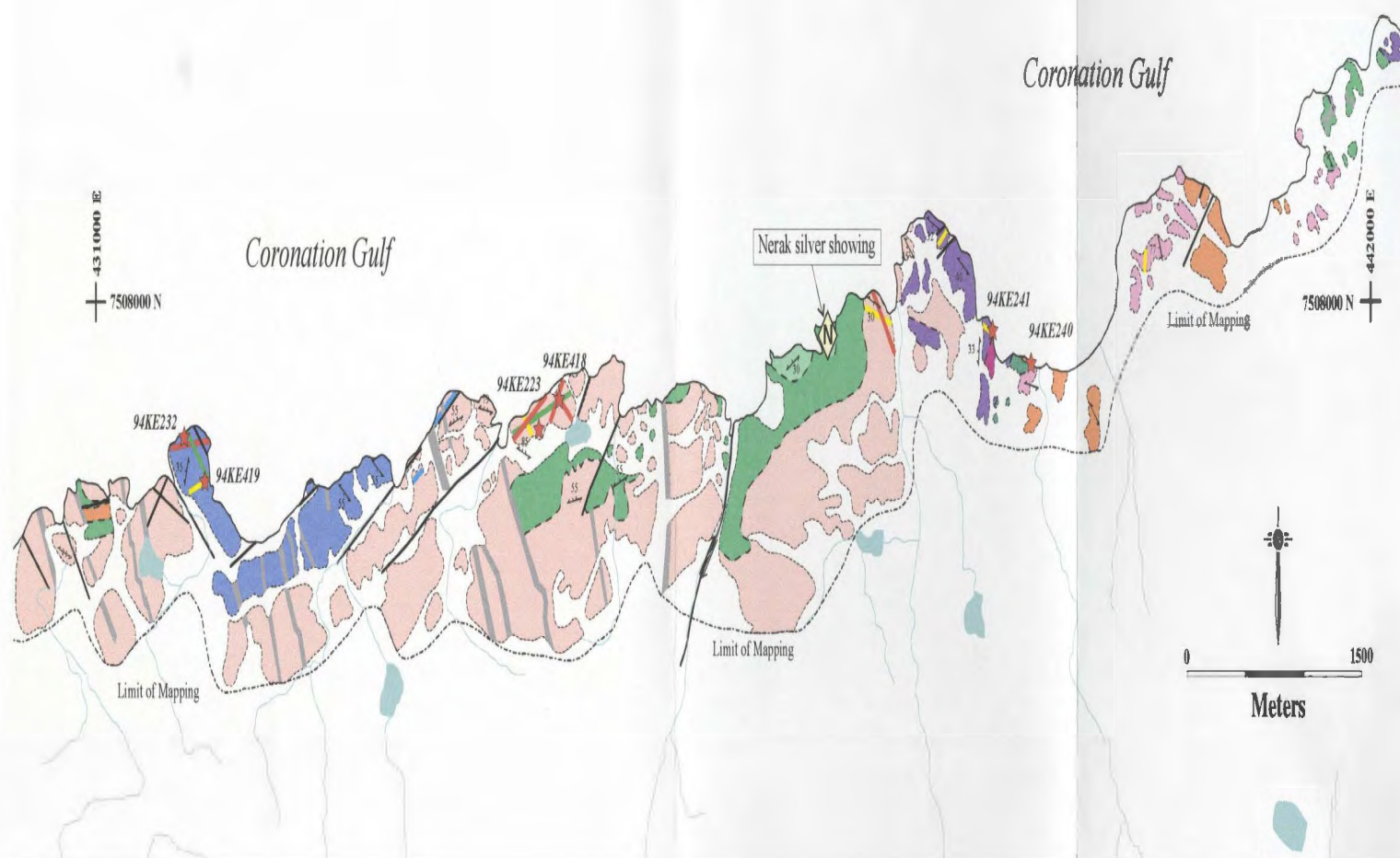
Archean

3.25-3.0 Ga High-grade Gneisses

Tonalite-granodiorite gneiss

Granite gneiss

Pyroxene-bearing mafic gneiss; finely layered, pyroxene-bearing mafic to intermediate gneiss

Biotite-garnet paragneiss, variably migmatitic

Monzogranite gneiss

2.9-2.88 Ga Granites

'Nerak granite'

Pegmatitic granite

2.87-2.85 Ga Minor Intrusive Rocks

Boudinaged diorite dyke

Granodiorite dyke

Syenogranite pegmatite

Post-2.85 Ga Intrusive Rocks

Green mafic dyke

Proterozoic

Mackenzie dykes (ca. 1267 Ma; Lecheminant and Heaman, 1989)

Symbols

★ Geochronology Sample Location

Fault: offset unknown, with offset

Foliation: vertical, inclined, trend

Gneissosity or migmatitic layering: vertical, inclined, trend

Geological contacts

Outcrop limits

the first three dyke sets, each unit has a distinctive composition, strain state and relative age, and is discussed more fully below.

2.2 Lithological Units

2.2.1 Tonalite to granodiorite gneiss

This unit is confined to the eastern part of the study area. The rock is a fine- to medium-grained, granoblastic, biotite-hornblende, tonalite to granodiorite gneiss with a medium to dark grey weathered surface and a dark grey fresh surface. It typically contains the mineral assemblage biotite (30-45%), plagioclase (25-30%), quartz (10-15%), K-feldspar (0-10%), +/- chlorite. Accessory minerals include zircon, titanite and apatite. Recrystallized quartz and feldspar occur as cm-scale lensoid segregations surrounded by thin, biotite-rich layers (Figure 2.2a). In localised areas of higher strain, quartzofeldspathic segregations define a prominent centimetre-scale compositional layering. This layering is deformed by a number of northwest trending, shallowly plunging, upright to recumbent folds that may represent F_2 structures refolded about the main S_3 fabric. This unit is interpreted as the oldest of the gneissic rocks on the basis of its complex structures and degree of recrystallization. Deformed trains of metre-scale mafic xenoliths are present locally. These xenoliths could be disagregated blocks of mafic gneiss but their linear distribution suggests they may represent boudinaged mafic dykes.

Figure 2.2

Figure 2.2a: Tonalite to granodiorite gneiss showing recrystallized lensoid segregations of felsic minerals. Megacrystic granite vein at top of photo is weakly deformed and cuts the fabric in the tonalite. Compass for scale.

Figure 2.2b: Granite gneiss with centimetre-scale layering and granoblastic texture. Lens cap is 6 cm in diameter.

2.2.2 Granite gneiss

This unit occurs in a single outcrop in the east part of the study area and is surrounded on all sides by the tonalite gneiss described above. It is a leucocratic, fine-grained, granoblastic monzogranite to granite gneiss, with a white- to light pink weathered surface and a white- to light-grey fresh surface (Figure 2.2b). The typical modal composition is plagioclase (30-35%), quartz (25-30%), K-feldspar (25-30%), biotite (3-7%), chlorite (1%) +/- amphibole with accessory zircon, monazite and apatite. Compositional layering in this unit is defined by centimetre-scale quartzofeldspathic layers separated by millimetre-scale biotite-chlorite layers. The quartzofeldspathic layers locally contain medium-grained, rounded phenocrysts of plagioclase up to 1 cm in diameter, possibly remnants of larger megacrysts. The limited extent of this unit suggests it may be a small felsic intrusion into the tonalite gneiss, or a partial melt derived from the tonalite gneiss during peak metamorphism. The structural style and degree of recrystallization exhibited is the same as that seen in the tonalite gneiss, suggesting the two rocks have undergone the same thermal and deformational history.

2.2.3 Mafic gneiss

Mafic gneiss is present throughout the study area as blocky screens and xenoliths that are elongated parallel to the regional foliation. The largest of these mafic gneiss blocks covers approximately 1km by 500m in the east-central part of the map sheet (Figure 2.1) and hosts the Nerak silver showing. Mafic gneiss is fine- to coarse-grained, mafic to ultramafic, and layered on a centimetre- to half meter-scale. The unit is characterized by

Figure 2.3

Figure 2.3*a*: Granulite facies mafic gneiss showing compositional layering and tonalitic, anatectic melt segregations, both concordant with layering and in boudin necks. Hammer handle is 30 cm long.

Figure 2.3*b*: Finely layered subunit of the mafic gneiss. This subunit is more intermediate in composition than the mafic gneiss. Hammer handle is 30 cm long

alternating Hb-Pl layers and Hbl-Pl-Opx-Cpx layers. The latter typically contain plagioclase (25%), pyroxenes consisting of orthopyroxene (hypersthene, 20%) and clinopyroxene (possibly augite, 10%), altering to hornblende (30%), biotite (2%) and actinolite (10%). Layering in these rocks is cut by veins and veinlets of leucotonalite, which have diffuse boundaries with the host gneisses (Figure 2.3a). They are interpreted as a locally derived melt phase of the mafic rocks. The veins are composed of anhedral, medium grained quartz (5-10%) and plagioclase (90-95%), and have irregular, diffuse boundaries. They also contain large (5+ cm), euhedral to subhedral pyroxene crystals with hornblende or magnetite rims.

No primary structures are preserved in the gneiss, although the apparently conformable association of these mafic rocks with paragneiss to the west of the study area suggests a possible supracrustal origin. In the western part of the study area, rusty weathering, siliceous, garnet and magnetite/sulphide-bearing blocks or layers, interpreted as metamorphosed iron formation, occur at the contact between the mafic gneiss and the paragneiss.

At two locations within the main block of the mafic gneiss near the Nerak silver showing, granoblastic finely-layered to laminated, plagioclase- and epidote-rich mafic rocks occur in conformable contact with the more mafic gneiss (Figure 2.3b). The mineral assemblage of this unit is plagioclase (25-60%), hornblende (20-30%), orthopyroxene (5-15%) and actinolite (15-20%) and epidote (1-5%). Quartz was not observed in the samples. The bulk composition of these rocks is consistent with a mafic to intermediate, volcanic origin.

2.2.4 Migmatitic paragneiss

Paragneiss occurs in both the eastern and western parts of the map area. This unit is migmatitic, with granoblastic texture, a schistose biotite-garnet-rich paleosome and a medium- to coarse-grained granodiorite to tonalite neosome (Figure 2.4a). The neosome forms stromatic to nebulitic veins ranging in width from a few millimeters to half a meter across. The presence of garnet and aluminosilicates suggests it is derived from melting of the sedimentary rocks, not part of a later intrusive phase. The typical mineral assemblage is as follows: quartz (20-50%), plagioclase (20-35%), biotite (10-20%) and garnet (5-30%), Fe-sulphides (pyrite, pyrrhotite) (1-2%) +/- K-feldspar +/- cordierite, +/- sillimanite +/- chlorite, with accessory zircon and monazite. In general, the paragneiss is quartz-rich and lacks significant amounts of aluminosilicate, suggesting a psammitic bulk composition. No primary structures or detrital quartz or feldspar grains have been preserved.

On the extreme western edge of the map area is an outcrop of paragneiss that contains up to 10% sillimanite as 5+ cm aggregates within a biotite-rich paleosome. In most cases the aluminosilicate has been altered to an aphanitic, waxy-green mass of sericite and quartz, but some of the larger pods still retain cores of recognizable sillimanite. The typical mineral assemblage at this outcrop is quartz (20-35%), plagioclase (20-35%), biotite (15-25%), garnet (5-15%), sillimanite (0-10%) and muscovite (0-5%) +/- chlorite, with accessory zircon. No K-feldspar was observed in these rocks, although it is present in metasedimentary rocks further to the west. The protolith for this unit is interpreted as a more pelitic member of the sedimentary rocks.

Figure 2.4

Figure 2.4*a*: Upper amphibolite to granulite facies paragneiss showing well-developed migmatitic layering and concordant tonalitic neosome. Paleosome layers may contain up to 20% garnet. Field of view approximately 3 m.

Figure 2.4*b*: Strongly deformed monzogranite gneiss with abundant angular mafic xenoliths and well developed compositional layering. Field of view approximately 4 m.

At one sample location (94KE240M) the migmatitic paragneiss contains minor hornblende and actinolite as well as biotite and garnet. The hornblende and actinolite appear to be the products of retrograde alteration of orthopyroxene. The significance of this mineral assemblage is discussed in greater detail in Ch. 3.

2.2.5 Monzogranite gneiss

This unit occurs in the west-central part of the map area and is bounded on the east and west by late brittle faults and to the south by Quaternary overburden, obscuring its contact relationships. The gneiss is leucocratic, medium- to coarse-grained and locally contains recrystallized K-feldspar megacrysts. The composition is monzogranitic, with the following mineral assemblage: plagioclase (40-45%), quartz (25%), K-feldspar (15-20%), biotite (5-10%), muscovite (1-2%), chlorite (1%) with accessory zircon, titanite and apatite. Compositional layering consists of alternating, discontinuous, centimeter-scale quartzofeldspathic leucosome and biotite-rich melanosome layers (Figure 2.4b). This unit contains abundant large xenoliths of massive amphibolite, which may be either disagregated individual layers of mafic gneiss or fragmented mafic dykes, and rare xenoliths of tonalite gneiss. The extent of recrystallization and migmatization suggest that this unit may be part of the older gneiss sequence.

2.2.6 'Nerak granite'

This foliated sparsely megacrystic biotite granite was informally named after the Nerak silver showing (Kelly, 1984; Vogg, 1984), where large dykes of granite intrude the main body of the granulite facies mafic gneiss. This unit is leucocratic, with a pink- to white weathered surface and a pinkish-grey fresh surface. K-feldspar (25-35%) occurs as 3-4 cm long megacrysts with rectangular euhedral to subhedral outlines or as fine- to medium-grained, sub- to anhedral crystals between megacrysts. Quartz (35%) and plagioclase (30%) are present as medium- to fine-grained anhedral masses between the biotite and K-feldspar. Medium- to fine-grained, subhedral biotite (3-10%) is present and typically altered to chlorite. In one location, in proximity to migmatitic paragneiss, garnet is present in trace quantities. Accessory minerals include zircon, apatite, monazite and allanite.

The granite is massive to well foliated, to almost gneissic, with igneous textures well preserved in the massive parts (Figure 2.5*a*). Areas of higher strain are randomly distributed and are characterized by a wispy foliation or layering defined by biotite-rich schlieren and, at even higher strain, preferred orientation of the megacrysts. Contacts between areas of higher strain and more massive granite are typically gradational. Biotite schlieren are deformed by broad, open F_3 folds (see Ch. 3), which trend roughly northeast. This unit contains abundant angular mafic xenoliths similar to those in the monzogranite gneiss. The eastern contact of the 'Nerak granite' appears gradational with a more pegmatitic-looking megacrystic granite (described below), suggesting both are derived from the same magmatic source.

Figure 2.5

Figure 2.5a: 'Nerak granite' with sparse, euhedral K-feldspar megacrysts and well preserved igneous texture. Lens cap is 6 cm in diameter.

Figure 2.5b: Megacrystic granite showing rounded, seriate megacrysts of K-feldspar and minor deformation. Bluish mineral colour in quartz is thought to be due to anatase inclusions. Hammer handle is 30 cm long.
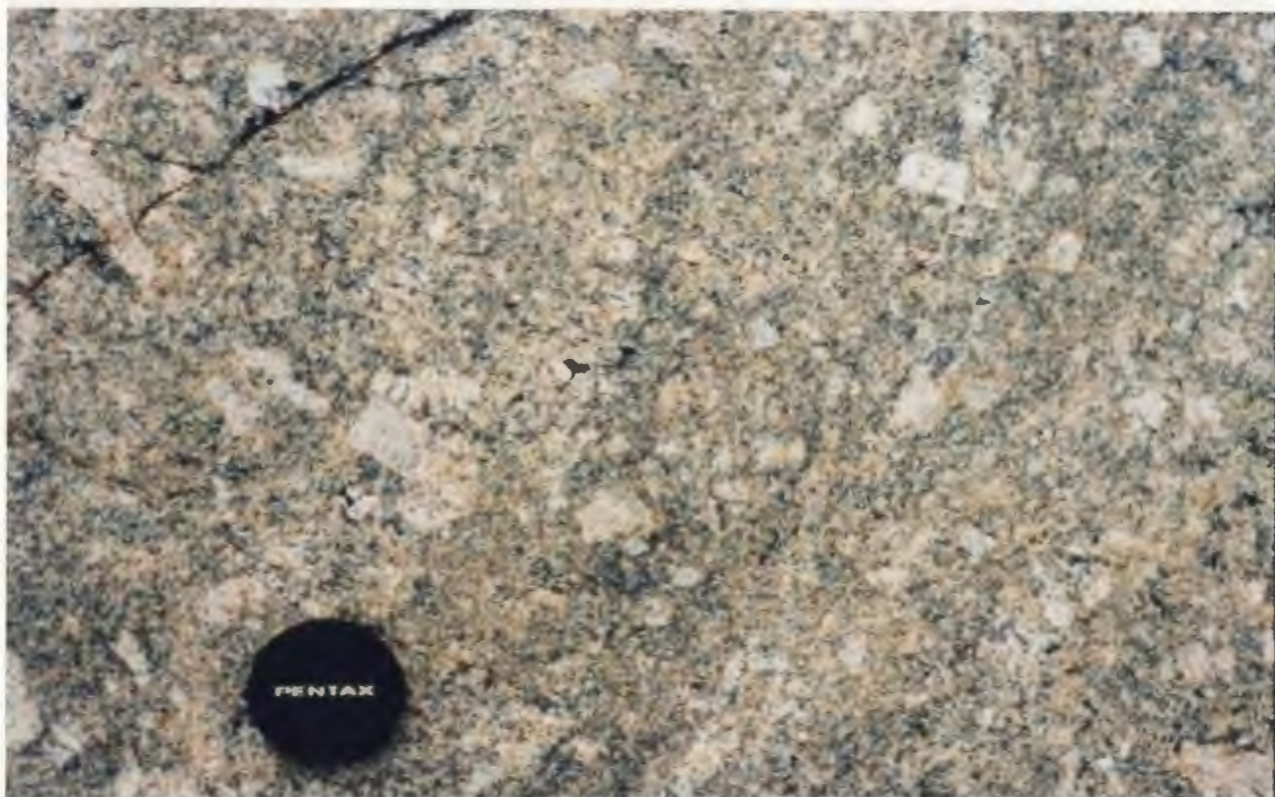
2.2.7 Pegmatitic granite

This unit is a very coarse-grained to pegmatitic biotite syenogranite with a white to yellowish-white weathered surface and a light greyish-white fresh surface. It is characterized by rounded, subhedral, seriate megacrysts of K-feldspar (35-40%), ranging from < 0.5 cm up to 30 cm across (Figure 2.5b). These megacrysts are unzoned although some are perthitic and some have graphic texture. Plagioclase (30-35%), is present as medium- to coarse-grained, seriate, subhedral to anhedral crystals. Quartz (20-25%) appears as fine- to coarse-grained, anhedral crystals interstitial to the feldspars and has a distinctive blue color, possibly from the presence of anatase. The mafic mineral is medium- to coarse-grained, euhedral to subhedral chlorite (2-7%) after biotite. Minor amphibole is locally present in proximity to mafic rafts. Garnets (1%) up to 2 cm in diameter are also present locally in proximity to paragneiss xenoliths. Accessory zircon, apatite and allanite are also present.

Fabric in the granite consists of a weak foliation defined by the preferred orientation of biotite and 'stringers' of feldspar megacrysts. The seriate, rounded nature of the megacrysts suggests that this unit was emplaced as a crystal 'mush'. This unit has intruded the granitoid orthogneisses, the mafic gneiss and the paragneiss, both parallel to and cross cutting the gneissosity, and contains abundant xenoliths of paragneiss and mafic gneiss.

2.2.8 Boudinaged diorite dyke

Diorite to tonalite dykes are present in the western and central parts of the study area, in both the monzogranite gneiss and the 'Nerak granite'. These dykes are medium- to fine-grained, dark grey weathering and composed of plagioclase (40-65%), hornblende (0-15%; in both brown and blue-green varieties), biotite after hornblende (10-25%), quartz (10-30%) and ilmenite (1-2%). Accessory minerals include titanite, apatite and zircon.

The dykes range from 20-50 cm wide and are boudinaged at a low angle to, and display a moderate internal foliation parallel to, the main S_3 fabric present in the host rocks (see Ch. 3 for description of structural elements). Dyke margins are irregular, have no visible chilled contacts, and are locally crenulated parallel to the fabric in the host rocks. The enveloping surface of the dyke segments cuts the host rock fabric at a low angle and suggests that the emplacement of these dykes may have occurred during the later stages of S_3 deformation (Figure 2.6*a*). The dykes also cut the angular mafic xenoliths present in both the monzogranite gneiss and the 'Nerak granite'.

2.2.9 Foliated granodiorite dykes

This unit consists of light grey weathering, fine-grained, sparsely K-feldspar porphyritic granodiorite dykes that occur throughout the study area (Figure 2.9*b*). Modal mineralogy consists of plagioclase (35-40%), quartz (40-45%) and biotite (5-10%). The dykes contain K-feldspar (5-10%) as matrix as well as small (<0.5 cm) phenocrysts. No amphibole was visible in the sample. Accessory minerals include titanite, apatite, zircon

Figure 2.6

Figure 2.6a: Boudinaged diorite dyke hosted in monzogranite gneiss. Note uneven dyke margins and dyke cutting gneissic fabric at low angle in upper right of photo. Hammer handle is 30 cm long.

Figure 2.6b: Two generations of syenogranite pegmatite. The pegmatite dykes cut both the fabric in the 'Nerak granite' and the boudinaged diorite dyke (visible in top left). Hammer handle is 30 cm long.

and allanite. These dykes are typically 0.5 meter wide and cut the main S_3 fabric in the host rocks at a moderate to high angle as well as cutting the diorite dykes mentioned above. A weakly to moderately developed internal foliation is present parallel to the foliation in the host rocks. Dyke margins are straight and have no visible chilled contacts.

2.2.10 Syenogranite pegmatite dykes

Internally zoned, undeformed, pink weathering dykes of biotite syenogranite pegmatite to aplite are present throughout the study area. The typical mineralogy is K-feldspar (40-60%), quartz (25-45%), plagioclase (10-15%), biotite/chlorite (2-3%), and magnetite (1-2%). These dykes are typically 0.5-1.0 metre wide and cross all of the other units, including the diorite and granodiorite dykes mentioned above. Pegmatite dyke margins are straight and chilled contacts are present in some. There appears to be more than one generation of pegmatite (Figure 2.6b) and, although compositionally identical, they cut each other at a high angle.

2.2.11 Other minor intrusive rocks

A series of ultramafic xenoliths occur in the western part of the study area. These xenoliths are present in the monzogranite gneiss and the 'Nerak granite', and range from 10 cm to 4-5 m across (Figure 2.7a). All have been altered to greenschist facies assemblages, with the primary minerals being replaced by chlorite, actinolite, serpentine and talc +/- epidote. These xenoliths may represent an ultramafic dyke suite that intruded

Figure 2.7

Figure 2.7a: Ultramafic xenolith hosted in the 'Nerak granite'. These xenoliths may be the remnants of an older ultramafic dyke set. Hammer handle is 30 cm long.

Figure 2.7b: Young granite showing characteristic fine grain size and lack of deformation. Lens cap is 6 cm in diameter.

the granitoid units and was boudinaged and altered during later tectonic and intrusive events. Alternatively, they may be part of an older unit that was entrained by the granite gneiss and 'Nerak granite' when they intruded. Because of their limited extent and poor state of preservation, the relative age and contact relationships of these rocks are hard to determine.

A fine-grained, green weathering, mafic dyke occurs in one location in the central part of the study area. It is 2-3 m. wide, trends roughly east west and is cut by late brittle faults and Mackenzie dykes (ca. 1267 Ma; LeCheminant and Heaman, 1989). The dyke is not cut by any of the other intrusive rocks, including the syenogranite pegmatite dykes. Mafic minerals have been altered almost entirely to fine-grained, actinolite (50%) with sericitized plagioclase (30-35%) visible as fine-grained phenocrysts. Quartz (5%) and carbonate (calcite?) (1-5%) are present, along with hematized Fe-sulphides (10%).

2.2.12 Young granite

This unit is located to the southeast of the study area, near 'Beaver lake' (Figure 1.2). It consists of a biotite-rich, leucocratic to mesocratic, light pink to red, fine-grained, equigranular granite (Figure 2.7*b*). The typical mineral assemblage consists of plagioclase (30-35%), quartz (25-30%), K-feldspar (25%), olive-green biotite (5-10%) and magnetite/ilmenite (2-3%), with accessory titanite, allanite, zircon and apatite. Titanite is present as medium to large euhedral to subhedral crystals which appear to be of igneous origin. Allanite is present as small, subhedral, zoned crystals, which have considerable radiation damage.

The granite is in intrusive contact with the gneissic and metasedimentary rocks of the Uplift, and locally contains xenoliths of older gneissic rocks. It is massive to weakly foliated, with a fabric defined by alignment of micas or elongation in quartz grains. On the basis of contact relationships, well preserved igneous texture and lack of significant deformation, this unit was interpreted as being one of the youngest in the Uplift.

2.3 Contact Relationships

The relative ages of units in the study area, especially the older gneissic and supracrustal rocks, are poorly constrained since the original intrusive and/or depositional contacts have been obscured during high grade metamorphism and transposed into the regional gneissosity. In addition, the later granites intrude preferentially along pre-existing anisotropies, such as unit contacts. However, several features are visible which suggest original contact relationships. In one locality in the western part of the study area (Figure 2.1), where the contact between the tonalite gneiss and the mafic gneiss is exposed, the mafic gneiss appears to cut the fabric of the tonalite gneiss at a low angle (Figure 2.8a). Xenoliths of the layered mafic gneiss are present in the orthogneiss, as well as trains of unlayered amphibolite xenoliths. These xenoliths display the same degree of recrystallization and deformation as the older gneissic rocks while their distribution and lack of layering suggests that they may have been dykes (Figure 2.8b). No similar raft trains were observed in either the mafic gneiss or paragneiss. It is possible that these massive amphibolite xenoliths represent the remains of feeders for the mafic gneiss. In the few areas where the contact between the mafic gneiss and the paragneiss is

Figure 2.8

Figure 2.8a: Contact between the mafic gneiss and the tonalite gneiss. The mafic gneiss appears to truncate the fabric in the orthogneiss at a low angle. Rock in the upper part of the photo is megacrystic granite vein. Compass for scale.

Figure 2.8b: Overview of station 94KE241 showing the contact between the tonalite gneiss (left, medium grey) and the granite gneiss (right, light grey), as well as the trains of mafic xenoliths (centre). Field of view is approximately 100 m wide.
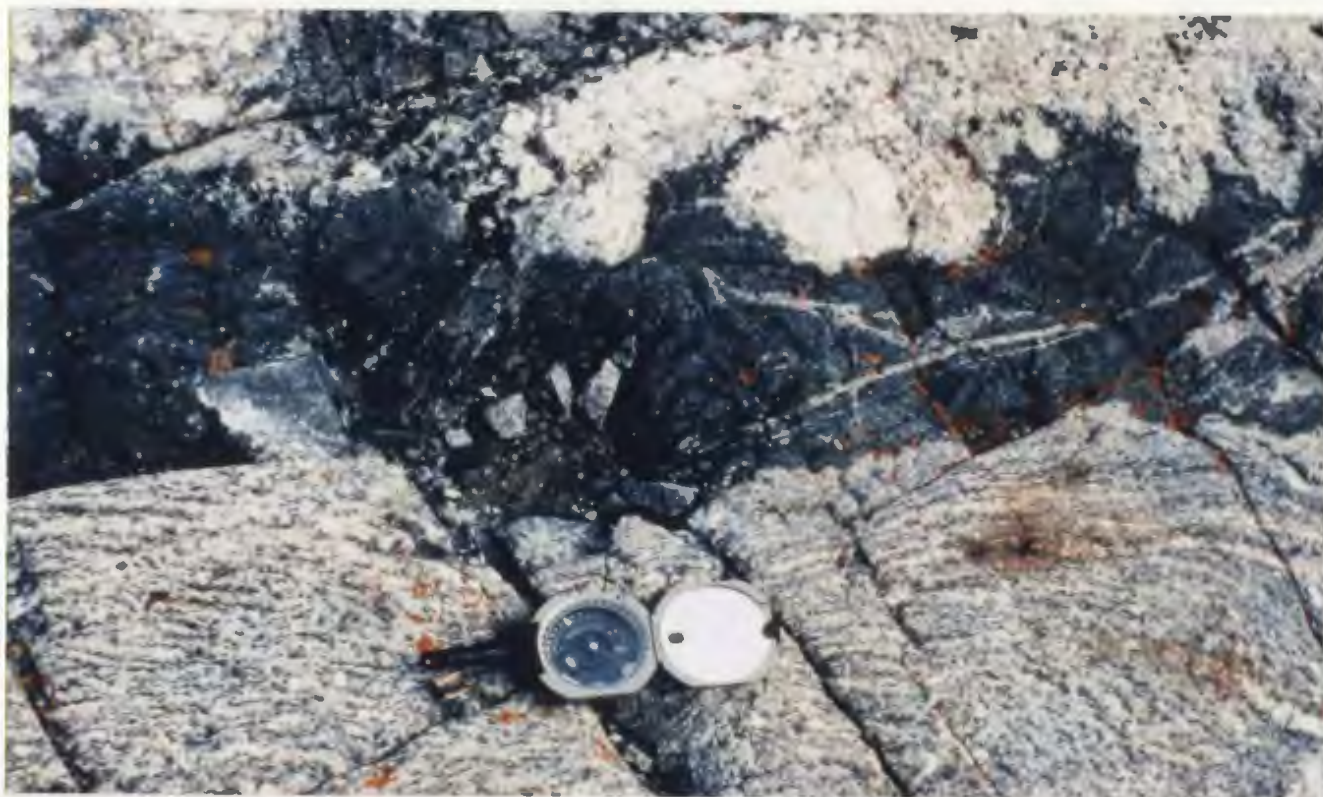
exposed, it is parallel and apparently conformable. As well, boudinaged, magnetite/sulphide-bearing, garnetiferous chert blocks, thought to be metamorphosed iron-formation, occur at or near this contact in the western part of the study area. The orthogneiss/mafic gneiss/paragneiss package may represent an old (>2.8 Ga) basement/volcanic/sediment succession that has undergone high-grade metamorphism.

The nature of the contact between the monzogranite gneiss and the surrounding rocks is unclear, since this unit is fault bounded on both its eastern and western edges. Compositionally, it resembles the 'Nerak granite', but its degree of recrystallization and migmatization suggests it may be part of the older gneiss package.

The pegmatitic granite and the 'Nerak granite' are intrusive into the other, older gneissic rocks at the coast. This can be seen particularly well at the Nerak silver showing, where large dykes of 'Nerak granite' intrude the main body of mafic gneiss (Figure 2.9*a*). The contact between the 'Nerak granite' and the pegmatitic granite is partially obscured by faulting but appears to be gradational, with progressively larger, rounder megacrysts developing eastward from the Nerak silver showing.

The contact relationships between the minor intrusive units in the study area are best illustrated by Figure 2.9*b*. In this photo, the oldest unit is the diorite/tonalite dyke, which is boudinaged in the host granite fabric. The granodiorite dyke is only slightly deformed and cuts both the diorite dyke and the host rock fabric at a high angle. This dyke set was probably emplaced late syn-deformation. The syenogranite pegmatite cuts both of the above mentioned dyke sets and the host rock fabric, and is undeformed. This implies that the emplacement of the pegmatite was post-deformational.

Figure 2.9

Figure 2.9*a*:   Dykes of 'Nerak granite' intruding the main body of the mafic gneiss at the Nerak silver showing. Hammer handle is 30 cm long.

Figure 2.9*b*:   The three minor intrusive rock units showing contact relationships. The boudinaged diorite dyke appears in the lower left of the photo and is truncated by the foliated granodiorite dyke (centre). Both are cut by an aplitic phase of the syenogranite pegmatite (top to bottom). Compass for scale.
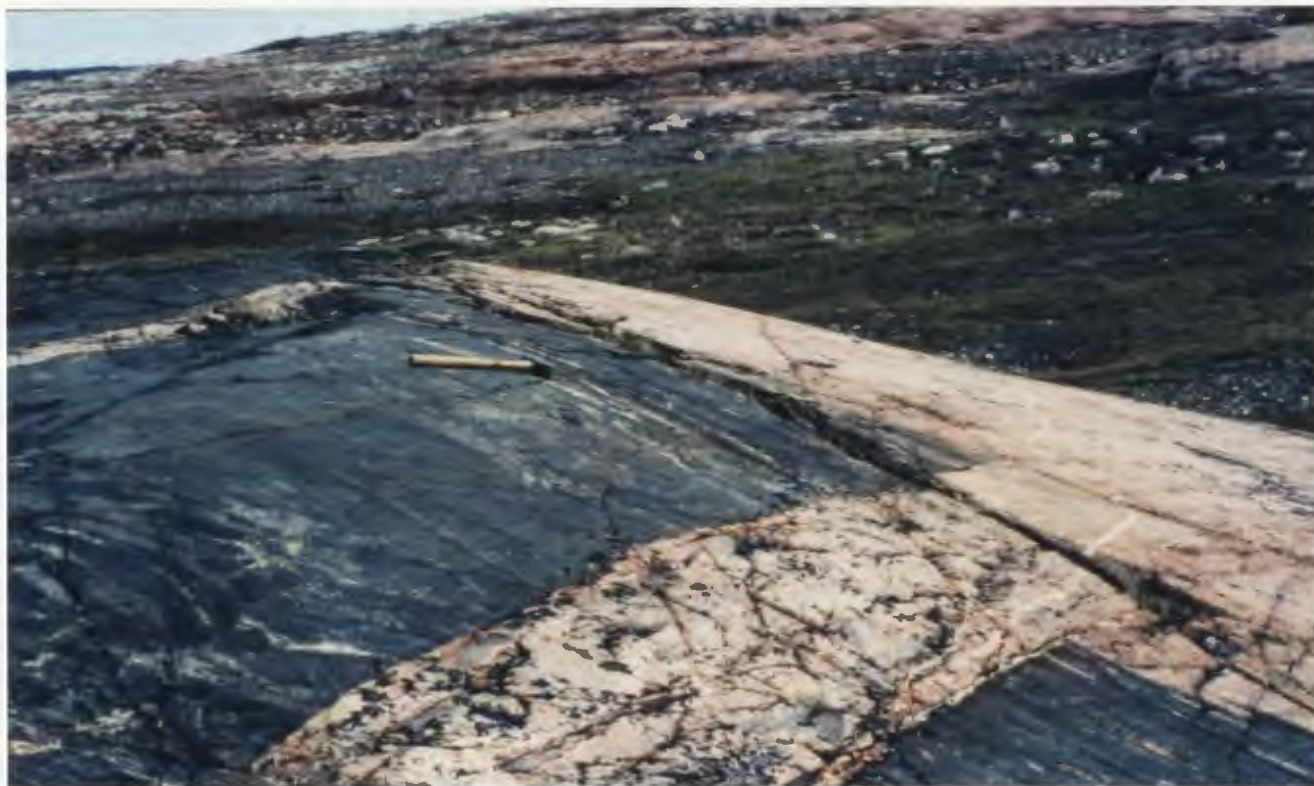
The relative age of the green, mafic dyke is more problematical. It is cut by Mackenzie dykes and late brittle faults, but nowhere along its length is it cut by any of the other dykes. This apparent relationship may be due to poor exposure of the dyke, but, if true, would mean that these mafic dykes are the youngest, undated intrusive rocks at this location.

Chapter 3: Structure and Metamorphism

3.1 Introduction

As outlined in Chapter 1, most supracrustal rocks in the Slave Province appear to undergone high temperature-low to medium pressure (HT-L/MP), greenschist to upper amphibolite facies metamorphism. To date, granulite facies rocks have been found in only four localities, all in the western half of the Slave Province (Figure 3.1). The distribution of the various metamorphic grades is patchy, implying that peak P-T conditions were achieved after regional deformation. Regional low-pressure metamorphism has been attributed to both extensive granitoid intrusion after peak deformation (Card and King, 1992) or to the differential erosion of crust whose geotherm has been disturbed by extensional thinning (Thompson, 1978). Broadly speaking, both the peak of deformation and metamorphism were synchronous with the intrusion of 2.62-2.59 Ga granitoid plutons (Thompson, 1989).

Regional polyphase deformation in the Slave Province resulted in the development of several generations of folds, cleavages and schistosities in syndeformational granitoids,
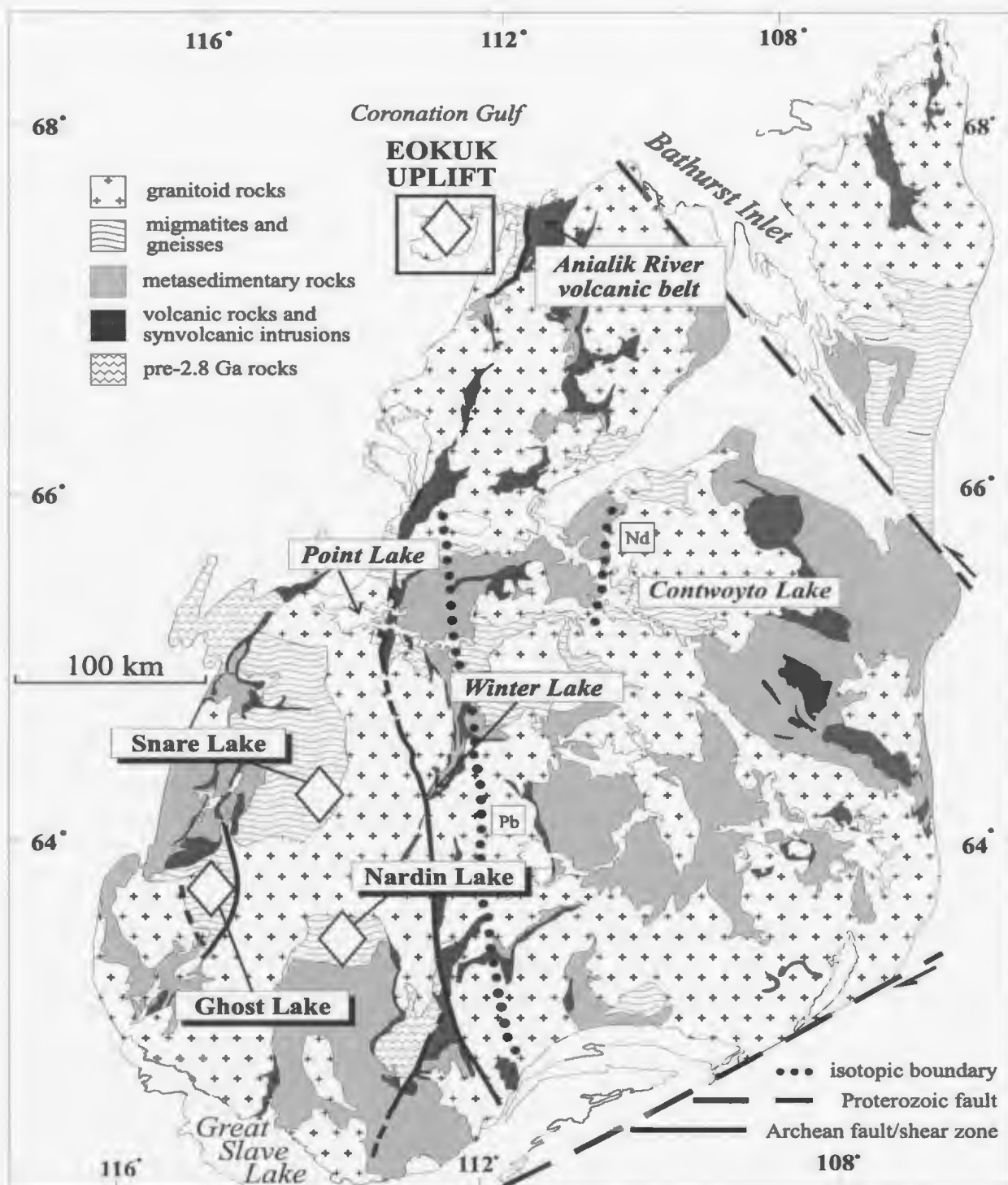
Figure 3.1: Slave Structural Province showing the location of the areas discussed in text. Locations of granulite-grade rocks are marked with diamonds, locations discussed in structural section are highlighted in italics. Isotopic age boundaries for Nd and Pb are shown with black dots (Nd: Davis and Hegner, 1992; Pb: Thorpe et al., 1992)

supracrustal rocks and older gneiss units. Two studies provide estimates of the nature and timing of deformation in the northern and central Slave Province have particular relevance to the Eokuk Uplift. The first, a study of the Kangguyak gneiss belt and the Anialik River volcanic belt (Figure 3.1), revealed an early collisional event between 2.65-2.64 Ga, when the gneisses were thrust eastward over the volcanic belt during westward directed subduction (Relf, 1995). A period of extension between 2.64-2.61 Ga was followed by an ESE-WNW regional shortening event syn- to post-2.60 Ga (Relf, 1995). In contrast, a transect across the central Slave Province from Point Lake to Contwoyto Lake (Figure 3.1), outlined two distinct episodes of crustal shortening. The first of these episodes took place at ca. 2650 (Relf, 1992) and resulted in the formation of an early set of folds and faults at Point Lake. This early fold and thrust belt is thought to have developed over an east-dipping subduction zone (Relf, 1992). The regional thermal peak metamorphism was synchronous with the second shortening event, which appears to have occurred at roughly 2610-2600 Ma across the transect (King et al., 1992; Relf, 1992). Collision in a continental arc setting, along with calc-alkaline magmatism, is thought to have been the cause of this later tectonothermal event (Relf, 1992; 1995). The results of these two studies indicate episodes of deformation occurred at different times and in different tectonic environments in the northern and central Slave Province.

3.2 Granulite Facies Metamorphism in the Slave Province

Granulite facies rocks have been reported from 4 localities in the Slave Province: Ghost Lake, Snare Lake, Nardin Lake and the Eokuk Uplift (Figure 3.1; Henderson and

Chacko, 1995; Stubley et al., 1995; Jackson, 1996; Pehrsson and Chacko, 1997 *a&b*). In this section, the metamorphism, structure, thermobarometry and U-Pb ages for the other high-grade terranes, apart from the Eokuk Uplift, are reviewed.

The Nardin Lake area is part of 30 x 40 km domain dominated by migmatitic turbiditic rocks (Figure 3.1) that defines a pronounced aeromagnetic high (Stubley et al., 1995). The migmatitic turbiditic rocks contain the sub-assemblage garnet-cordierite-K-feldspar-sillimanite, indicating moderate pressure, upper amphibolite facies conditions. The absence of orthopyroxene in intercalated amphibolites suggests these rocks may have been metamorphosed only to amphibolite facies (Stubley et al., 1995). However, a Sil-Cdr-Kfs pelite from the highest grade part of the metamorphosed supracrustal rocks gives P-T conditions of 500-600 MPa at 700-750 ^{0}C (Bethune and Carmichael, 1998). This indicates conditions were at the amphibolite to granulite facies transition and implies that granulite facies may have been achieved locally.

The Ghost Lake area, which is coincident with a roughly triangular 80 x 30 km aeromagnetic high, is underlain by granulite to upper amphibolite facies rocks (Figure 3.1). The units in the area are mainly granitoid gneiss, migmatitic to diatexitic metasedimentary rocks and K-rich granitoid rocks with subordinate mafic metavolcanic rocks. The highest-grade metasedimentary rocks have the assemblage Pl-Bt-Cdr-Grt +/- Kfs +/- Sil. Large, podiform occurrences of blue, gem quality cordierite are common. Orthopyroxene-bearing metasedimentary rocks also occur though they are not common. Granitoid gneiss at high grade typically has the assemblage Pl-Qtz-Kfs-Cpx-Opx-Bt, which implies metamorphism under low to medium pressure-high temperature (L/MP-HT) conditions (Henderson and Chacko, 1995). The age of granulite facies

metamorphism, from preliminary U-Pb analyses of zircon from a mafic granulite from the

Forked Lake area, appears to be 2.59 Ga (Perks and Chacko, 1997). This is

contemporaneous with ages of both a megacrystic granite (2598 +/- 4 Ma) and an

orthopyroxene-bearing granite (2589 +/-2 Ma) from the same area (Perks and Chacko,

1997), and suggests that magmatism may have provided some of the heat needed for LP-

HT metamorphism.

Metamorphic and structural studies carried out in the Snare Lake area consist of a

transect roughly 100 km long between Snare Lake in the west and Winter Lake in the east

(Figure 3.1; Pehrrson and Chacko, 1997 *a&b*). This area is coincident with a large

aeromagnetic anomaly and is underlain by supracrustal gneiss interlayered with granitoid

gneiss and massive to megacrystic monzogranite sheets. The supracrustal rocks consist

of metasedimentary and mafic migmatite, diatexite and amphibolite (Pehrsson and

Chacko, 1997b). Assemblages in the supracrustal rocks range from Grt-Cdr-Kfs in pelitic

paragneiss, Opx-Grt-Bt in psammitic paragneiss to Opx-Cpx +/- Hbl in mafic migmatite.

P-T determinations on Grt-Opx-Pl-Qtz assemblages in metasedimentary rocks 6 km to the

south of the transect indicate peak pressure of 600-700 MPa at 800-900 ^{0}C (Pehrsson and

Chacko, 1997a). On average, P-T conditions across the transect range from 675-800 ^{0}C

and 600-700 MPa. U-Pb zircon ages from a leucosome in a migmatitic paragneiss are ca.

2587 Ma with an inherited component at 2640 Ma (S. Pehrsson, pers. comm.).

Broadly speaking, structures in all three areas are characterized by shallow to

subhorizontal migmatitic to gneissic which has been deformed by later, upright open

folds, producing dome and basin interference patterns (Henderson and Schaan, 1993;

Stubley et al., 1995; Pehrrson and Chacko, 1997b).

3.3 Metamorphism and Structure in the Eokuk Uplift

The following two sections provide a brief synopsis of the metamorphic grades and structural styles of rocks in the Eokuk Uplift. The first section deals with distribution of rocks of various metamorphic grades across the Uplift and includes P-T estimates on four representative samples of pelitic and mafic rocks of different grades. The second section deals with the structures present in the study area and the relative timing of deformation.

3.3.1 Metamorphism

Rocks within the Eokuk Uplift were metamorphosed to predominantly amphibolite facies and, within the study area along the Coronation Gulf coast, granulite facies. In general, metamorphic grade increases both east and west of a narrow central zone of lower to middle amphibolite facies schistose metavolcanic and metasedimentary rocks (Figure 3.2). Outside this central zone, middle to upper amphibolite facies migmatite and gneiss predominate (Jackson, 1996). Mafic rock units contain the assemblage Hbl-Pl (+/-Bt +/-Qtz) at all grades. In the lower amphibolite facies metavolcanic rocks, epidote is locally present, while at granulite facies, orthopyroxene and clinopyroxene are present. In the metasedimentary rocks, the assemblage Grt-Bt-Qtz-Pl (+/-Ksp) is present at all grades. The lower amphibolite facies metasediments consist of two varieties. The first is iron-rich, garnet-biotite schist interlayered with quartz-rich, biotite-muscovite +/- garnet schist. The second is a biotite-muscovite (cordierite, andalusite, sillimanite +/-garnet)
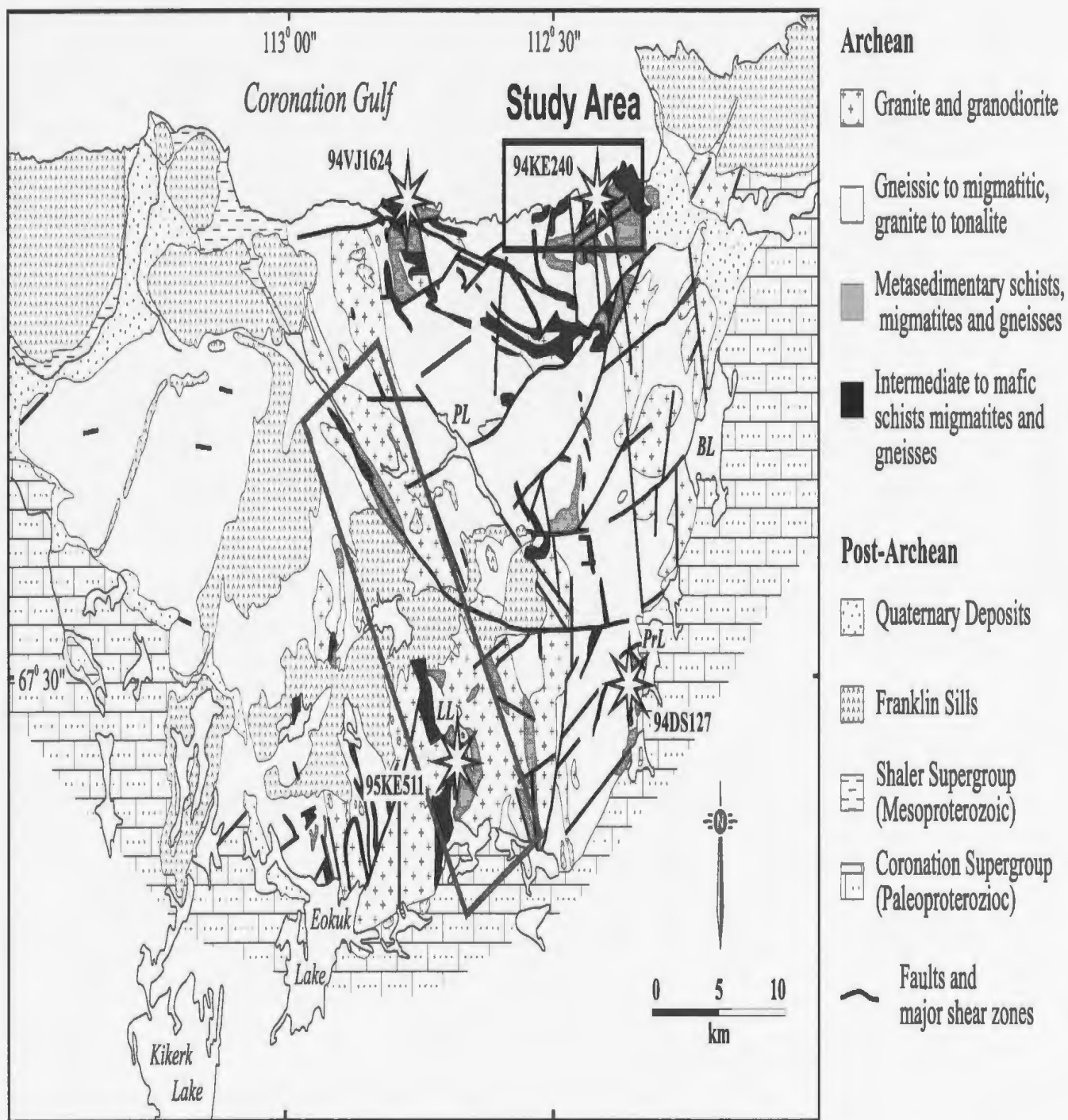
Figure 3.2: Geological map of the Eokuk Uplift. Study area is shown by the black box. Grey box shows the approximate extent of lower to mid-amphibolite facies supracrustal rocks. *LL*, 'Larry's lake'; *PL*, 'Purina lake'; *PrL*, 'Profile lake'; *BL*, 'Beaver lake' (informal names). The stars show the locations and station numbers of samples discussed in text. Modified after Jackson, (1994).

pelite which is interlayered with psammite and locally graded (Jackson, 1996). At upper amphibolite facies, the metasedimentary rocks are granoblastic quartzofeldspathic migmatites and gneisses that are commonly garnetiferous and contain combinations of biotite, muscovite, sillimanite, cordierite and hornblende.

In order to quantify the P-T conditions in the study area, three pelite samples and one mafic gneiss sample with typical mineral assemblages have been studied in detail. They were chosen to be representative of the peak mineral assemblages in each area and to give an idea of the range of metamorphic conditions across the Eokuk Uplift.

The first pelite sample is from the schistose, iron-rich member near 'Larry's lake' (95KE511). The pelites at 'Larry's lake' are biotite-rich and appear to have a turbiditic protolith, since graded bedding is still preserved in some locations. Cordierite is abundant throughout these sediments and andalusite occurs locally as coarse, euhedral crystals in pods with quartz and feldspar. Garnet is abundant in isolated layers and occurs as mm-scale euhedral crystals. Thin sections of the pelitic sample from the 'Larry's lake' area contain the assemblage Qtz-Bt-Grt-Pl-Cdr-St. No muscovite is present, which would preclude the formation of K-feldspar. Minor fibrolitic sillimanite is intergrown with biotite. Garnets are euhedral and have rotated inclusion trails implying deformation was ongoing during metamorphism. Staurolite occurs as skeletal, relict grains enclosed in cordierite (Figure 3.3a). Similar reaction textures are seen in Fe-rich pelitic rocks from elsewhere in the Slave Province, particularly at Point Lake and in the Yellowknife greenstone belt. These textures are thought to be a result of either the Fe-rich nature of the sediments or of rapid metamorphism, both of which would allow staurolite to coexist with cordierite. The staurolite in the sample is probably not a product of an early period

Figure 3.3

Figure 3.3a: Photomicrograph of the pelite from 'Larry's lake' (94KE511). Note relict staurolite (St) overgrown by cordierite (Cdr- dashed outline). Field of view is 1.5 mm.

Figure 3.3b: Photomicrograph of the pelite from 'Profile lake' (94DS127). Sillimanite (Sil) occurs as anhedral grains in association with biotite, and appears to be altering to quartz and fine-grained muscovite. Field of view is 1.1 mm
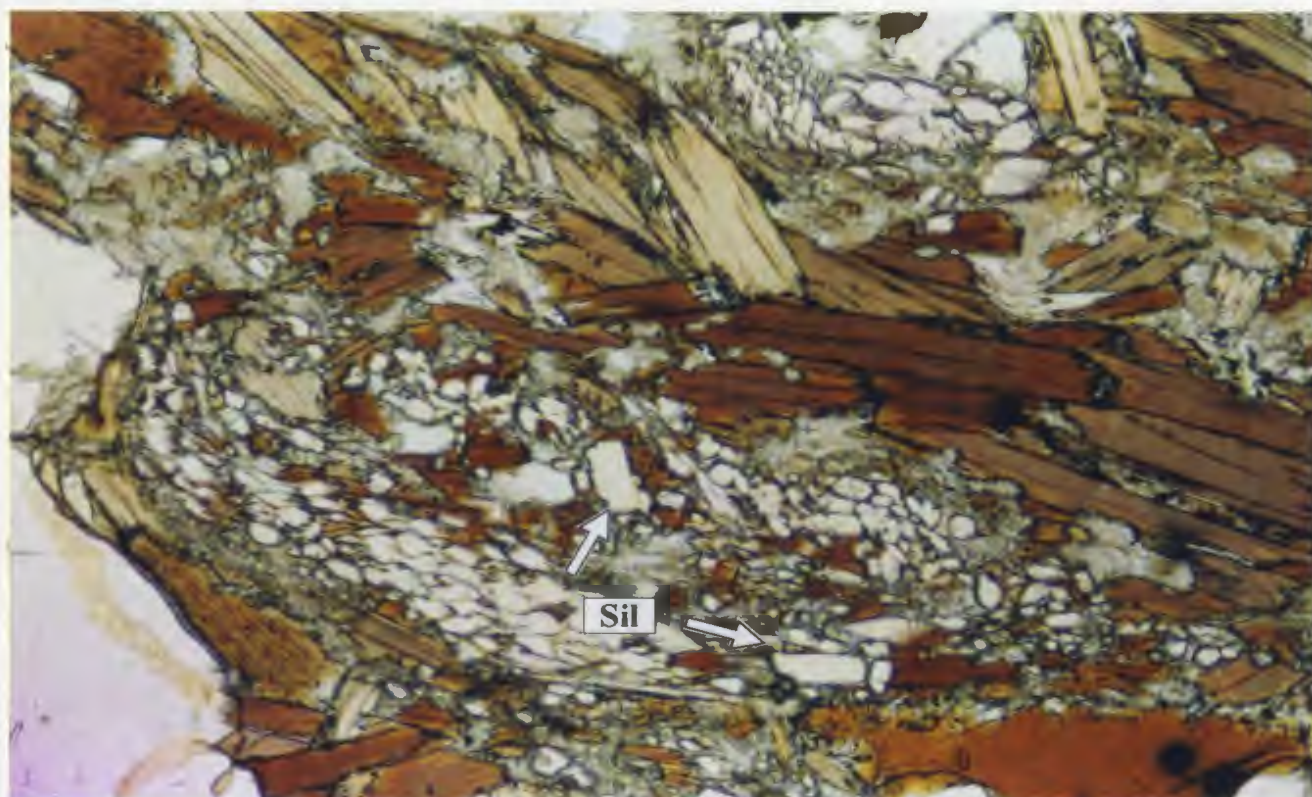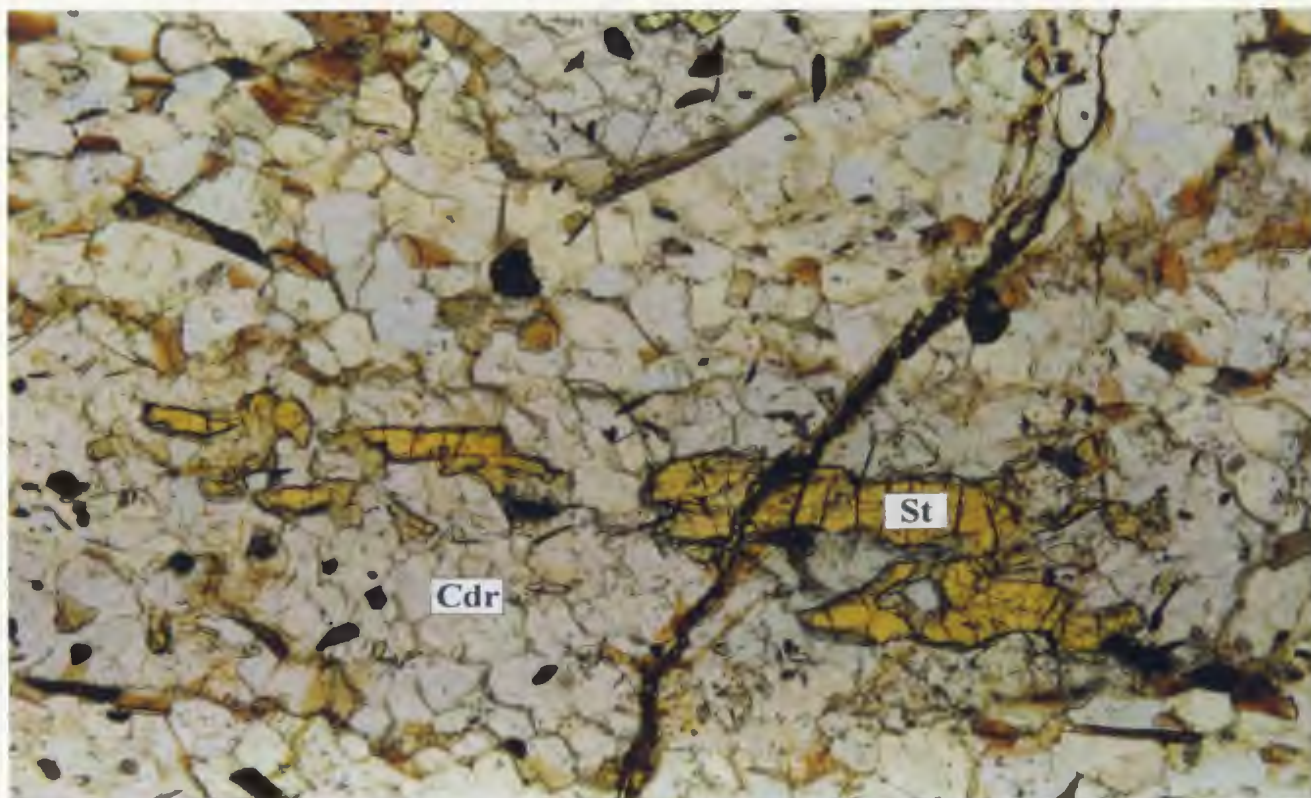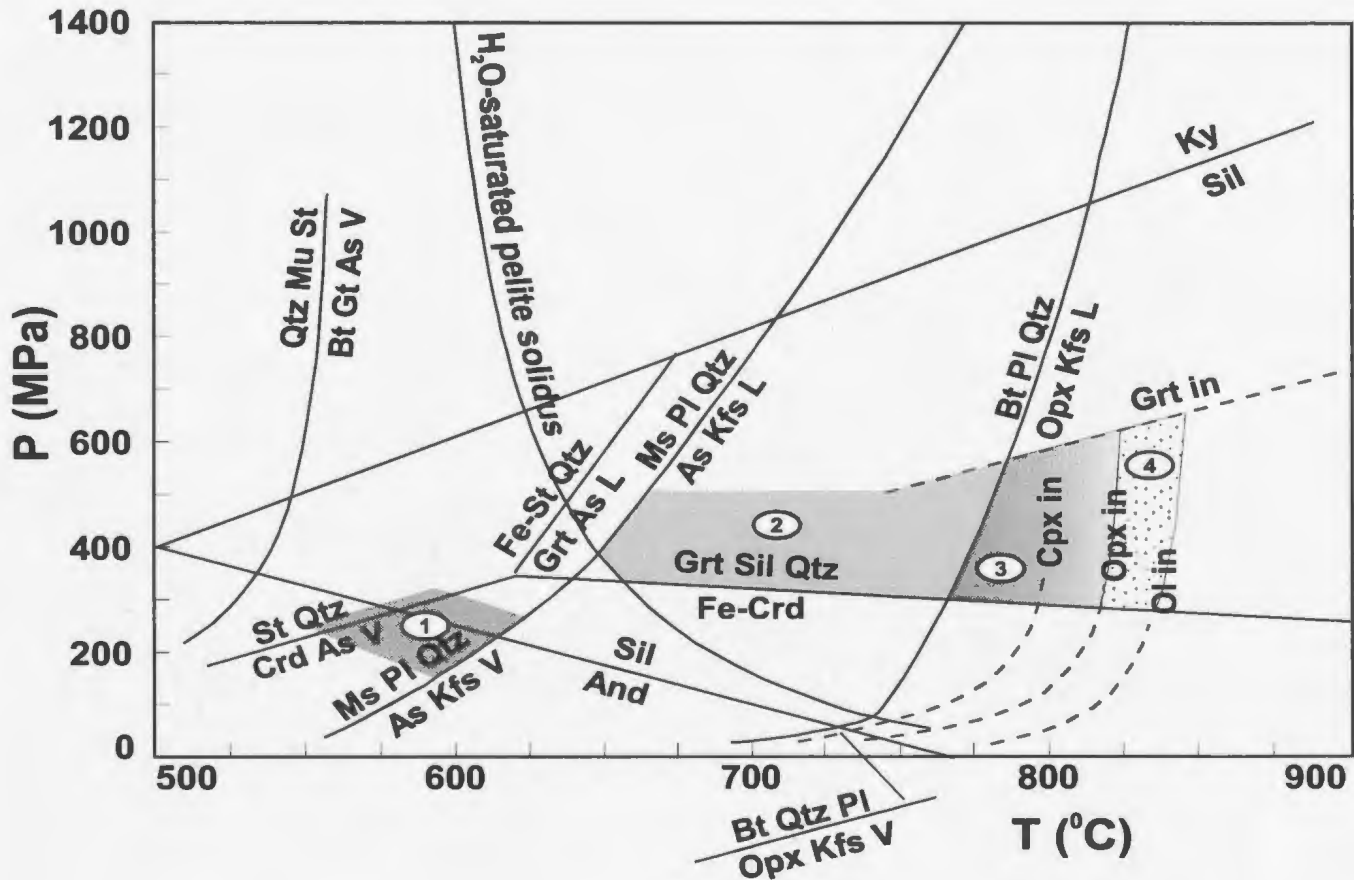
Figure 3.4: P-T diagram showing reaction boundaries for vapor-absent melting reactions in pelites (black lines) and amphibolite to granulite facies transition reactions for mafic rocks (dotted lines). Shaded areas show inferred peak P-T conditions for the various samples mentioned in the text: (1) 94KE511; (2) 94VJ1624 and 94DS127; (3) 94KE240M; (4) granulite facies mafic gneiss. From Spear (1993); Carmichael et al. (1987); Yardley (1981) and Holdaway and Lee (1977).

of high pressure metamorphism, but rather represents a relic of a lower grade of the same LP-HT conditions that produced the cordierite (Thompson, 1978; Jackson, 1984). From the mineral assemblage present in this rock, peak P-T conditions are estimated to be between 200-300 MPa and 500-625 ^{0}C (Figure 3.4).

The second pelite sample comes from the iron-poor, quartz-rich migmatites 2 km southwest of 'Profile lake' (94DS127) (Figure 3.2). These rocks are paragneisses with granoblastic texture and compositional layering defined by cm-scale bands of biotite-rich melanosome alternating with tonalitic leucosome. In thin section, the sample has a mineral assemblage of Qtz-Pl-Bt-Grt-Sil (Figure 3.3b). No cordierite was observed in this sample and K-feldspar is a minor component in the leucosome. Garnets are fractured, resorbed and partially altered to biotite. Retrograde alteration is extensive. Partial melting in this sample suggests that temperatures must have exceeded 650 ^{0}C. P-T estimates from the mineral assemblage in this rock range from 650-750 ^{0}C at 300-500 MPa.

Attempts to quantitatively determine peak P-T conditions for migmatitic paragneiss in the study area have been frustrated by the extensive, greenschist facies alteration in the rocks. The presence of sillimanite and absence of cordierite indicate that these gneisses formed in a HT-L/MP metamorphic environment. At station 94VJ1624 (Figure 3.2), migmatitic paragneiss has the assemblage Pl-Qtz-Bt-Grt +/-Ksp +/- Sil. The sillimanite in this sample is resorbed but has an atypical equant crystal habit, suggesting it may be a pseudomorph of andalusite (Figure 3.5a). No fibrous sillimanite is visible in hand sample. The mineral assemblage in this rock is consistent with peak P-T conditions similar to those at 'Profile lake'.

Figure 3.5

Figure 3.5*a*: Photomicrograph of migmatitic metapelite at station 94VJ1624. This metapelite has the assemblage Qtz-Pl-Bt-Grt-Sil-Ksp, indicative of moderate pressure upper amphibolite to granulite facies conditions. The sillimanite in the photo has a blocky, equant crystal habit that suggests it may be a pseudomorph of andalusite. Field of view is 2.3 mm.

Figure 3.5*b*: Photomicrograph of Al-poor, Fe-rich migmatitc metapsammite at station 94KE240. Mineral assemblage consists of Qtz-Pl-Bt-Grt-Act-Hbl. The actinolite and blue-green hornblende may to be the result of lower amphibolite alteration of orthopyroxene (see Fig. 3.6b). Field of view is 2.3 mm
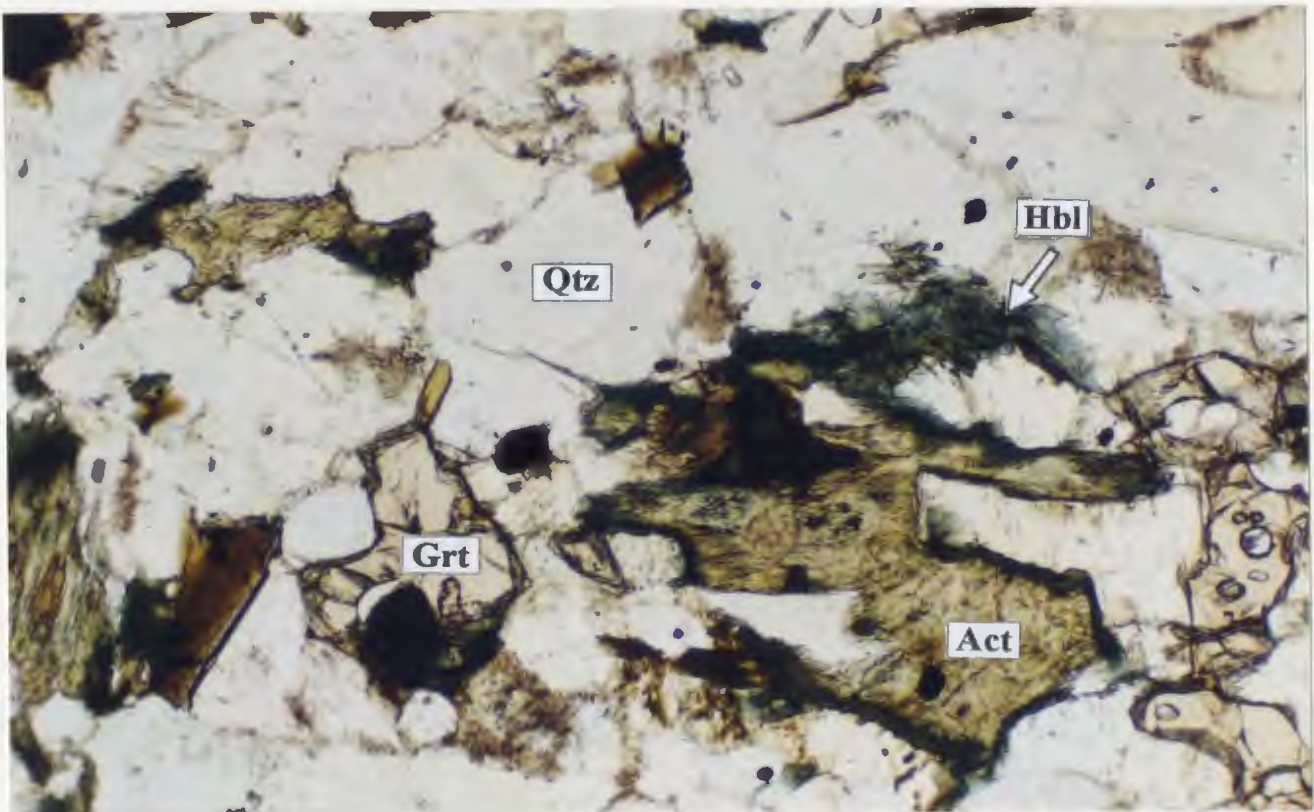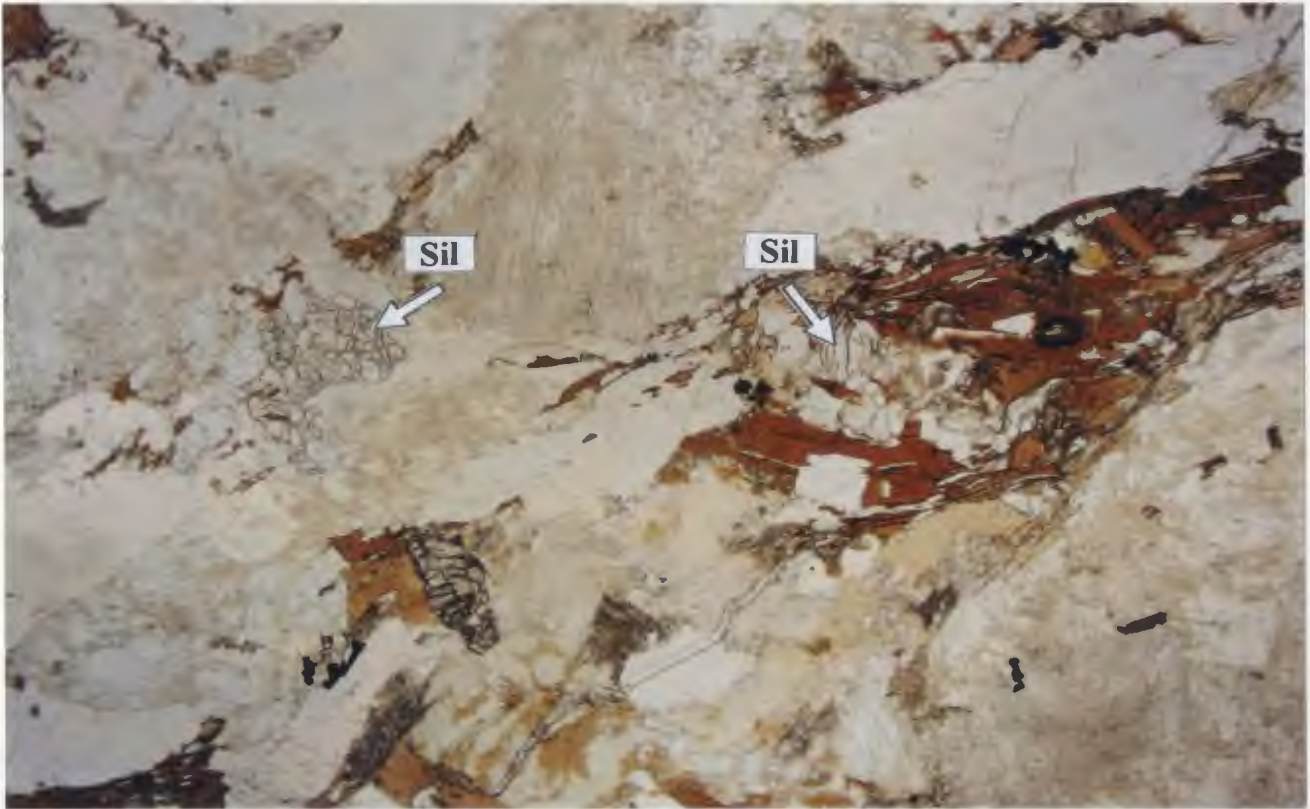
Within the study area, a paragneiss identified as a psammite (94KE240) contains the assemblage Pl-Qtz-Bt-Grt-Hbl-Act. The hornblende and actinolite occur as aggregates of actinolite rimmed with blue-green hornblende suggesting retrograde actinolite growth (Figure 3.5b). Similar aggregates of actinolite and hornblende, surrounding relict orthopyroxene, are seen in the mafic gneiss and are interpreted as a lower amphibolite to greenschist facies retrograde reaction from peak granulite facies conditions. The similarity in reaction textures suggests that the original mafic mineral in these metasediments may have been orthopyroxene. The alumina-poor, iron-rich composition of this sedimentary rock would be compatible with the formation of orthopyroxene at lower granulite temperatures. If this is the case, then peak temperatures in this section of the Uplift must have exceeded 750 ^{0}C (Figure 3.4).

A better estimate of the peak P-T conditions can be gained from the adjacent mafic gneisses. In granulite facies mafic gneiss in the study area, both orthopyroxene and clinopyroxene are visible in hand samples and thin sections. Euhedral metamorphic orthopyroxene up to 5 cm in diameter is common in tonalitic leucosome in the mafic migmatite (Figure 3.6a). In thin section, these rocks display a granoblastic texture, with both orthopyroxene and clinopyroxene present, in addition to green-brown hornblende, plagioclase +/- quartz (Figure 3.6b). The lack of garnet in the mafic gneiss suggests the granulites formed at low pressure, probably not above 500 MPa (Figure 3.4; Spear, 1993). Preliminary major element geochemistry samples from the granulite grade mafic gneiss indicates no excess of iron or silica in the rocks (V. Jackson, pers. comm., 1996), which would delay the formation of garnet until higher pressures (Spear, 1993). The absence of cordierite in the surrounding metasediments, combined with the absence of garnet in the

Figure 3.6

Figure 3.6*a*: Euhedral orthopyroxene developed in the tonalitic leucosome of the mafic gneiss. The dark mineral rim around the pyroxene is a mixture of hornblende and magnetite. Lens cap is 6 cm in diameter.

Figure 3.6*b*: Photomicrograph of the mafic gneiss showing granoblastic texture and typical hornblende-plagioclase-orthopyroxene-clinopyroxene mineral assemblage. Field of view is 2.3 mm.
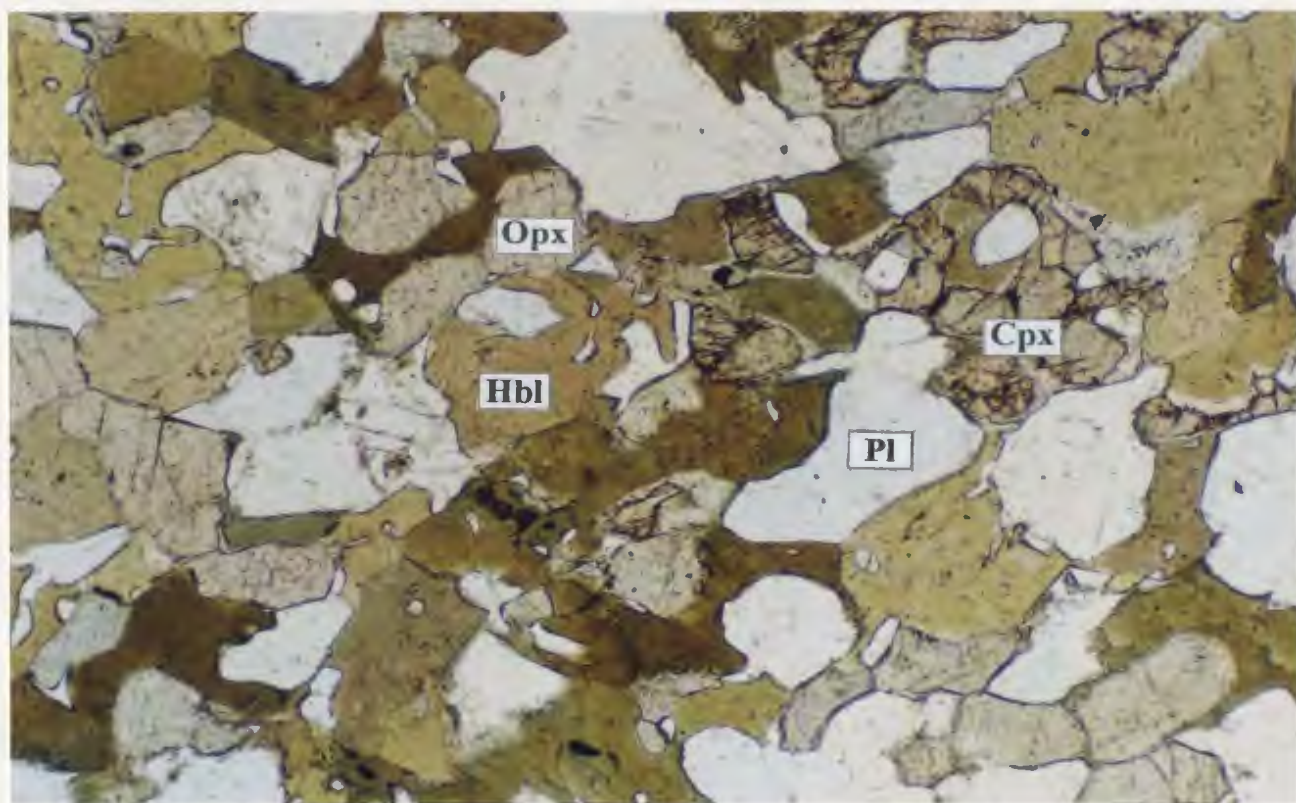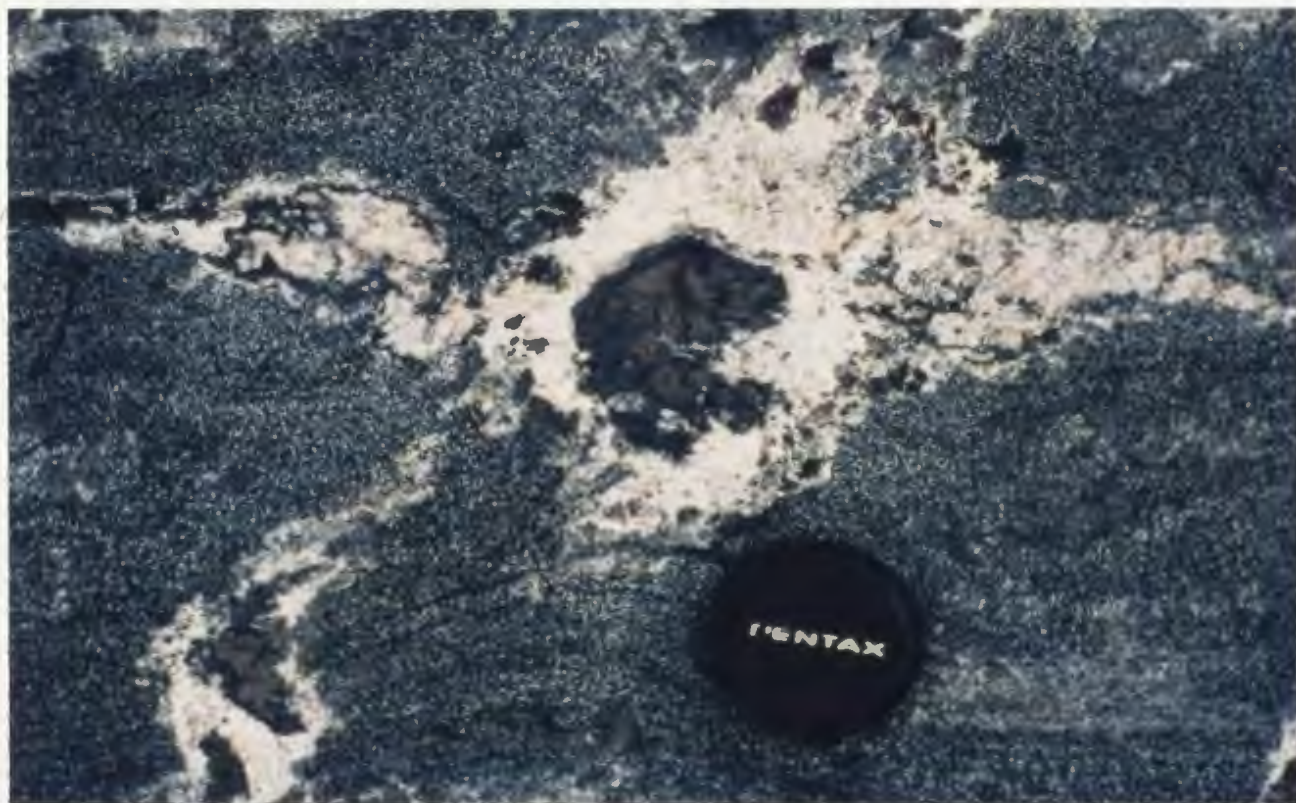
mafic gneisses themselves, would suggest peak P-T conditions between 800-850 ^{0}C and 300-600 MPa (Figure 3.4).

The orthogneisses contain no assemblages diagnostic of high-grade metamorphism. However, in thin section, most display granoblastic textures, with short, straight mineral grain boundaries and many small round grains developed. This is in contrast to the megacrystic granites that, though showing retrograde alteration and slight recrystallization along grain boundaries, have well preserved igneous textures. Megacrystic granitic rocks do not show the degree of melting, recrystallization or any mineral assemblages that would suggest they have undergone high-grade metamorphism.

At least two episodes of lower grade metamorphism are discernable from textural evidence in thin section. First, there appears to have been an amphibolite facies event connected with the intrusion of the megacrystic granites. Almost total replacement of pyroxene, especially clinopyroxene, by hornblende occurs near the contact between the mafic gneiss and megacrystic granite. Hornblende also appears growing in fractures and in the axial planar cleavages of folds in the mafic gneiss and as reaction rims on pyroxene crystals (Figure 3.6*a*). Second, a pervasive, though patchy, greenschist grade overprint is visible in most rocks of the study area. This has led to the alteration of biotite and garnet to chlorite in the paragneiss (Figure 3.7*a*), and the alteration of orthopyroxene to blue-green hornblende and actinolite in the mafic gneiss (Figure 3.7*b*). In areas where the mafic gneiss has undergone lower amphibolite to greenschist alteration, relict pyroxene is surrounded by felty aggregates of actinolite which are, in turn, rimmed by dark, blue-green hornblende (Figure 3.7*b*).

Figure 3.7

Figure 3.7a: Photomicrograph of migmatitic paragneiss from the study area showing chlorite alteration in garnet (center of photo) and sericitization of plagioclase. Field of view is 7.5 mm.

Figure 3.7b: Photomicrograph of the mafic gneiss with orthopyroxene altering to blue-green hornblende and actinolite as a result of lower amphibolite to greenschist facies overprint. Note also the almost complete sericitization of the plagioclase. Field of view is 7.5 mm.
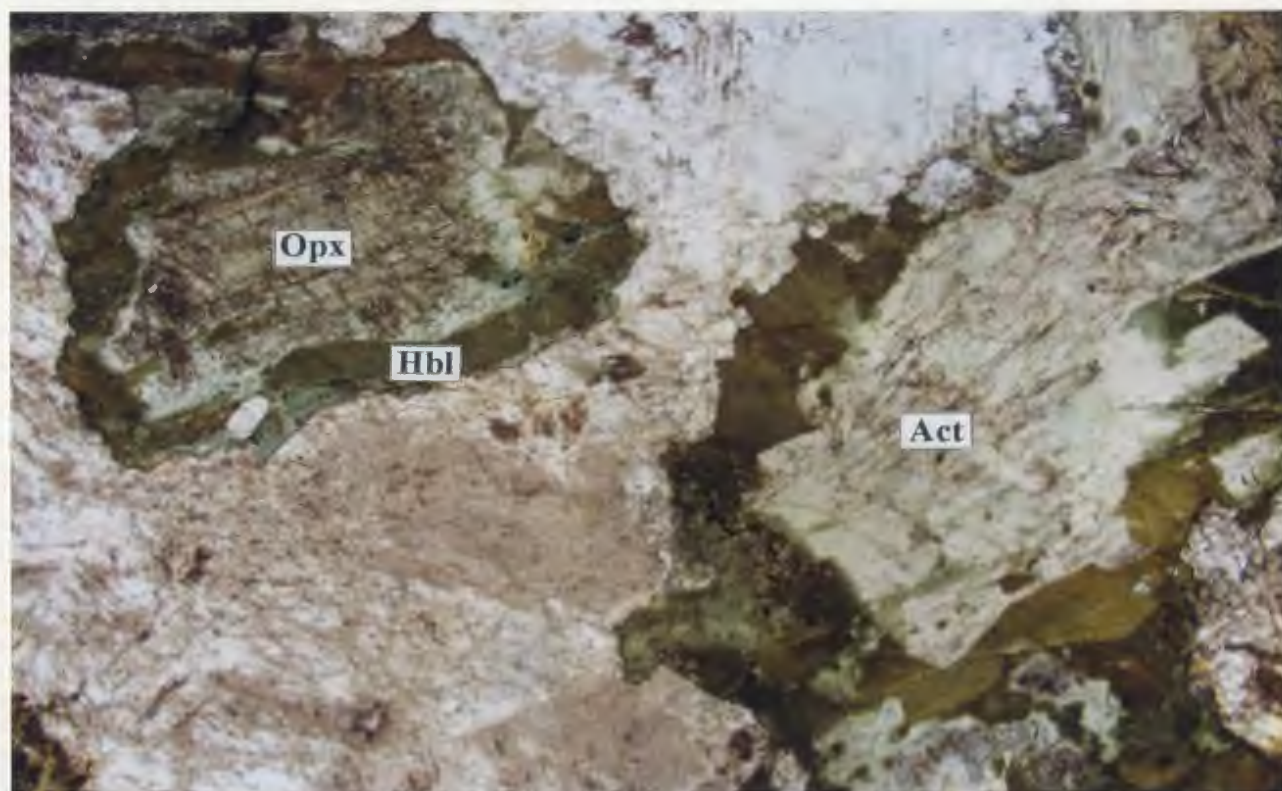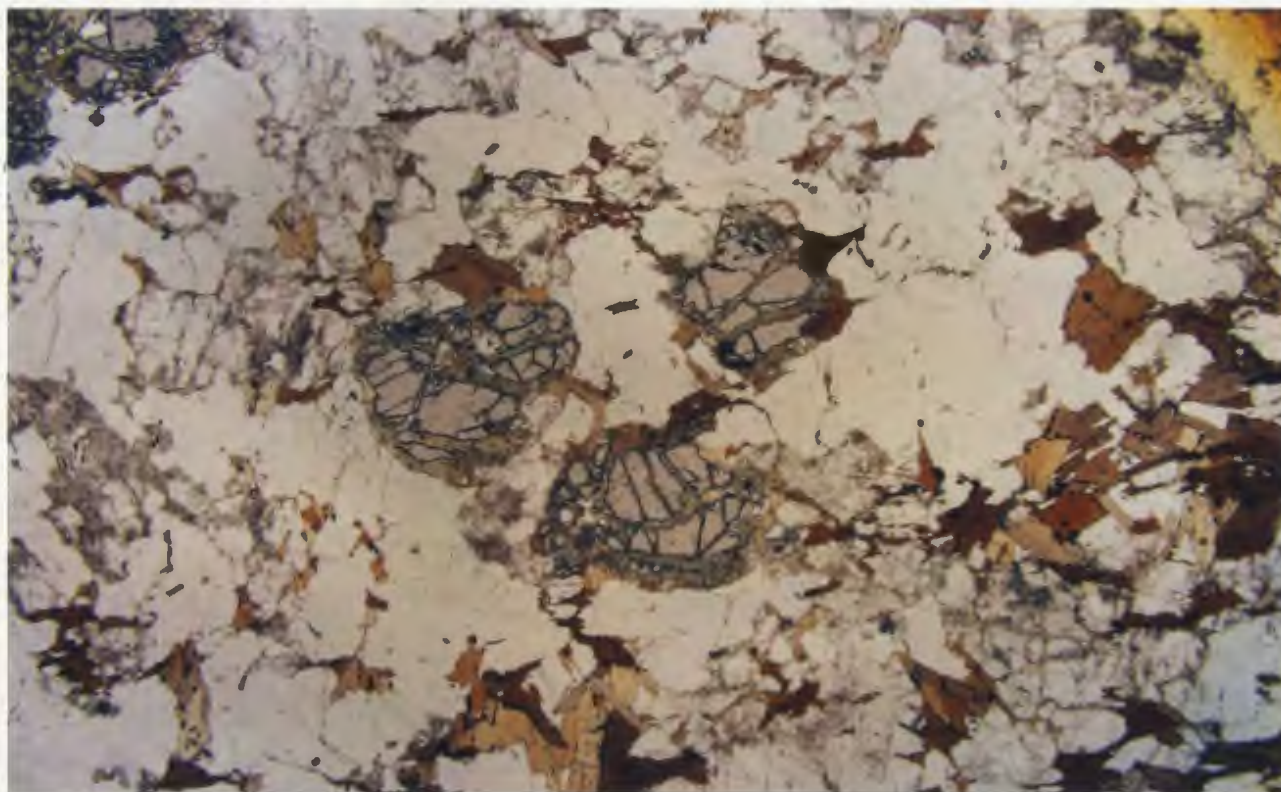
3.3.2 Structures in the Eokuk Uplift

The degree of deformation of rocks in the study area is heterogeneous and encompasses a wide variety of strain states from polydeformed migmatites in high-grade rocks to massive granite plutons. There appears, in certain areas, to be a link between metamorphic grade and structural style. This relationship apparently exists between the S_2 structures, which appear to be restricted to the high-grade rocks, and the S_3 structures, which are widespread throughout both high and lower grade rocks. This section describes the main structural fabrics present in rocks of the Uplift, with attention to S_2 and S_3, while the following section attempts to determine the relative timing of these events with respect to metamorphism. Structural data and interpretation for this section are from Jackson (1996).

The most prominent fabric in the Uplift is a compositional layering and coplanar foliation designated $S_{0,1}$. In lower grade supracrustal rocks it is defined by bedding (S_0), flattened detrital grains or flattened pillows. In amphibolite to granulite grade rocks, it is defined by gneissic or migmatitic layering (S_1).

The earliest recognizable fold set in the Uplift consists of tight to isoclinal, shallowly plunging, upright to recumbent, long-limbed folds of the S_1 fabric, designated F_2 (Figure 3.8 a, b). These folds are not common and are typically refolded into type 3 interference patterns by a third set of structures (F_3)(Figure 3.9a). In the amphibolite facies metasedimentary rocks, there is an F_2 associated axial planar foliation (S_2) that is absent in the mafic rocks. S_2 axial planar foliations are also found in the granulite grade rocks in the study area, where they occur as mineral segregations (plagioclase and pyroxene in mafic gneiss, mica, quartz and plagioclase in metasedimentary rocks) in association with

Figure 3.8

Figure 3.8a: Granulite facies intermediate gneiss showing shallowly plunging F_2 structures. Plunges of folds and dips of associated axial planar foliations are from $15\text{-}30^0$

Figure 3.8b: Tight, reclined, shallowly plunging F_2 fold of migmatitic layering at station 94KE240. Note undeformed megacrystic granite truncating structures in the fold hinge and on the upper limb of the fold. The granite also contains xenoliths of metasediment visible in the upper central part of the photo.

recumbent folds. These recumbent structures are thought to be F_2 folds since they are refolded by a later fold set.   In general, large-scale F_2 folds are only recognizable from reversals in dip direction along the axial trace of later folds.

The most common outcrop and map-scale folds of $S_{0,1}$ are long-limbed, open to isoclinal F_3 folds. These have rounded hinges and mainly northwest-southeast, or locally north-south, trending axial traces. Fold axes plunge from near-horizontal to vertical and locally have opposing plunge directions. Symmetric to asymmetric similar F_3 folds are abundant in some gneissic to migmatitic rocks and appear to have been formed by slip and concomitant granitoid (neosome?) injection along planes parallel to the F_3 axial trace. The S_3 axial plane foliation varies from a weak foliation to a banding that is only distinguishable from $S_{0,1}$ in F_3 fold hinges zones, as it is parallel or subparallel to $S_{0,1}$ on the limbs of F_3 folds. This banding is thought to be due to granitoid injection along fold axial planes. The main foliation in many granite-granodiorite intrusions is correlated with S_3, and many of the mafic enclaves within these rocks outline mesoscale F_3 folds.

F_4 meso- and macro-scale folds, and related planar and linear fabrics, are defined mainly in the eastern and south-central parts of the Uplift. In the south part of the Uplift, S_4 is associated with a penetrative west-southwest striking foliation. An associated lineation (L_4) is shallowly to steeply plunging and northwest to northeast trending. Granitic intrusions near 'Beaver lake', which truncate gneissic to migmatitic layering, contain a weakly to moderately developed northeast striking foliation which has been tentatively associated with S_4.

Hoffman et al. (1984, and references therein) have documented the deformation of the Paleoproterozoic Coronation Supergroup during the development of the Wopmay Orogen

Figure 3.9

Figure 3.9*a*: Hinge of tight F_2 fold in the mafic gneiss with anatectic melt infilling tension gashes in more competent layers in the gneiss. Dark spots within melt segregations are euhedral to subhedral orthopyroxene crystals suggesting granulite facies metamorphism was coeval with F_2 folding.

Figure 3.9*b*: Outcrop diagram showing an F_2 fold reoriented by a later F_3 fold in a type 3 fold interference pattern. Axial traces of the two fold sets are marked with dotted lines.

after Jackson (1996)
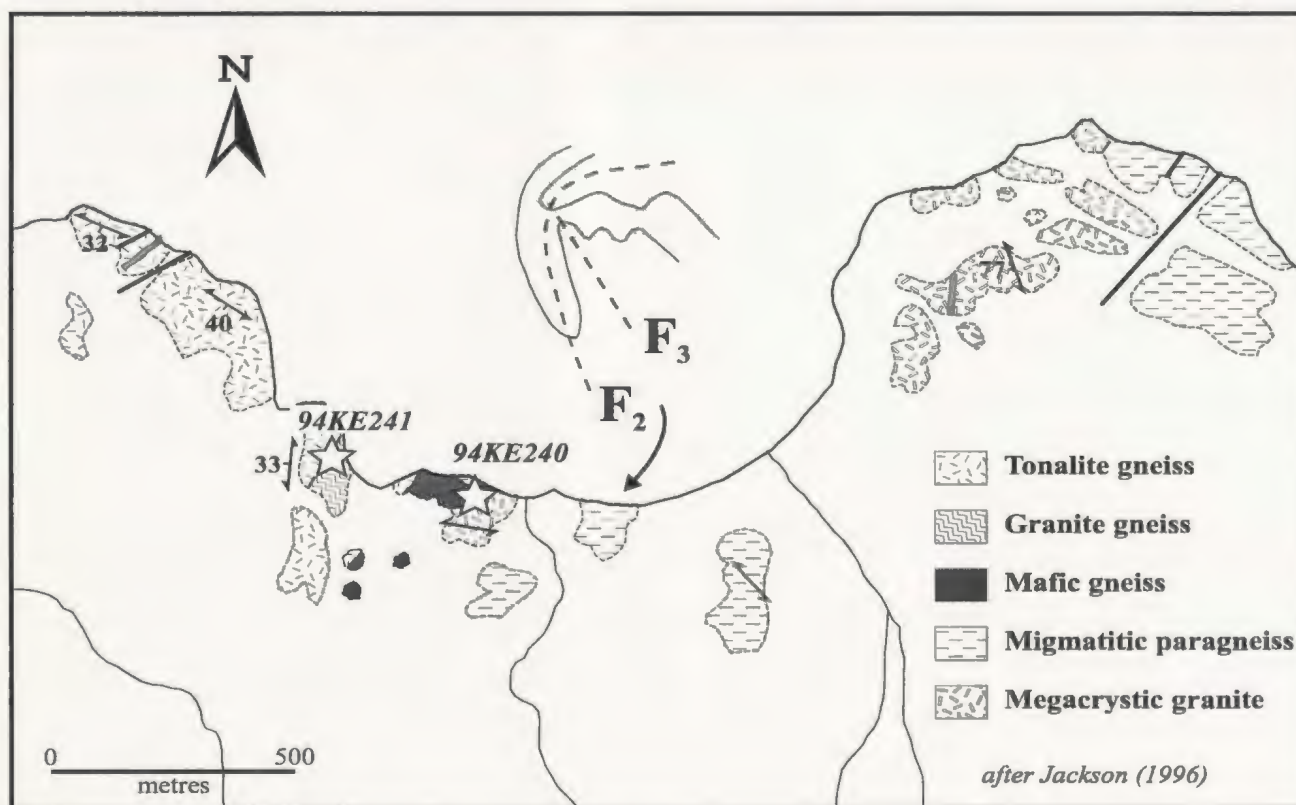
and place the involvement of the Archean basement (including the Eokuk Uplift) as post-Calderian (post ca 1.90 to 1.89 Ga) east-vergent folding and thrusting. Subsequent deformation during the Tree River event resulted in folding of the Coronation Supergroup and the underlying Archean basement about gently plunging northeast- or southeast trending fold axes. The final deformation event (ca. 1.84 to 1.81 Ga) attributed to the Wopmay Orogen (Hoffman and Bowring, 1984) generated conjugate, northeast-dextral and northwest-sinistral brittle transcurrent faults. These are the most obvious Proterozoic features within the Eokuk Uplift and many of these faults extend into the main area of the Slave craton. The rocks of the overlying Neoproterozoic Shaler Supergroup and Franklin diabase sills are flat lying and undeformed.

3.3.3 Relative timing of F_2 and F_3

Within the study area, structures identified as F_2 and F_3 display distinctly different styles and orientations. F_2 folds are typically tight to isoclinal, upright to recumbent, shallowly plunging and appear to be confined to the upper amphibolite to granulite facies gneissic units. Evidence for the timing of F_2 with respect to granulite metamorphism comes from isoclinally folded rocks in the mafic gneiss. At one location, anatectic melt segregations containing euhedral to subhedral orthopyroxene can be seen in tension gashes in more competent layers in the hinge of the fold (Figure 3.9a). The presence of these pyroxenes in the melt suggests that granulite facies conditions were synchronous with F_2 folding and the production of the tension cracks. In addition, the melt segregations appear to cut the earlier S_1 gneissic layering (see Figure 3.6a). An equal

Figure 3.10a: Equal area stereoplot showing the distribution of fold axes from the upper amphibolite to granulite grade gneisses at the Coronation Gulf coastal section of the Eokuk Uplift. These shallow to moderately plunging, northwest trending fold axes are interpreted to represent the original, F_2 structures. The smaller cluster of measurements in the center of the diagram may indicate steepening of the original, shallowly plunging, F_2 folds by later F_3 structures.

Upper amphibolite to granulite gneiss
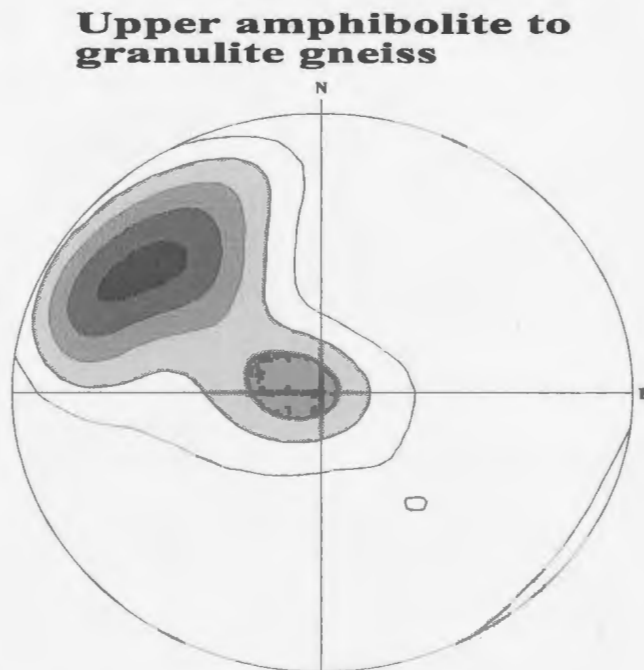
N = 79
Peak position : 308.7 / 29.6

Figure 3.10b: Equal area stereoplot showing the distribution of fold axes from the megacrystic granites in the Coronation Gulf coastal section of the Eokuk Uplift. The doubly plunging nature of these folds is apparent from the diagram, suggesting that two deformational events, possibly F_3 and the later F_4, were neccessary to produce this pattern. Although these folds appear coplanar with those produced by F_2, the different distribution, steeper plunge and evidence from contact relationships all suggest that F_3 is a distinct event post-dating F_2.

Megacrystic granite
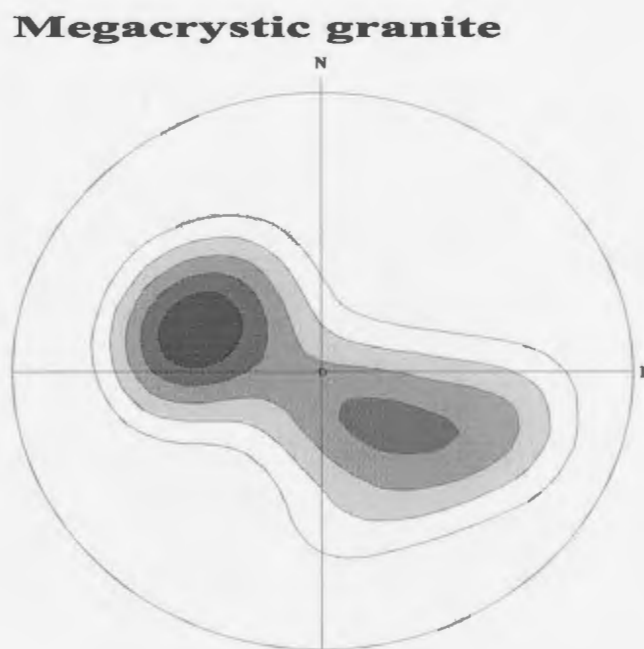
N = 68
Peak position : 293.2 / 55.2

area stereographic plot of fold axes from upper amphibolite to granulite grade supracrustal gneiss and orthogneiss from the Coronation Gulf coast shows that the folds associated with the high grade gneisses are predominantly shallowly plunging and northwest trending (Figure 3.10a). The small cluster of measurements with steeper plunges may be a result of refolding of the original shallowly plunging structures during the F_3 deformation event.

The deformation associated with F_3 appears to have affected both the high-grade gneisses and the megacrystic granites. F_3 folds tend to be open, upright and moderately to steeply plunging. In the megacrystic granites, zones with preserved massive igneous textures grade into areas characterized by apparent F_3 folds defined by biotite schlieren. In the gneisses, the structures are more complex, with shallowly dipping F_2 folds refolded about more steeply dipping F_3 folds. In one location in the paragneiss, a reclined, shallowly plunging F_2 fold is refolded about a northwest trending F_3 fold axis (Figure 3.9b). Isolated low strain zones preserve the original contact relationships between the megacrystic granites and the high-grade gneissic rocks. Here, shallowly plunging F_2 folds in granulite facies mafic and metasedimentary gneisses are truncated by undeformed, unmigmatized megacrystic granite (Figure 3.8b). This preservation of original contact relationships suggests that deformation in the granites post-dates both high-grade metamorphism and the F_2 deformation event.

A stereographic plot of fold axes from the megacrystic granites indicates northwest and southeast striking, moderately to steeply plunging folds (Figure 3.10b). The doubly plunging nature of these fold axes suggests that two deformation episodes are represented, one to create the original fold set and a subsequent event approximately

perpendicular to the first, to create, domed, doubly plunging structures. It is possible that the northeast-southwest trending, S_4 event, which may post-date the young granites, may be responsible for this later deformation.

3.4 Discussion

Deformation in the rocks of the study area shows a progression from early S_1 gneissosity to shallowly plunging/dipping S_2 and finally, refolding about open upright S_3 structures and possible reorientation of F_3 folds by S_4 (Figure 3.11). Granulite facies mineral assemblages in structures associated with F_2 folding argue that F_2 and granulite metamorphism were coeval. The truncation of shallow D_2 structures by undeformed megacrystic granite in areas where the original contacts are preserved suggests that granite intrusion post-dated D_2 and granulite metamorphism. D_3 apparently post-dates granite intrusion, since both granites and gneisses are deformed by this event. It appears likely that F_2 and F_3 represent deformation events that took place under distinct tectonic and metamorphic conditions.

Harley (1989) has described a common structural pattern seen in many granulite terranes where early pre- to syn-metamorphic flat-lying structures have been refolded by later coplanar low angle or flat-lying structures. These shallow early structures are refolded about varied steep to upright large, scale structures. Similar patterns exist in both the high-grade rocks of the Eokuk Uplift and the granulite facies rocks of the southern Slave Province.

D₄

S_4- shallow to steeply
dipping foliation and lineation
F_4 folds
(confined to southern part of Uplift)

intrusion of 'young granite'?

D₃

F_3- open, steeply plunging,
NW-SE trending folds;
S_3-steep foliation

megacrystic granite intrusion

M_2- amphibolite facies metamorphism

D₂

F_2- tight to isoclinal, upright to
recumbent, shallowly plunging folds

M_1- granulite facies metamorphism

D₁

early gneissosity

Figure 3.11: A summary of the intrusive, metamorphic and deformation events in the Coronation Gulf area, Eokuk Uplift.

Mineral assemblages in the high-grade metasedimentary gneisses in the study area are consistent with L/MP-HT conditions in excess of 750 ^{0}C. Mineral assemblages from granulite facies mafic gneisses suggest peak P-T conditions near 800-850 ^{0}C and 300-600 MPa. This is comparable to conditions found in the rocks of the southern Slave Province. No gem cordierite was observed in the metasedimentary gneiss, however, and it appears that peak metamorphic temperatures in the southern Slave may have been slightly higher. Evidence from Ghost Lake suggests that granulite facies metamorphism in the southern Slave Province was synchronous with granite-charnockite plutonism and that the plutons may have provided some of the heat necessary for metamorphism (Henderson and Chacko, 1995). In contrast, an amphibolite facies overprint on previously formed granulite facies rocks is synchronous with the intrusion of biotite-bearing, hydrous granites in the study area. This appears to have been followed by a later lower amphibolite to greenschist facies retrograde alteration, locally developed in both granites and gneisses.

Chapter 4: TIMS U-Pb Geochronology

4.1 Introduction

As noted in Chapter 1, occurrences of pre-2.8 Ga 'basement' rocks in the Slave Province are confined to areas west of 112^0 W. The location of the Eokuk Uplift at 112^0 to 113^0 30" suggests the possibility that the gneisses in the study area may be, in part, older than 2.8 Ga. Although previous researchers have identified the rocks therein as Archean (Craig et al., 1960; Hoffman et al, 1984), no geochronological data existed for the area until the present study was undertaken.

The samples selected for U-Pb age determination represent the major units in the field area, as well as minor units that constrain the field relationships and deformation events described in Chapters 2 and 3. Two samples of the oldest orthogneiss, a paragneiss unit and a separate monzogranite gneiss were dated. All of these units have experienced the upper amphibolite to granulite grade metamorphic event outlined in Chapter 3. Six younger intrusive units that cut the older gneiss package, and bracket the main deformational event in the study area were also dated. The ages of later lower

Figure 4.1: Geological map of the study area showing geochronology sample locations described in text (marked with stars and station numbers). Ages given are in Ma. z, zircon; m, monazite; t, titanite. Uncolored areas represent beach or Quaternary sediments.

amphibolite to greenschist grade metamorphic events not recorded by U-Pb systematics in zircon have been documented through the analysis of monazite and titanite from these rocks.

4.2 Analytical Methods

Samples were prepared at the Radiogenic Isotope Facility at Memorial University of Newfoundland, using standard crushing, density separation and magnetic separation techniques. These procedures are more completely described in Appendix 1. The abbreviations 'A' and '^{0}' refer to the amperage used in the initial magnetic mineral separation and the degree of tilt used in the final magnetic separation, respectively. Zircon, monazite and titanite single grains and multiple grain fractions were selected from the highest quality grains in various populations. The vast majority of analyses are of single grains and, unless otherwise noted, grains with cores were avoided. All fractions were strongly abraded to minimize the effects of surface Pb loss and, in the case of some zircons, to remove possible metamorphic overgrowths.

Zircon dissolution and column chemistry were completed using the methods of Krogh (1973), but modified to use smaller Teflon bombs and ion exchange columns. Quantities of reagents used are one tenth the volume of those reported in Krogh (1973). Titanite and monazite were dissolved in 7 ml Savillex containers using HF/HNO_3 and HCl, respectively. Extraction of U and Pb was by HBr column chemistry (Corfu and Stott, 1986) with an additional purification of U.

Isotope ratios were measured on a Finnigan-Mat 262 mass spectrometer with four Faraday detectors in multicollection mode and ^{204}Pb measured in the SEM-ion counter. Smaller samples were measured using the secondary electron multiplier-ion counter in peak jumping mode.

Stacey and Kramers (1975) model Pb isotopic compositions were used to correct for common Pb in excess of the laboratory blank. Linear regressions were done using the method of Davis (1982). Age uncertainties, errors on regression calculations and error ellipses on concordia plots are given at a 95% confidence limit. Decay constants used are those of Jaffey et al. (1971).

Sample locations and age data are shown in Figure 4.1. U-Pb data for zircon, monazite and titanite from 10 samples are presented in Table 4.1. Concordia diagrams for the samples are presented in Figures 4.3, 4.4, 4.7, 4.8 and 4.9.

4.3 U-Pb Results

4.3.1 Tonalite gneiss (94KE241GD)

This sample was taken from a fine to medium grained, granoblastic, biotite-bearing tonalite gneiss at station 94KE241 (Figure 4.1). Heavy mineral separates from this sample contain one zircon population. These are medium-sized (75-100 μm) brown prisms with square cross sections, sharp to slightly resorbed terminations and aspect ratios of 3:1 to 4:1. Internal zoning, visible under the microscope, is present in some grains, and was initially thought to represent inherited cores and later, metamorphic

Table 4.1: U-Pb Analytical Results

Fraction [a]	Weight (mg)	U	Pb rad [b] (ppm)	Pb (pg)	$\frac{^{204}Pb}{^{206}Pb}$	$\frac{^{208}Pb}{^{206}Pb}$	$\frac{^{206}Pb}{^{238}U}$	2σ	$\frac{^{207}Pb}{^{235}U}$	2σ	$\frac{^{207}Pb}{^{206}Pb}$	2σ	$\frac{^{206}Pb}{^{238}U}$	$\frac{^{207}Pb}{^{235}U}$	$\frac{^{207}Pb}{^{206}Pb}$
			Concentration Measured				Corrected Atomic Ratios [c]						Age (Ma)		
94KE241GD: Tonalite gneiss (438700 E, 7507875 N)															
Z1 brn prism	0.004	146	111.4	5	4816	0.1015	0.65035	266	23.3760	968	0.26069	38	3230	3243	3251
Z2 brn prism	0.005	234	180.5	5	8337	0.2106	0.61753	248	20.7287	830	0.24345	40	3100	3126	3143
Z3 brn prism	0.002	277	197.1	6	4039	0.0965	0.61718	296	20.9282	1018	0.24593	36	3099	3135	3159
Z4 znd prism	0.006	146	95.4	4	7837	0.0721	0.57261	290	19.7258	1018	0.24985	32	2919	3078	3184
Z5 znd prism	0.012	138	88.6	100	604	0.0436	0.58331	266	19.2718	1006	0.23962	52	2962	3056	3117
Z6 brn prism	0.006	86	64.7	4	5619	0.1133	0.63757	258	22.9212	908	0.26074	48	3179	3224	3251
Z7 brn prism	0.002	177	114.9	5	3428	0.0803	0.56617	264	19.8075	896	0.25374	52	2892	3082	3208
Z8 brn prism	0.002	212	144.1	12	1084	0.1005	0.58299	244	20.4254	866	0.25410	44	2961	3112	3211
94KE241: Granite gneiss (438750 E, 7507800 N)															
Z1 lbrn prism	0.002	583	369.7	16	3169	0.0824	0.55473	328	18.8065	1088	0.24588	54	2845	3032	3158
Z2 lbrn prism	0.004	513	309.7	50	1386	0.0814	0.53033	260	17.6913	882	0.24194	36	2743	2973	3133
Z3 lbrn prism	0.005	320	159.9	8	5546	0.0827	0.44153	186	14.2042	608	0.23332	34	2357	2763	3075
Z4 lbrn prism	0.005	691	155.6	37	1355	0.0066	0.22644	92	4.6996	182	0.15052	34	1316	1767	2352
Z5 lbrn prism	0.002	5402	310.6	9	3072	0.0925	0.05025	24	1.6419	74	0.23697	44	316	986	3100
M1 clr mf equant	0.001	3852	12071	8	21495	5.2446	0.56082	164	15.9926	514	0.20682	18	2870	2876	2881
M2 clr mf equant	0.002	3972	15614	21	11843	6.9434	0.55688	168	15.7961	522	0.20573	18	2854	2865	2872
M3 clr mf equant	0.003	2455	10285	17	16110	7.5090	0.55480	238	15.7128	704	0.20541	18	2845	2859	2870
94KE240M: Migmatitic paragneiss (439000 E, 7507725 N)															
M1 mf equant	0.008	877	7510.3	79	2991	16.3717	0.56211	168	16.0146	528	0.20663	20	2875	2878	2879
M2 mf frag	0.004	814	3279.1	23	4306	7.3276	0.54528	278	14.9205	760	0.19845	32	2806	2810	2814
M3 mf frag	0.002	676	1733.4	16	2832	4.0585	0.56309	218	15.8944	636	0.20472	28	2879	2870	2864
M4 mf equant	0.005	663	4446.6	8	15599	13.0346	0.54387	152	15.1608	474	0.20217	18	2800	2825	2844
M5 mf equant	0.010	757	5996.8	60	4368	15.0748	0.56094	214	15.9370	648	0.20606	18	2871	2873	2875
M6 mf frag	0.003	687	4543.3	8	7709	12.3713	0.56187	254	15.9345	736	0.20569	26	2874	2873	2872

	Concentration Measured					Corrected Atomic Ratios [c]							Age (Ma)		
Fraction [a]	Weight (mg)	U	Pb rad [b] (ppm)	Pb (pg)	$\frac{^{204}Pb}{^{206}Pb}$	$\frac{^{208}Pb}{^{206}Pb}$	$\frac{^{206}Pb}{^{238}U}$	2σ	$\frac{^{207}Pb}{^{235}U}$	2σ	$\frac{^{207}Pb}{^{206}Pb}$	2σ	$\frac{^{206}Pb}{^{238}U}$	$\frac{^{207}Pb}{^{235}U}$	$\frac{^{207}Pb}{^{206}Pb}$
94KE232B: Monzogranite gneiss (431800 E, 7507350 N)															
Z1 lbrn sq prism	0.003	331	215.8	101	325	0.0714	0.58395	214	18.3680	776	0.22813	40	2965	3009	3039
Z2 lbrn znd core	0.010	312	202.2	25	4196	0.1852	0.54175	184	15.3649	560	0.20570	20	2791	2838	2872
Z3 lbrn znd prism	0.004	233	116.5	5	4978	0.0556	0.45480	130	14.0645	438	0.22429	22	2417	2754	3012
Z4 lbrn znd prism	0.003	266	154.4	7	3419	0.0589	0.51949	366	17.0030	1200	0.23738	40	2697	2935	3103
Z5 lbrn prism	0.002	1035	427.1	26	1844	0.1030	0.37240	182	9.4928	468	0.18488	32	2041	2387	2697
Z6 lbrn prism	0.002	229	113.7	10	1286	0.0650	0.44983	174	13.5110	536	0.21784	38	2394	2716	2965
Z7 lbrn prism	0.004	159	93.9	7	2864	0.0912	0.53136	206	15.0193	580	0.20500	34	2747	2816	2866
Z8 lbrn prism	0.002	245	154.8	22	957	0.0629	0.56661	270	18.1510	874	0.23234	42	2894	2998	3068
M1 mf frag	0.002	220	281.5	115	136	1.3622	0.57666	334	16.2078	1268	0.20385	98	2935	2889	2857
M2 mf equant	0.002	323	388.3	93	202	1.2556	0.56522	628	16.1423	1866	0.20713	100	2888	2885	2883
M3 mf equant	0.002	533	11415.1	18	1784	42.1402	0.56961	378	16.1943	1014	0.20620	58	2906	2888	2876
T1 clr frags	0.035	9	5.8	56	183	0.3783	0.48984	262	11.7602	872	0.17412	88	2570	2586	2598
T2 clr frags	0.133	9	6.0	219	182	0.4067	0.49672	202	11.8763	548	0.17341	44	2600	2595	2591
T3 brn frags	0.094	54	34.4	194	827	0.3208	0.49326	166	11.8137	444	0.17370	20	2585	2590	2594
94KE223: 'Nerak granite' (435050 E, 7507575 N)															
Z1 pink prism	0.002	95	68.2	45	168	0.2625	0.56746	612	16.2468	1450	0.20765	152	2897	2891	2887
Z2 brn prism	0.010	137	96.0	38	1259	0.2564	0.55702	256	15.9434	702	0.20759	46	2854	2873	2887
Z3 pink frag	0.013	137	93.6	6	11236	0.2170	0.55776	230	15.7610	650	0.20495	32	2857	2862	2866
Z4 pink frag	0.011	181	125.4	39	1801	0.2455	0.55513	194	15.8452	576	0.20701	28	2846	2868	2882
Z5 brn prism	0.009	404	258.7	9	13877	0.1608	0.54474	186	15.4824	564	0.20613	20	2803	2845	2875
Z6 clr needles	0.004	598	298.0	11	6147	0.1708	0.42365	276	11.4748	758	0.19644	22	2277	2563	2797
M1 clr subh	0.001	2318	21105.2	37	2454	17.4233	0.56368	398	16.0579	1098	0.20661	50	2882	2880	2879
M2 clr subh	0.005	645	10294.1	15	7449	31.5474	0.56181	276	15.9796	808	0.20629	24	2874	2876	2877
M3 clr eu frag	0.003	1120	633.9	64	1352	0.1902	0.47153	266	13.2807	720	0.20427	50	2490	2700	2861
94KE240G: Megacrystic granite (439000 E, 7507725 N)															
Z1 brn prism	0.002	741	478.1	9	6434	0.1297	0.56115	240	15.9764	668	0.20649	38	2871	2875	2878

Fraction[a]	Weight (mg)	U	Pb rad [b] (ppm)	Pb (pg)	$\frac{^{204}Pb}{^{206}Pb}$	$\frac{^{208}Pb}{^{206}Pb}$	$\frac{^{206}Pb}{^{238}U}$	2σ	$\frac{^{207}Pb}{^{235}U}$	2σ	$\frac{^{207}Pb}{^{206}Pb}$	2σ	$\frac{^{206}Pb}{^{238}U}$	$\frac{^{207}Pb}{^{235}U}$	$\frac{^{207}Pb}{^{206}Pb}$
									Corrected Atomic Ratios[c]					Age (Ma)	
Z2 brn prism	0.002	478	302.9	9	3988	0.1335	0.54981	220	15.6035	590	0.20583	44	2824	2853	2873
Z3 brn prism	0.112	554	325.5	179	11249	0.1144	0.51832	154	14.4734	478	0.20252	16	2692	2781	2847
Z4 clr needles	0.006	604	232.6	328	253	0.0759	0.35705	210	8.7384	552	0.17750	36	1968	2311	2630
Z5 clr needles	0.009	1095	369.6	614	311	0.0940	0.31260	160	6.9638	386	0.16157	28	1754	2107	2472
Z6 clr needles	0.003	1504	492.7	169	565	0.0737	0.30896	106	6.7879	260	0.15934	22	1736	2084	2449
M1 clr euh frag	0.001	3540	3214.1	7	13477	0.6730	0.56043	260	15.8535	742	0.20517	30	2868	2868	2868
M2 clr ovoid	0.021	4103	16240	54	53543	7.1187	0.54890	350	15.4328	1010	0.20391	16	2821	2842	2858
M3 clr euh frag	0.004	4003	16204	35	15096	7.2940	0.54967	180	15.6694	554	0.20675	18	2824	2857	2880
M4 clr subh ovoid	0.002	4878	18511	21	14020	6.9059	0.54027	168	14.9881	512	0.20120	16	2785	2814	2836
94KE232A: Boudinaged diorite dyke (431800 E, 7507350 N)															
Z1 brn prism	0.001	100	64.4	7	530	0.1254	0.55919	552	15.9236	1262	0.20653	142	2863	2872	2879
Z2 brn prism	0.001	144	91.8	7	701	0.1321	0.55455	358	15.7468	1032	0.20594	58	2844	2862	2874
Z3 brn prism	0.004	131	107.0	78	278	0.4541	0.56967	428	16.2328	1188	0.20667	72	2906	2891	2880
T1 clr frags	0.123	4	2.6	217	88	0.2483	0.52371	250	13.4971	1090	0.18692	112	2715	2715	2715
T2 brn frags	0.066	20	18.0	124	375	0.7138	0.54691	296	15.0305	830	0.19932	50	2812	2817	2821
T3 brn frags	0.036	29	26.3	88	421	0.7146	0.55171	222	15.3175	658	0.20136	36	2832	2835	2837
T4 clr frags	0.126	4	2.5	160	119	0.1599	0.51486	192	13.2130	552	0.18613	42	2677	2695	2708
T5 clr frags	0.192	4	2.5	246	119	0.1709	0.50653	198	12.7355	640	0.18235	64	2642	2660	2674
94KE419: Granodiorite dyke (431950 E, 7507225 N)															
Z1 brn prism	0.002	221	144.1	5	3933	0.1457	0.56154	324	15.8627	940	0.20488	20	2873	2869	2865
Z2 brn prism	0.001	135	88.5	5	1345	0.1772	0.55263	318	15.5602	878	0.20421	48	2836	2850	2860
Z3 brn prism	0.003	257	171.9	97	276	0.1656	0.56725	210	16.0856	678	0.20567	36	2897	2882	2872
T1 brn frags	0.065	35	21.8	187	412	0.2122	0.51482	222	13.0743	622	0.18419	32	2677	2685	2691
T2 clr frags	0.071	4	2.9	177	71	0.3066	0.51009	318	12.6081	1874	0.17927	206	2657	2651	2646
T3 brn frags	0.046	52	35.1	130	607	0.3268	0.51845	278	13.2643	748	0.18556	40	2693	2699	2703
T4 clr frags	0.049	5	3.2	85	104	0.3264	0.49825	300	12.2720	1002	0.17863	90	2606	2625	2640
T5 brn frags	0.082	39	24.4	159	669	0.2248	0.51446	206	13.1297	536	0.18510	20	2676	2689	2699

Fraction [a]	Weight (mg)	U	Pb rad [b] (ppm)	Pb (pg)	$\frac{^{204}Pb}{^{206}Pb}$	$\frac{^{208}Pb}{^{206}Pb}$	$\frac{^{206}Pb}{^{238}U}$	2σ	$\frac{^{207}Pb}{^{235}U}$	2σ	$\frac{^{207}Pb}{^{206}Pb}$	2σ	$\frac{^{206}Pb}{^{238}U}$	$\frac{^{207}Pb}{^{235}U}$	$\frac{^{207}Pb}{^{206}Pb}$
T6 clr frags	0.093	7	4.8	188	127	0.3393	0.50258	204	12.4295	590	0.17937	46	2625	2637	2647
94KE418A: Syenogranite pegmatite (434975 E, 7507600 N)															
Z1 lbrn prism	0.004	2153	437.0	232	428	0.2686	0.17244	64	2.3349	104	0.09820	24	1026	1223	1590
Z2 yell prism	0.001	1222	303.1	89	285	0.1332	0.22461	76	4.6514	208	0.15020	40	1306	1759	2348
Z3 clr prism	0.002	464	255.1	19	1195	0.1546	0.47243	258	12.8189	684	0.19679	44	2494	2666	2800
Z4 clr prism	0.001	732	232.9	34	399	0.3006	0.25618	106	5.0293	240	0.14238	26	1470	1824	2256
M1 clr euh	0.003	586	3326.2	21	2817	10.5747	0.55654	234	15.5904	648	0.20317	38	2852	2852	2852
M2 clr euh	0.002	1147	6246.5	14	4743	10.1033	0.55557	290	15.5494	824	0.20299	28	2848	2850	2850
T1 brn frags	0.031	61	33.0	56	964	0.2088	0.45403	236	10.8103	562	0.17269	34	2413	2507	2584
T2 clr frags	0.341	21	11.9	606	387	0.1302	0.49404	164	11.7931	452	0.17313	24	2588	2588	2588
T3 clr frags	0.174	33	15.6	189	838	0.0994	0.43144	152	10.2283	386	0.17194	22	2312	2456	2577
T4 brn frags	0.135	41	22.8	147	1184	0.1242	0.49178	142	11.7131	372	0.17274	22	2578	2582	2584
T5 brn frags	0.130	46	25.3	169	1102	0.1239	0.49077	148	11.6917	396	0.17278	18	2574	2580	2585
94VJ253: Young granite (442575 E, 7502500 N)															
Z1 pink prism	0.007	211	115.3	10	4159	0.1785	0.47001	222	11.1893	506	0.17266	38	2484	2539	2584
Z2 sm clr needles	0.002	365	185.9	10	1932	0.2249	0.42332	190	10.0373	480	0.17197	28	2276	2438	2577
Z3 sm clr needles	0.001	1610	804.1	6	1473	0.2792	0.40235	348	8.9913	648	0.16207	84	2180	2337	2477
Z4 brn prism	0.001	367	171.7	9	741	0.1834	0.40242	222	9.2229	534	0.16622	44	2180	2360	2520
T1 brn euh frags	0.113	84	85.9	281	1059	1.2222	0.49427	170	11.8414	446	0.17376	18	2589	2592	2594
T2 brn euh frags	0.050	87	85.0	133	1032	1.1104	0.49273	192	11.7819	492	0.17342	22	2582	2587	2591

Notes: [a] Z, zircon; M, monazite; T, titanite; euh, euhedral; subh, subhedral; frag(s), fragments; mf, multifaceted; znd, zoned; clr, clear; b brown; lbrn, light brown; yell, yellow; all zircon and monazite analyses are single grains unless otherwise noted. UTM coordinates for each sample are presented in brackets. All UTM coordinates are for Zone 12 and NAD 1927.

[b] Total radiogenic Pb after correction for blank, common Pb and spike.

[c] Ratios corrected for fractionation, spike, 4-10 pg laboratory blank, initial common Pb (calculated using the model of Stacey and Kramers (1975) for the age of the sample), and 1 pg U blank. Uncertainties (2σ) on the isotopic ratios refer to the final digits.

overgrowths (Figure 4.2*a*). Eight of the best single zircons from the 1^0 magnetic and non-magnetic mineral separate were dated, two from the zoned population and six from the unzoned population.

Analytical Results

Data points from the eight analyses give a variety of discordant ages. Four analyses (Z1, Z6, Z7 and Z8, Figure 4.3*a*) define a discordia line with an upper intercept age of 3254 +13/-6 Ma, after error expansion (cf.: Davis, 1982) with a lower intercept of 682 +926/-1011 Ma. The two analyses from zoned zircons (Z4 and Z5) fall to the left of the line defined by the unzoned grains and therefore do not suggest the presence of older, xenocrystic cores. Based on the apparent absence of older cores and the igneous morphology of the zircons in this sample, 3254 +13/-6 Ma is interpreted as the crystallization age of the gneiss. The noncolinear distribution of some of the other analyses indicates these grains may have undergone a later phase of lead loss, possibly due to a metamorphic event.

4.3.2 Granite gneiss (94KE241)

This sample consists of a fine-grained, granoblastic, leucocratic biotite granite gneiss from station 94KE241. Only one population of zircon was present in the heavy mineral separates from this sample. These are medium-sized (74-100 μm), light brown prisms, with rounded, resorbed terminations and square cross sections. Aspect ratios are between 3:1 and 4:1. Many are turbid and most have darker centers, distinct internal zoning,

Figure 4.2

Figure 4.2: (*a*) euhedral brown zircon prisms from the tonalite gneiss (94KE241GD). Zircons with visible internal zoning are grouped at the top of the photo; unzoned zircon is on the bottom. (zircons 300-400 μm long) (*b*) zircon prisms from the granite gneiss (94KE241). All are turbid and have marked internal zoning and resorbed terminations. (zircons ~300 μm long) (*c*) euhedral prisms from the monzogranite gneiss (94KE232B). Internal zoning is present in the zircon grains along the top of the photo. (zircons 300 μm long)
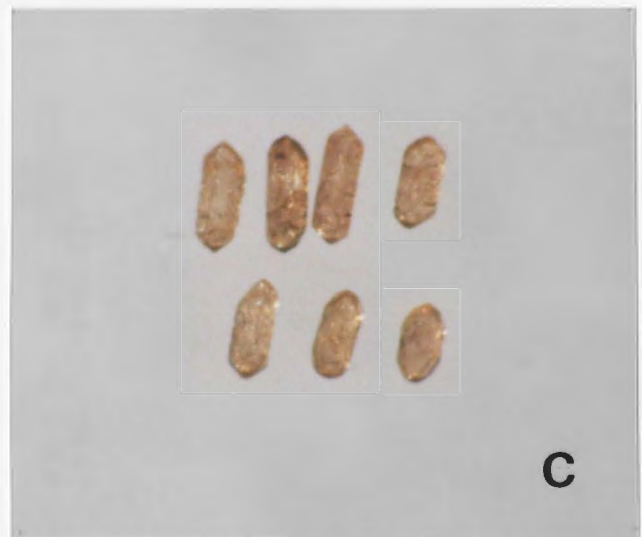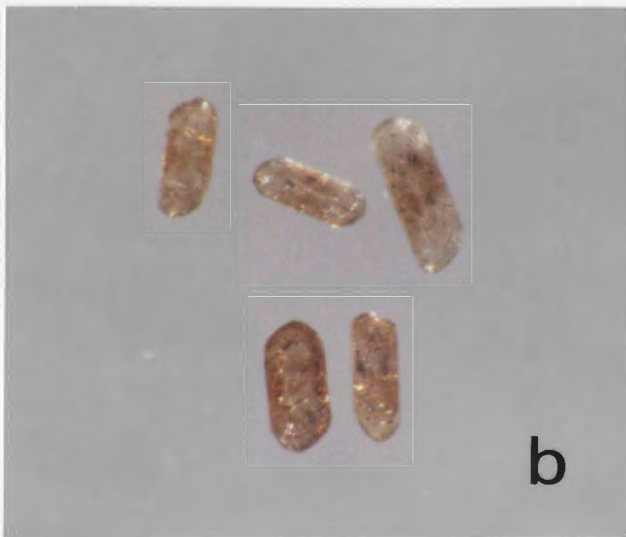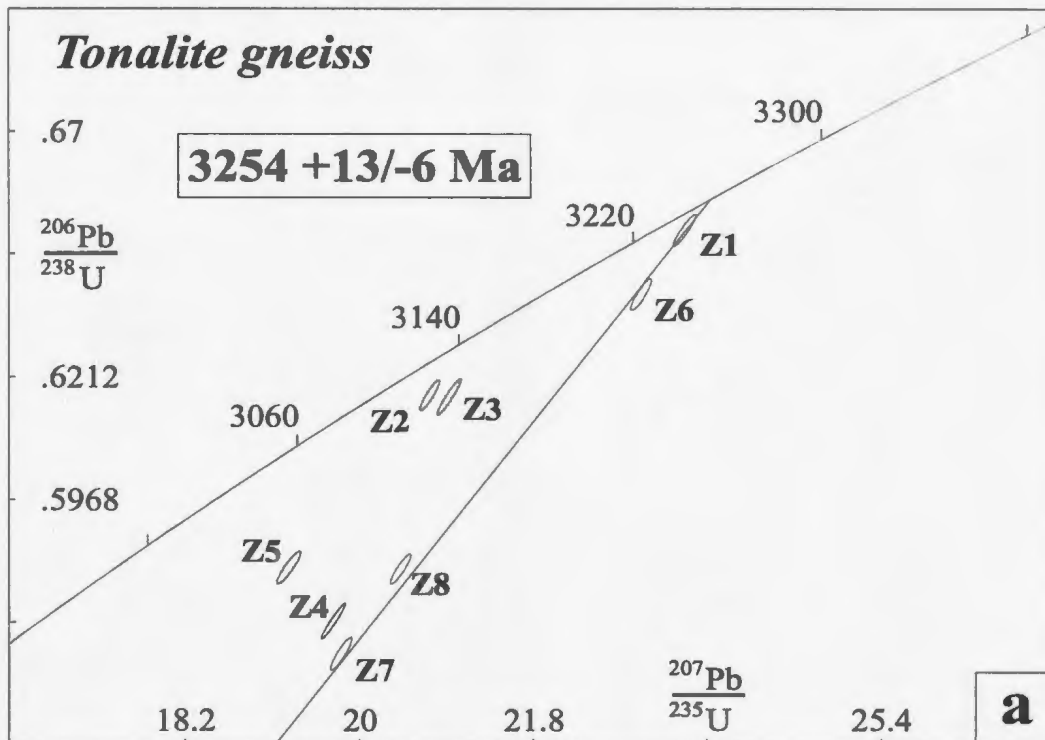
Figure 4.3a: U-Pb concordia diagram of zircon analyses from tonalite gneiss. Ellipses are for 2σ uncertainties.
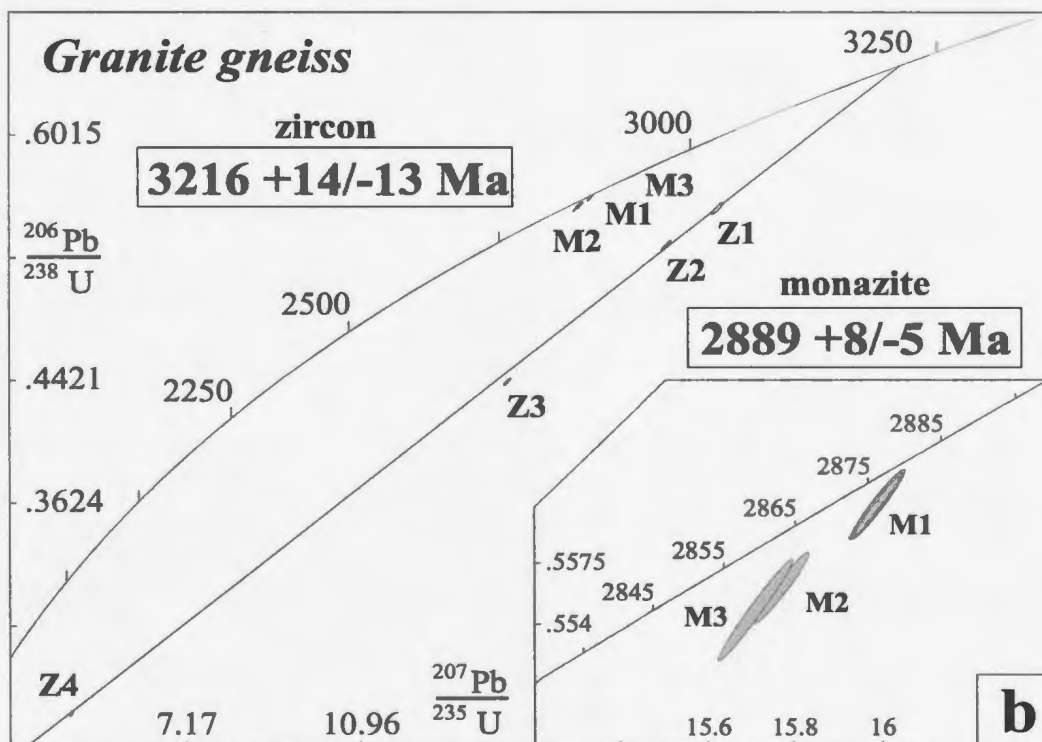
Figure 4.3b: U-Pb concordia diagram of zirconand monazite analyses from granite gneiss. Ellipses are for 2σ uncertainties. Z, zircon; M, monazite.

cracks and opaque inclusions (Figure 4.2*b*). Cathodoluminescence of polished grains reveals only igneous growth zoning; no xenocrystic cores are observed. Four single zircons from the 0^0 non-magnetic mineral separate and one single zircon from the 3^0 magnetic separate were selected for dating. These were strongly abraded to remove any possible overgrowths.

The sample also contains small, round to ovoid, deep yellow monazites (Figure 4.5*a*). Most of the crystals are turbid and contain opaque, metallic inclusions. Three single monazites from the 0.5-1.0 A magnetic separate were chosen for analysis and lightly abraded.

Analytical Results

Of the five single grain zircon analyses carried out, one (Z5) from the 0^0 non-magnetic mineral separate was 91.9% discordant and is not considered further. The remaining four points do not define a line. However, a line through the upper three points (Z1, Z2 and Z3) gives an upper intercept age of 3200 +58/-40 Ma and a lower intercept age of 375 +/-40 Ma, after error expansion. A line through Z1, Z2, and Z4, calculated after error expansion, gives an upper intercept age of 3216 +14/-13 Ma and a lower intercept age of 909 +/-40 Ma (Figure 4.3*b*). The single population of zircons, their igneous morphology and lack of visible xenocrystic cores, suggests that ca. 3200 Ma is the crystallization age of the gneiss. The slightly non-colinear nature of the data points may be the result of the relatively high uranium content (>500 ppm) of these zircons, with radiation damage resulting in multistage Pb loss during later metamorphic events.

Data points from the three single monazites analyzed form a cluster near concordia. A regression line through all three points gives poorly constrained upper and lower intercept ages of 2889 +104/-7 Ma and 1788 +736/-382 Ma, respectively (Figure 4.3*b*). Pinning the lower intercept of the regression line at 1800 +/-50 Ma generates an upper intercept age of 2889 +8/-5 Ma and a lower intercept of 1798 +233/-192 Ma. The choice of 1800 Ma to pin the lower intercept is based on the approximate age defined by lower intercepts from other samples and corresponds to the final deformational event attributed to the Wopmay Orogen. The ~350 Ma difference in zircon and monazite ages is discussed in more detail below, but it would appear the monazites are a product of a thermal event at ca. 2890 Ma.

4.3.3 Migmatitic paragneiss (94KE240M)

The sample of the migmatitic paragneiss comes from station 94KE240 and consists of well-layered, migmatitic, granoblastic Qtz-Pl-Bt-Gt paragneiss. Only monazite was analyzed from the migmatitic paragneiss (Figure 4.1). Zircon analyses for this rock are presented in Chapter 5. Monazite consists of small (<75 μm), light yellow to tan, very round to ovoid grains and grain fragments. One monazite grain, excluded from analysis, displays a distinct core and overgrowth (Figure 4.5*b*), suggesting at least two phases of monazite crystallization in this rock. Most grains have minor orange staining and no visible inclusions. Six of the best single monazites from the 0.5-1.0 A mineral separate were picked for analysis.
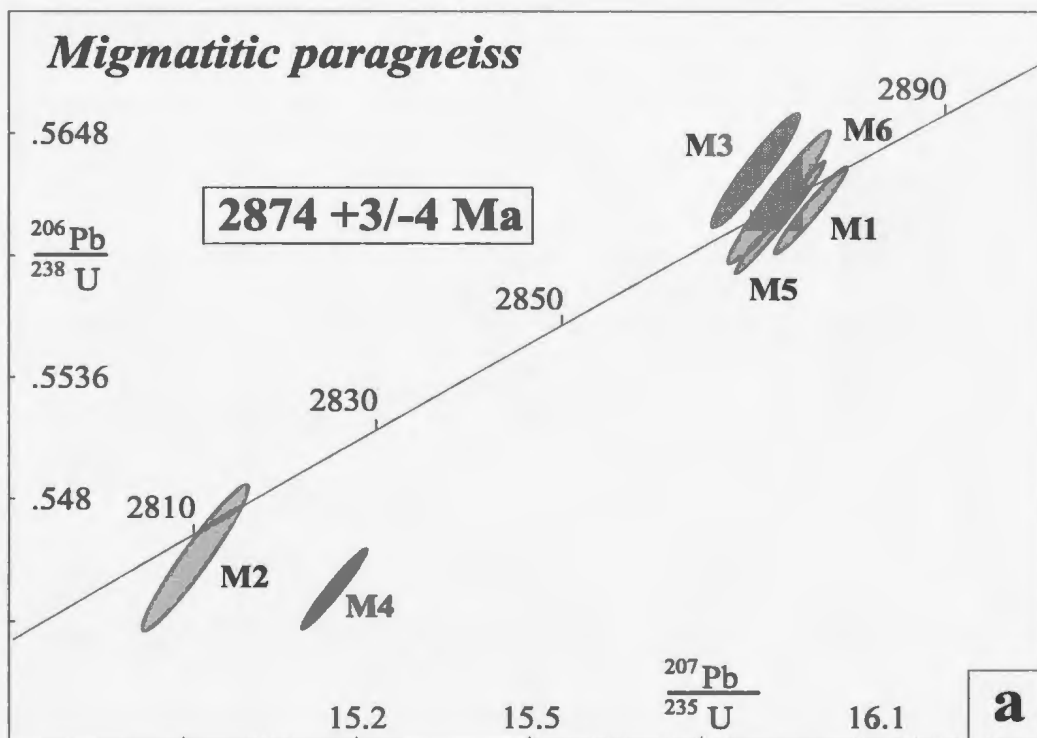
Figure 4.4a: U-Pb concordia diagram of monazite analyses from the migmatitic paragneiss (94KE240M). Ellipses are for 2σ uncertainties.
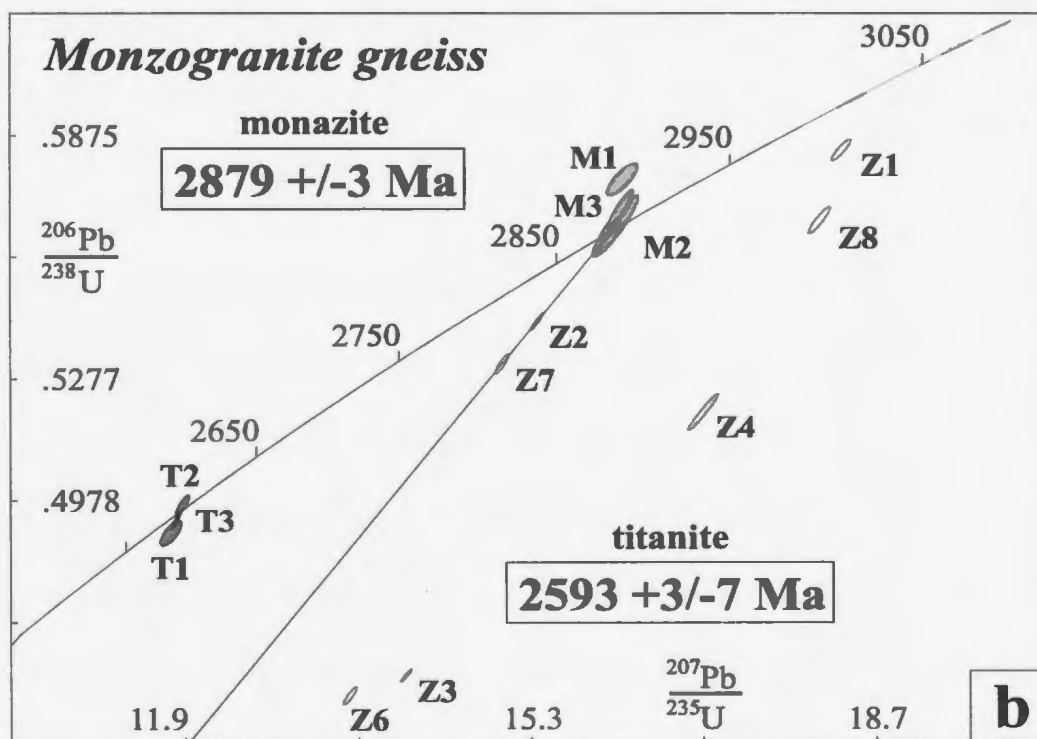
Figure 4.4b: U-Pb concordia diagram of zircon, monazite and titanite analyses from the monzogranite gneiss (94KE232B). Ellipses are for 2σ uncertainties. Z, zircon; M, monazite; T, titanite.

Analytical Results

Of the six single monazites analyzed, four of the resulting data points cluster on or near concordia, with one (M4) 1.9% discordant (Figure 4.4a). Two analyses (M5 and M6) are concordant, with overlapping uncertainties. The average ^{207}Pb/^{206}Pb age of these grains is 2874 +3/-4 Ma. One analysis (M1) is 0.32% discordant with a ^{207}Pb/^{206}Pb age of 2879 +/-2 Ma. Another analysis (M2) is concordant, within uncertainty, and gives a younger ^{207}Pb/^{206}Pb age of 2814 +/-1 Ma. The presence of monazites with cores and overgrowths suggests that the 2879 Ma age for M1 may represent either partial resetting of an original detrital population of monazite by later, high grade metamorphism or it may be the crystallization age of monazite in this rock. The 2874 Ma age for the concordant analyses may indicate a second monazite forming event or it may be a mixed age produced by a metamorphic event post-2814 Ma.

4.3.4 Monzogranite gneiss (94KE232B)

The monzogranite gneiss at Station 94KE232 is medium- to coarse-grained, biotite-bearing, granoblastic and has discontinuous cm-scale compositional layering. The zircons from the monzogranite gneiss are light brown igneous prisms with square to rectangular cross-sections and pointed to slightly resorbed terminations. Most grains have inclusions and are cracked. Some also have internal zoning, possibly representing cores and metamorphic overgrowths (Figure 4.2c). Eight single grains from the 0^0 magnetic and nonmagnetic mineral separates were chosen for dating

Figure 4.5

Figure 4.5: (*a*) monazite from the granite gneiss (94KE241) showing the small size and rounded anhedral habit of these grains. (monazites 150-200 μm in diameter) (*b*) monazite grain from the migmatitic paragneiss (94KE240M) with a distinct core and overgrowth. (monazite is 150 μm in diameter) (*c*) monazite crystals from the megacrystic granite (94KE240G). Note the euhedral to subhedral crystal habit. The grain in the upper right of the photo has a rounded core and euhedral overgrowth. (cored monazite is 350 μm in diameter)
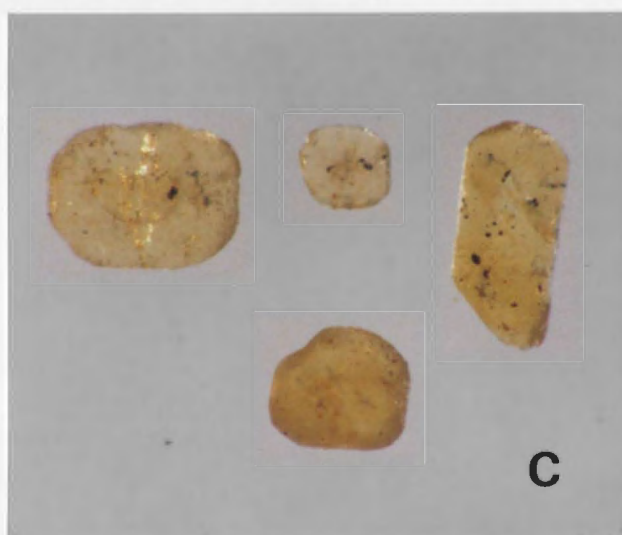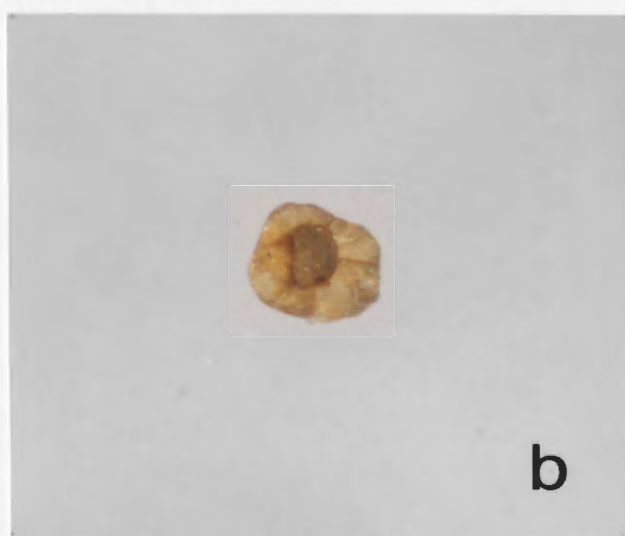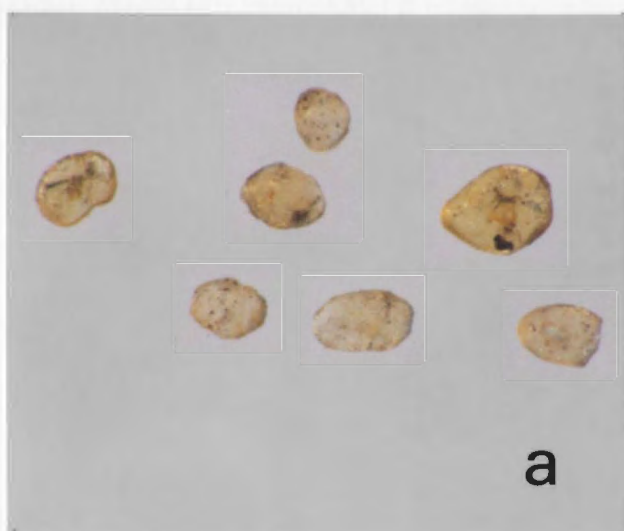
Monazite occurs in the sample as small- to medium-sized, round to ovoid, dark yellow grains and grain fragments. Most grains are turbid and have opaque, metallic inclusions and orange staining. Three single grains were picked from the 0.5-1.0 A mineral separate and lightly abraded.

Titanite occurs as dark brown to colourless, anhedral fragments. No zoning is apparent in the titanite. In thin section, the titanite appears as anhedral platy crystals along the cleavage planes of biotite that has undergone alteration to chlorite. This suggests that the titanite formed during a greenschist facies thermal event. One multiple grain fraction of brown titanite and two fractions of colourless titanite were picked for analysis.

Analytical Results

Data points from the eight zircon analyses are variably discordant (Figure 4.4b), and do not define a line. One analysis (Z5) is 28% discordant and is not included in this data set. Z2, Z3 and Z4 are all grains with internal zoning, and the data points from these analyses are widely distributed, suggesting there may be xenocrystic cores in some grains or a complex Pb-loss history. However, two data points (Z2 and Z7) form a colinear array with the monazite data, which is discussed more fully below. The three least discordant zircon analyses yield $^{207}Pb/^{206}Pb$ ages of 3103 +/-2 Ma (Z4, 16% discordant), 3068 +/-2 Ma (Z8, 7.1% discordant) and 3039 +/-2 Ma (Z1, 3.0% discordant). All of these analyses confirm the presence of older zircons, whether primary or xenocrystic, in this gneiss.

Two of the monazite analyses produce data points which are concordant to slightly negatively discordant and which define an average $^{207}Pb/^{206}Pb$ age of 2879 +/-3 Ma (Figure 4.4b). This is consistent with the metamorphic monazite ages from the other two gneisses. In addition, when the two colinear zircon analyses (Z2 and Z7) are included in the regression calculation, the line produced yields an upper intercept age of 2877 +4/-3 Ma after error expansion. This is the same age, within uncertainty, as that from the monazite analyses alone, and suggests synchronous crystallization of monazite and zircon.

The titanite analyses for this sample yield a cluster of concordant to slightly discordant data points. T2 and T3 are concordant within uncertainty at 2593 +3/-7 Ma (Figure 4.4b). T1 is 1.3% discordant, with a $^{207}Pb/^{206}Pb$ age of 2598 +/-8 Ma. The significance of this metamorphic age discussed below.

4.3.5 'Nerak granite' (94KE223)

The 'Nerak granite' sample comes from station 94KE223 and consists of a massive K-feldspar megacrystic biotite granite (Figure 4.1). The sample contains three distinct zircon populations. The most abundant are small (<75 μm), colourless, elongated to needle-like prisms with slightly rounded terminations and aspect ratios of 6:1 to 8:1. One fraction of the best 0^0 non-magnetic prisms was picked for analysis. The second population consists of equant, brown to pinkish brown, multifaceted prisms and prism fragments (Figure 4.6a). Aspect ratios are typically 1:1 to 2:1. Most are cracked and many show turbid cores and clear overgrowths. Small, clear inclusions, which may be

Figure 4.6

Figure 4.6: (*a*) brown prismatic zircons from the 'Nerak granite' (94KE223). Note the sharply pointed terminations and the lack of apparent internal zoning. (zircons 400 μm long) (*b*) pink zircon prisms from the 'Nerak granite'. Zircons have a complex bipyramidal morphology with well developed, higher-order crystal faces. No internal zoning is visible. (zircons 500 μm long) (*c*) equant brown prisms from the megacrystic granite (94KE240G). The zircon in the upper left has an opaque core and clear overgrowth, with radiating fractures from the core into the overgrowth. (zircons 500 μm long) (*d*) small, light brown zircon prisms from the granodiorite dyke (94KE419). (largest zircon 300 μm long) (*e*) turbid, tabular zircon prisms from the syenogranite pegmatite (94KE418A). (zircons 150-250 μm long)
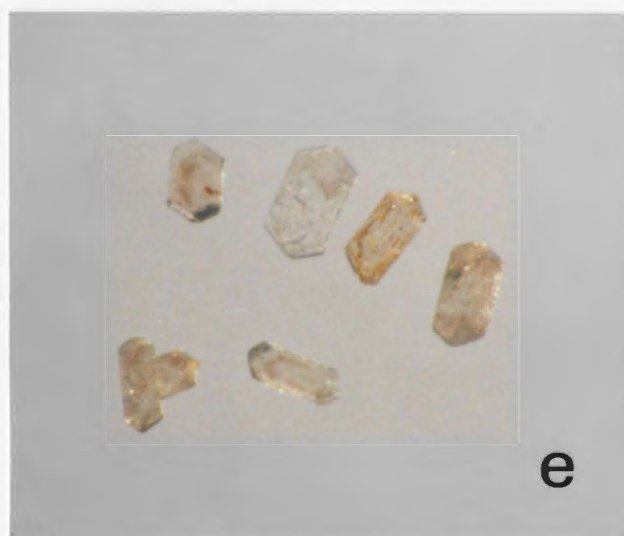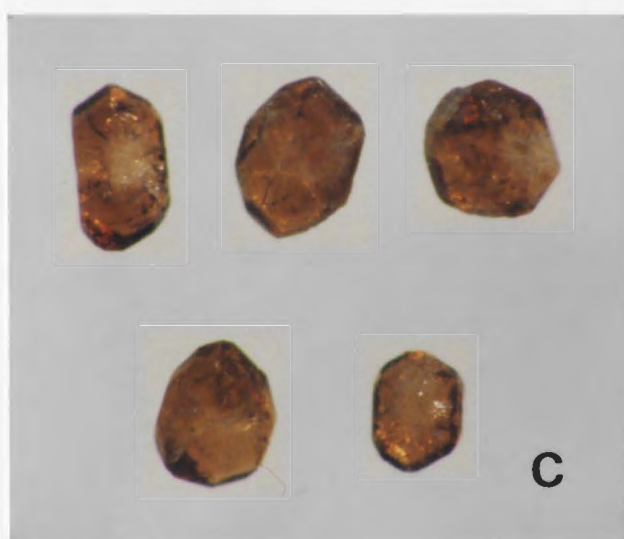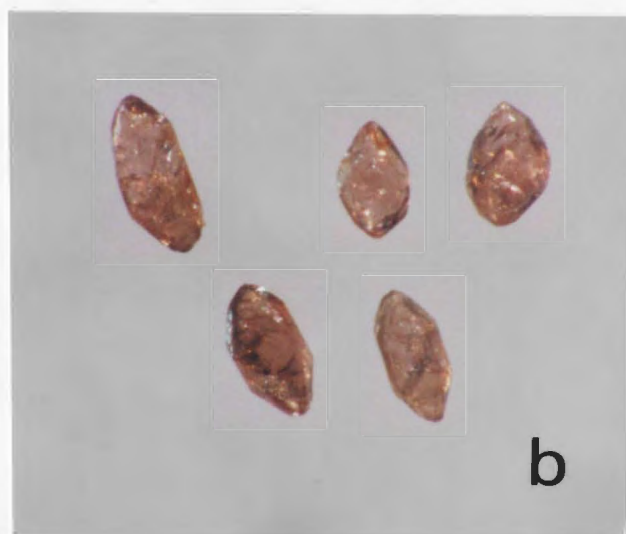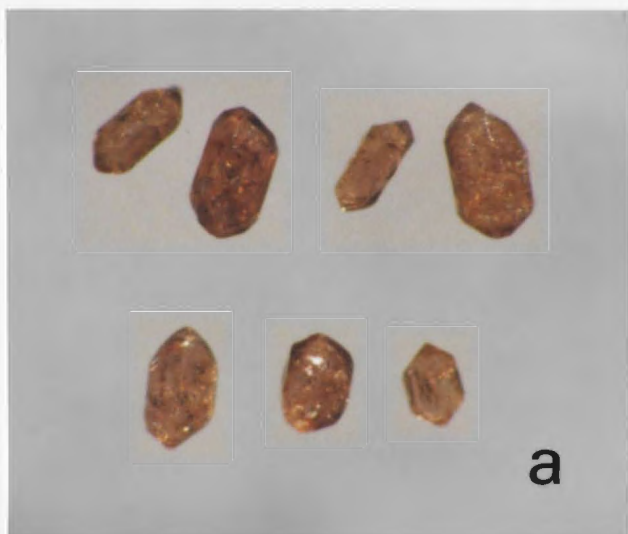
fluid or apatite, are present in some. Two of the best 0^0 non-magnetic prisms were picked from this population. The third population consists of large, pink, clear zircon fragments with well developed, higher-order crystal faces. Rare complete crystals have a pointed, bipyramidal morphology with cores and internal zoning (Figure 4.6*b*). Three intact single grains from the 0^0 non-magnetic mineral separate were picked for analysis.

Monazite from this sample consists of light to dark yellow, clear to slightly turbid, euhedral to subhedral, grains and fragments. Three single monazite grains from the 0.5-1.0 A magnetic separate were picked for analysis.

Analytical Results

Of the six zircon analyses obtained, 5 yield data points which define a discordia line with an upper intercept age of 2887 +/-2 Ma and a lower intercept of 642 +/-21 Ma with a probability of fit of 12.3% (Figure 4.7*a*). One zircon analysis (Z3) from the pink population has a younger $^{207}Pb/^{206}Pb$ age of 2866 +/-3 Ma with 0.52% discordance. One possible explanation for this zircon age is that Z3 is on a shallow lead loss line to a younger metamorphic event.

Of the three single monazite grains analyzed, two (M1 and M2) are concordant and have overlapping error ellipses, while M3 is 15.7% discordant (Figure 4.7*a*). The average $^{207}Pb/^{206}Pb$ age calculated from M1 and M2 is 2878 +5/-3 Ma. This upper intercept age is similar, within uncertainty, to the $^{207}Pb/^{206}Pb$ age of 2887 +/-12 Ma for the concordant zircon analysis Z1. This similarity in ages for the monazite and zircon indicates either a common primary crystallization age or, if the monazites are metamorphic in origin, the metamorphic event is nearly coeval with granite intrusion and crystallization.
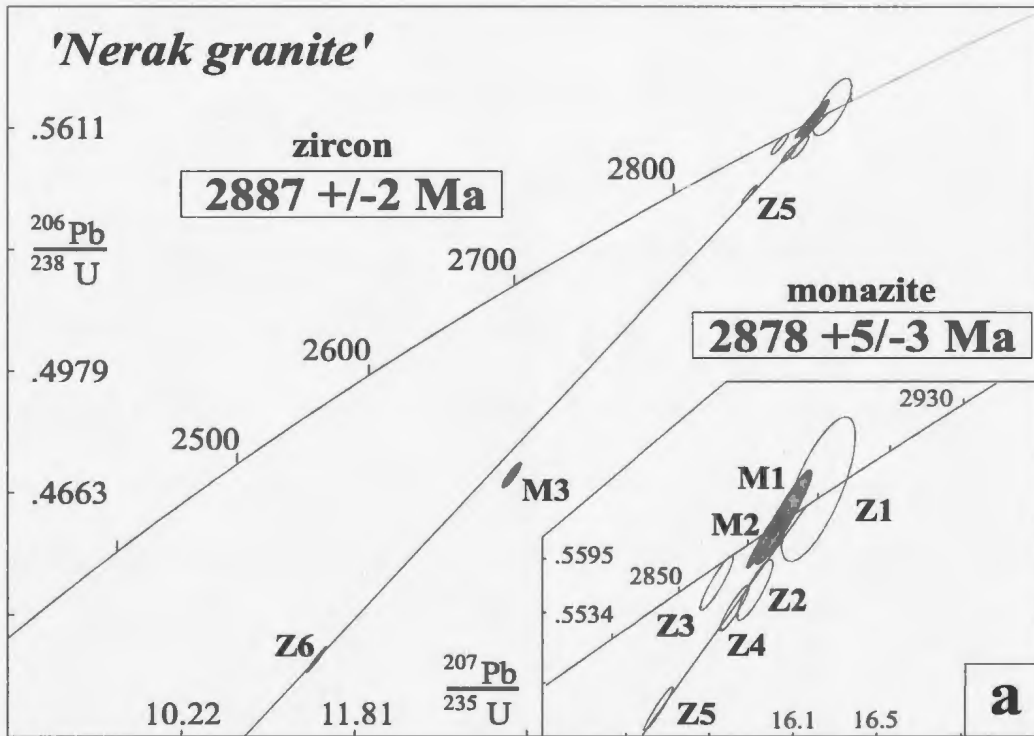
Figure 4.7a: U-Pb concordia diagram of zircon and monazite analyses from the 'Nerak granite' (94KE223). Ellipses are for 2σ uncertainties. Z, zircon; M, monazite.
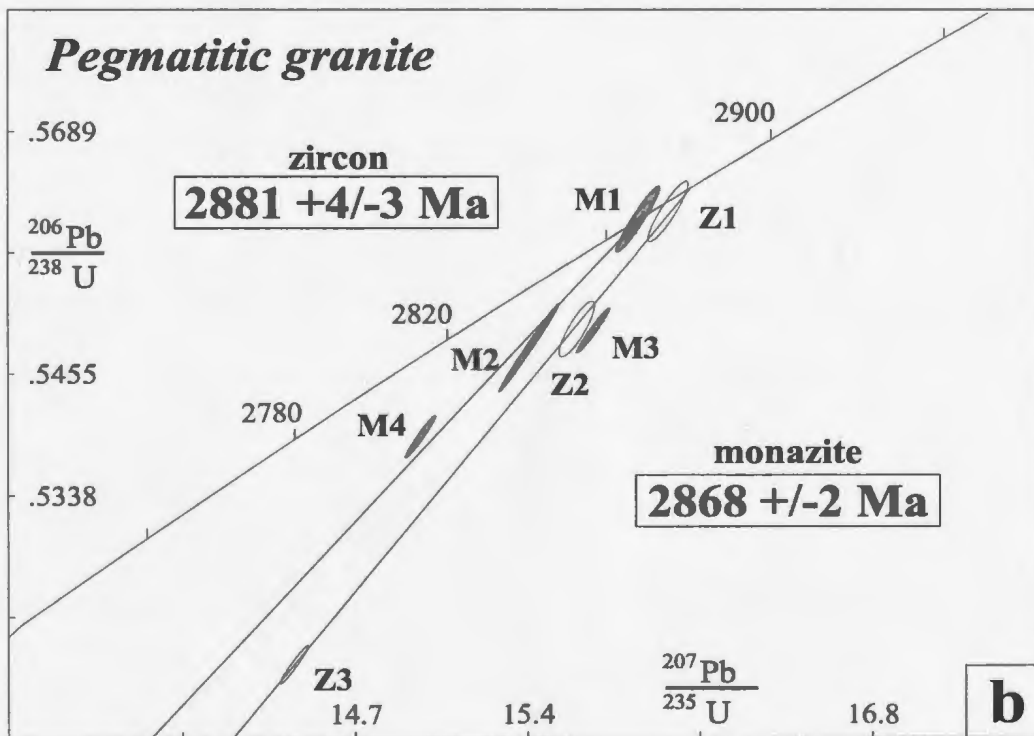
Figure 4.7b: U-Pb concordia diagram of zircon and monazite analyses from the pegmatitic granite (94KE240G). Ellipses are for 2σ uncertainties. Z, zircon; M, monazite.

4.3.6 Pegmatitic granite (94KE240G)

The pegmatitic granite from station 94KE240 is a white, weakly foliated, coarse-grained to pegmatitic biotite syenogranite. This sample contains two populations of zircon, of which the most numerous are small, colourless, elongated to needle-like prisms with pointed terminations and square cross-sections. Aspect ratios range from 5:1 to 7:1. None display obvious cores or internal zoning. Three fractions of the best 0^0 non-magnetic prisms were picked for analysis. A second, less abundant population consists of large (> 100 μm), dark brown zircons with aspect ratios of 1:1 to 3:1, the shapes of which vary between slightly elongated, square-cross section prisms and more equant grains with well developed, higher-order crystal faces. Many zircons from this second population have turbid, ovoid cores surrounded by radially fractured, clear overgrowths (Figure 4.6c). Three single zircons from the 0^0 non-magnetic separate were picked and strongly abraded to remove overgrowths.

Monazite from this sample occurs as small, light yellow to light brown, flattened oval to tabular shaped grains and grain fragments. Most are turbid with opaque inclusions and orange staining. One grain was found with a distinct core and overgrowth (Figure 4.5c). Four clear unzoned single monazites from the 0.5-1.0 A separate were picked for analysis.

Analytical Results

The three fractions of small needles, Z4, Z5 and Z6, are 29-33% discordant and non-colinear (not shown in Figure 4.7b) and were not used to determine the age. Zircons of

this population have higher (600-1500 ppm) uranium values than the brown population. This, combined with their size, could result in considerable U and Pb loss from radiation damage. The remaining three data points from the brown prisms define a discordia with a probability of fit of 34%, an upper intercept age of 2881 +4/-3 Ma and a lower intercept age of 876 +78/-73 Ma (Figure 4.7*b*). The 2881 Ma upper intercept is interpreted as the crystallization age of the granite.

Data points for the four monazite analyses are non-colinear, but one (M1) is concordant, yielding a $^{207}Pb/^{206}Pb$ age of 2868 +/-2 Ma, which is interpreted to be the crystallization age of the monazite (Figure 4.7*b*). One fraction (M3) plots to the right of both the discordia lines formed by both monazite and zircon and is discussed further below.

4.3.7 Boudinaged diorite dyke (94KE232A)

The diorite dyke at station 94KE232 is fine-grained, hornblende and biotite bearing and has a moderate internal foliation. Two populations of zircons are present in the mineral separates. One population consists of small, purple-brown, multiply faceted, clear grains that are interpreted as metamorphic overgrowths on igneous zircon and were not dated. The second population consists of small (<75 μm), purple-brown prismatic grains with rounded, slightly resorbed terminations and aspect ratios between 3:1 and 4:1. They are normally clear with multiple opaque inclusions and rare clear inclusions. No visible cores or internal zoning were observed under microscopic examination. Rare,

Figure 4.8

Figure 4.8a: Two populations of titanite from the diorite dyke (94KE232A). Large subhedral crystals of brown titanite are visible in the upper right of the photo. Anhedral, clear titanite grains (lower left) have grown with blue-green hornblende and chlorite in the fracture at the upper right to left of the photo. Field of view is 2.3 mm.

Figure 4.8b: Anhedral titanite from the granodiorite dyke (94KE419). This titanite occurs as overgrowths on an opaque mineral, possibly ilmenite, and is shown cutting the internal foliation of the dyke (arrows). Field of view is 2.3 mm.
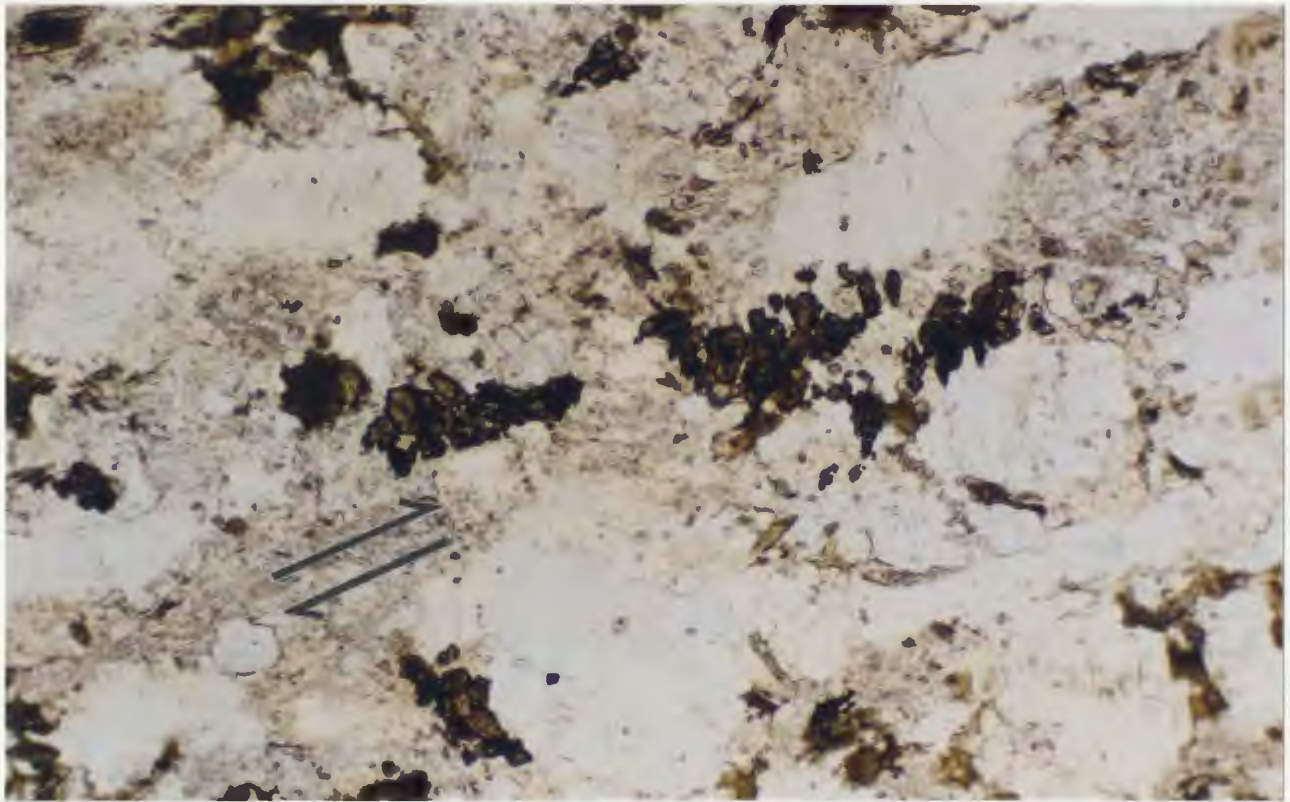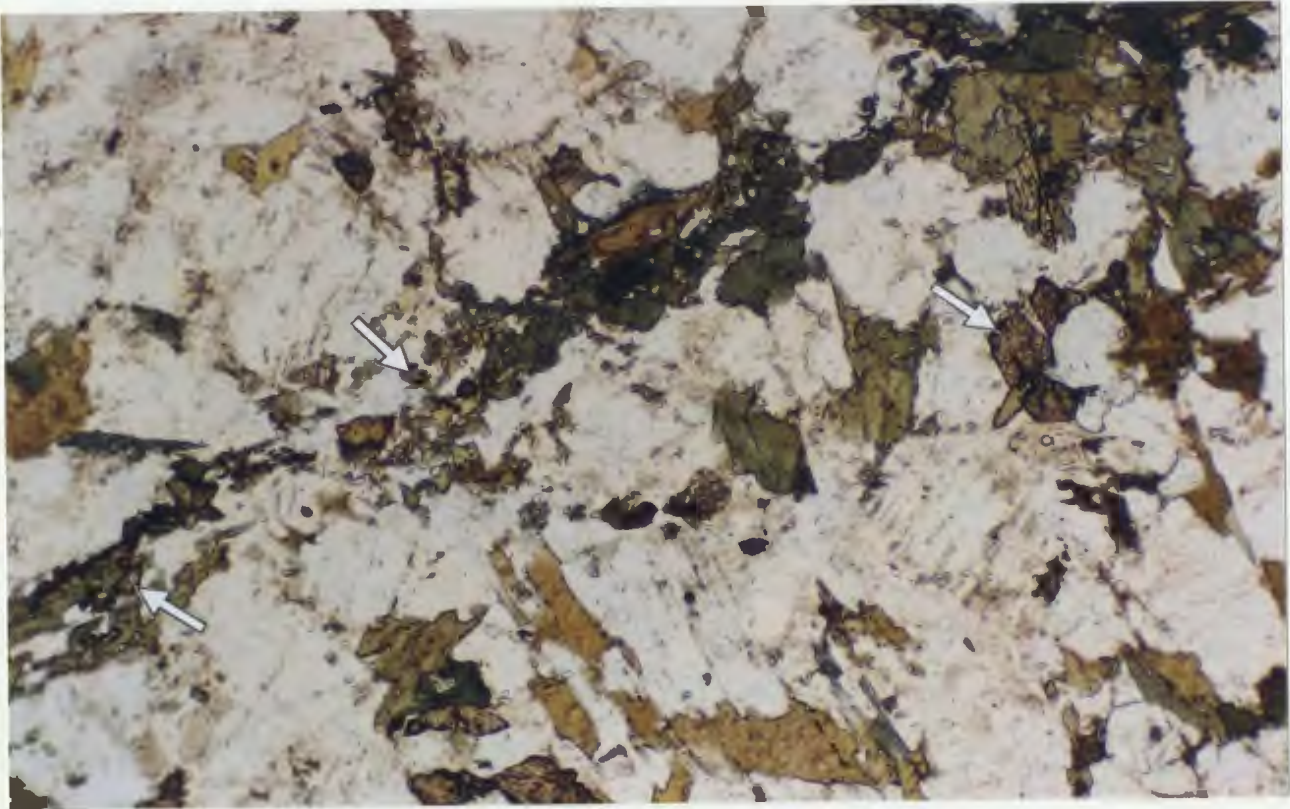
large (<100 µm) equant, multifaceted grains occur which may be xenocrystic. Three single zircons were picked from the 0^0 non-magnetic and magnetic mineral separates.

Titanites from this sample consist of anhedral fragments varying in colour from dark brown to colourless. Most are turbid and contain opaque inclusions. Rarely, an abrupt variation in colour from dark brown to colorless occurs within single grains and could represent different ages of titanite growth. In thin section, the brown titanite occurs as relatively larger, subhedral to anhedral resorbed grains associated with hornblende and biotite. The colourless titanite grains occur as small, anhedral aggregates associated with the development of blue-green hornblende and actinolite along fractures in the rock (Figure 4.8a). Five multiple grain fractions of titanite, two from the dark brown population and three from the colourless population were picked from the 1.7 A mineral separate.

Analytical Results

Data points from the zircon analyses form a linear array at or slightly above concordia (Figure 4.9a). A discordia line defined by these points has an upper intercept of 2877 +5/-4 Ma, a lower intercept of 530 +738/-646 Ma with a 66% probability of fit, and is interpreted to be the emplacement age of the dyke.

The titanite analyses indicate two distinct ages of crystallization. The dark brown titanites (T2 and T3) yield data points that are concordant within error and do not overlap, with $^{207}Pb/^{206}Pb$ ages of 2837 +/-2 and 2821 +/-2 Ma, respectively (Figure 4.9a). One
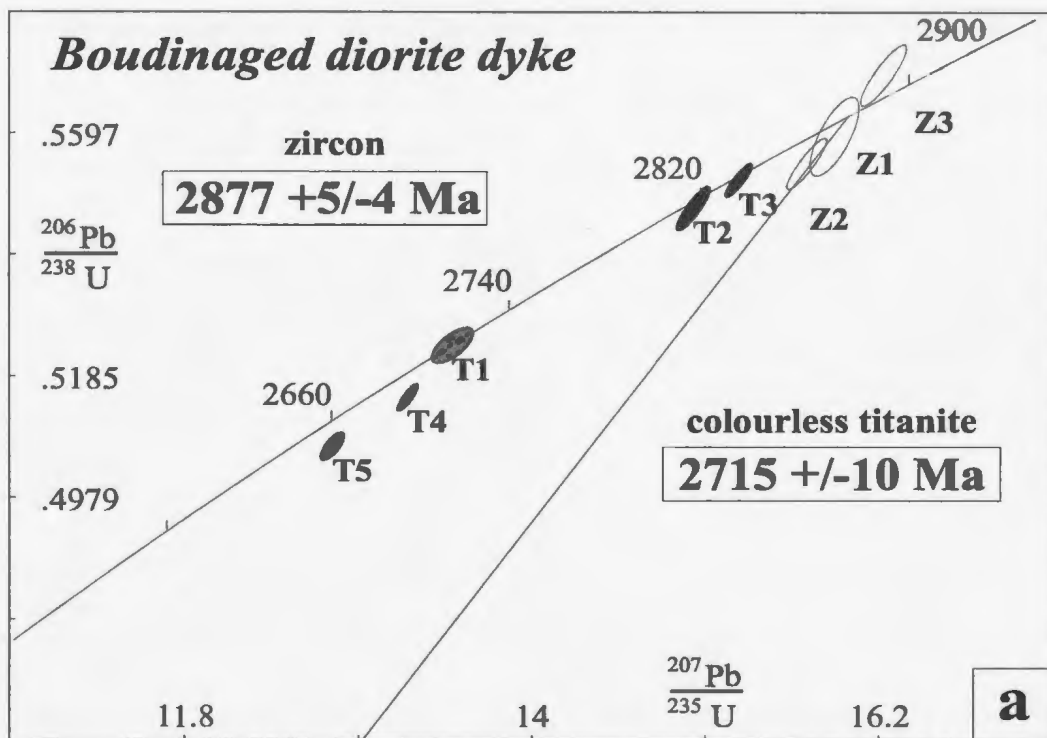
Figure 4.9a: U-Pb concordia diagram of zircon analyses from boudinaged diorite dyke (94KE232A). Ellipses are for 2σ uncertainties. Z, zircon; T, titanite. Black ellipses are brown titanite; grey ellipses are colourless titanite.
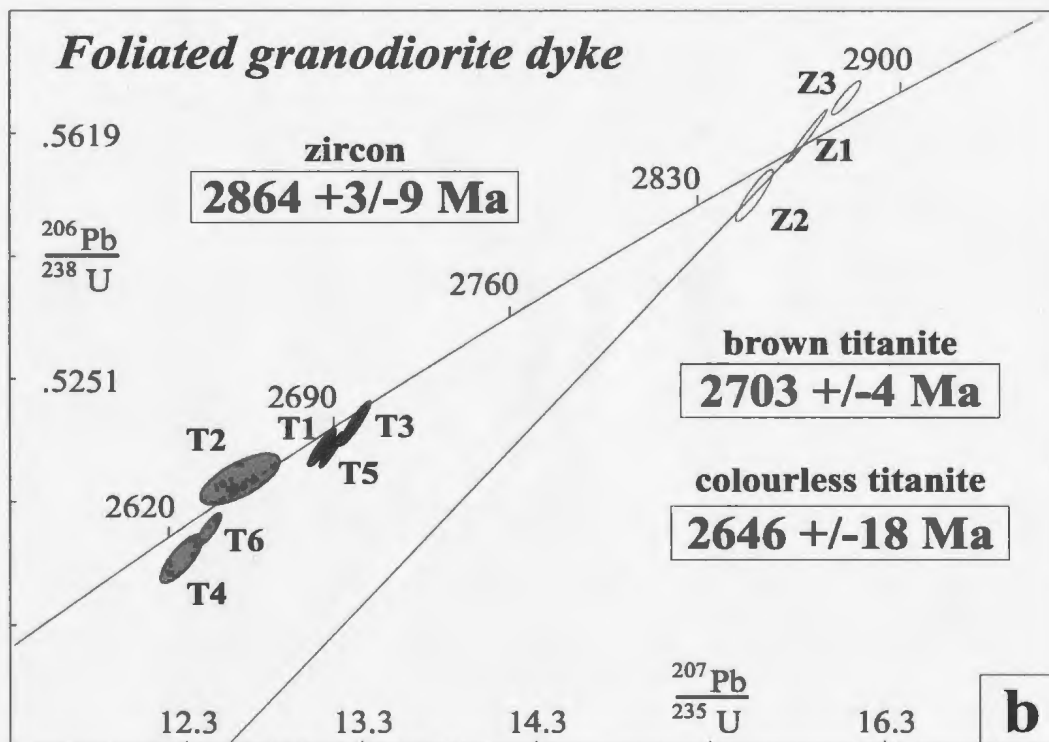
Figure 4.9b: U-Pb concordia diagram of zircon analyses from foliated granodiorite dyke (94KE419). Ellipses are for 2σ uncertainties. Z, zircon; T, titanite. Black ellipses are brown titanite; grey ellipses are colourless titanite.

colourless titanite analysis (T1) is concordant, with a $^{207}Pb/^{206}Pb$ age of 2715 +/-10 Ma. The remaining clear titanite data points appear to define a shallow discordia line.

4.3.8 Granodiorite dyke (94KE419)

The granodiorite dyke at station 94KE419 is fine-grained, sparsely K-feldspar porphyritic and biotite bearing. Zircon in the heavy mineral separate occurs as small (<75μm), clear, brown to light brown prisms with square cross sections and rounded terminations. No cores or internal zoning were visible (Figure 4.6d). Three of the best single zircons were chosen from the 0^0 non-magnetic mineral separate.

Titanites from this sample consist of anhedral fragments ranging in colour from colourless to dark brown, with light brown varieties predominating. In thin section, all titanite has an anhedral, metamorphic crystal habit. Some titanite grains appear to have grown across the foliation present in the thin sections and may post-date deformation (Figure 4.8b). No grains with distinct colour zoning, such as those seen in the diorite dyke, are visible. Three multiple grain fractions of colourless and brown titanite from the 1.7 A mineral separate were chosen for analysis.

Analytical Results

Data points for the zircon analyses form a linear cluster below to slightly above concordia and define a discordia line with an upper intercept at 2864 +3/-9 Ma, and a lower intercept of 1052 +841/-393 Ma with a 44 % probability of fit (Figure 4.9b). This is interpreted as the crystallization age of the dyke.

The six titanite analyses yield data points that fall into two distinct clusters. One fraction of brown titanite (T3) is concordant at 2703 +/-4 Ma. The age of the concordant brown titanite is taken as the age of crystallization for this population. Of the colourless titanite, one (T2) is concordant, within uncertainties, with a $^{207}Pb/^{206}Pb$ age of 2648 +/-18 Ma (Figure 4.9b). The age of the concordant colourless titanite is taken as the crystallization age of this population. Given the anhedral morphology of these titanites, the pattern produced by these analyses suggests two discrete metamorphic titanite-forming events.

4.3.9 Syenogranite pegmatite dyke (94KE418A)

This sample comes from an undeformed biotite syenogranite pegmatite dyke at station 94KE418. Zircon from this sample is medium-sized (75 µm), stubby, tabular, prisms of poor quality (Figure 4.6e). All are turbid to some degree, with igneous growth zoning defined by alternating light brown and colourless bands. About 1% of the zircon is amber to light yellow in colour, but this appears to be a surface discolouration as it is lost during abrasion.

Monazite occurs as large crystals or crystal fragments that are brown to dark orange and completely turbid. Rare, clear monazites are small, euhedral to subhedral grains. Two single monazites from the 0.5-1.0 A mineral separate were chosen for analysis.

Titanite consists of anhedral, platy fragments, ranging in color from dark brown to colourless. In thin section, the titanite can be seen growing in biotite cleavage planes where it is altered to chlorite (Figure 4.10a). There appears to be no abrupt colour

Figure 4.10

Figure 4.10*a*: Metamorphic titanite from the syenogranite pegmatite. Note titanite grains growing in the cleavage planes in biotite altering to chlorite. The large grain in the lower left is titanite overgrowing ilmenite. Biotite crystal is 1 mm wide

Figure 4.10*b*: Large, euhedral titanite crystals from the young granite. Titanite in centre of photo is 800 μm long.
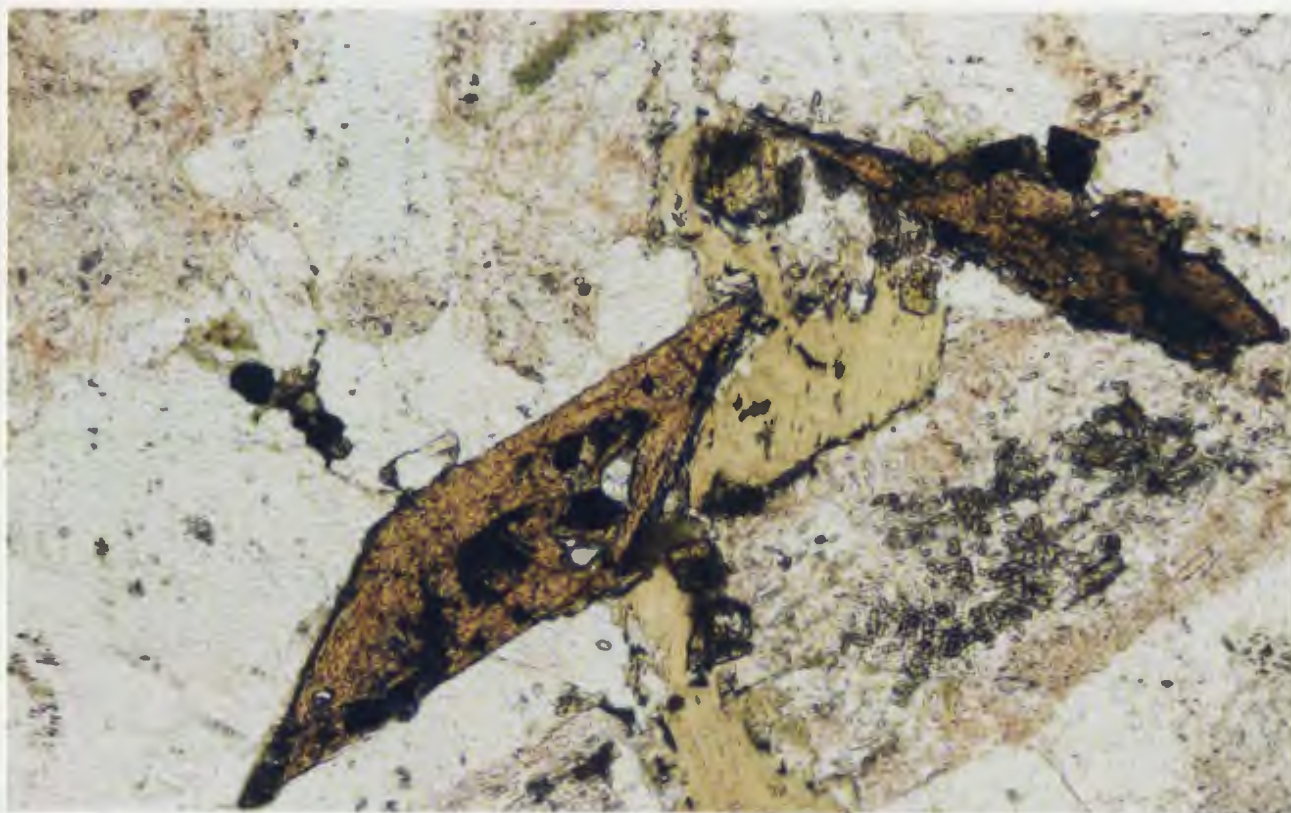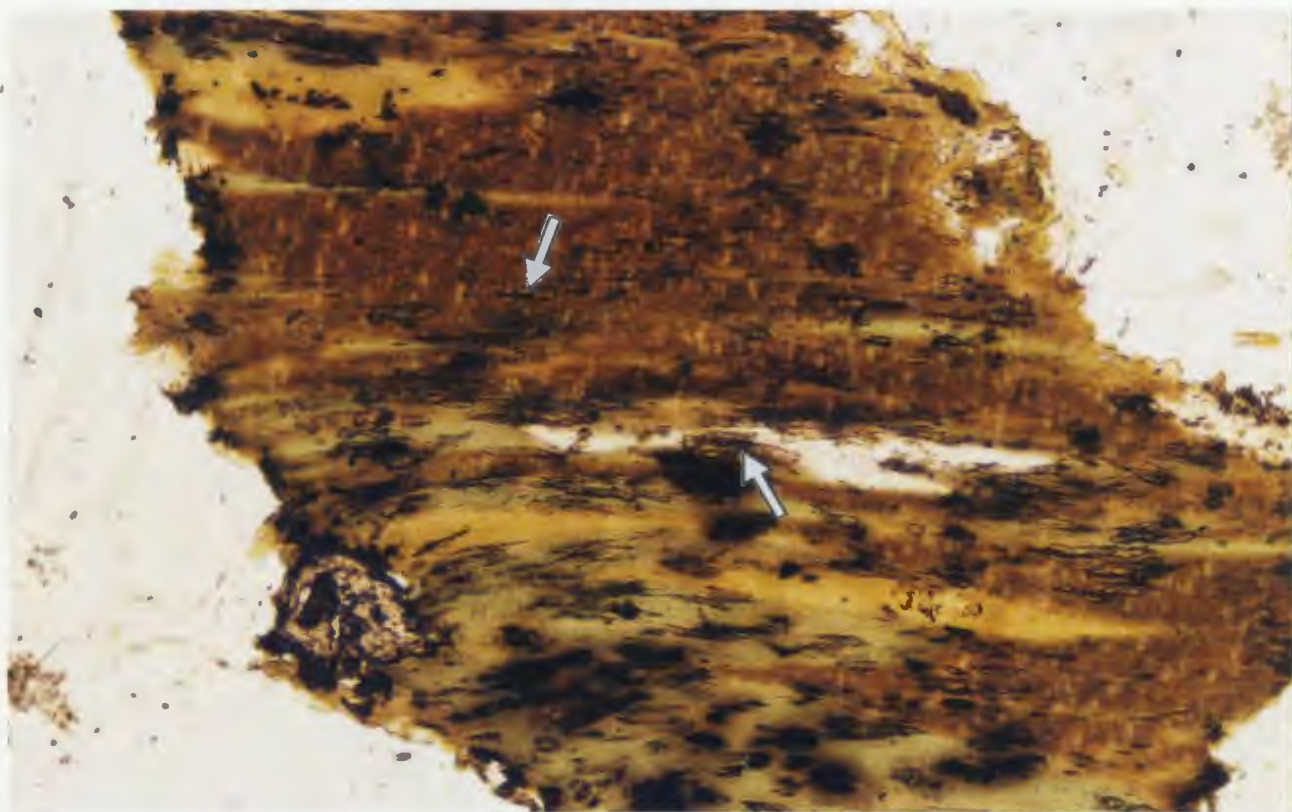
zoning, as is the case with titanite from the diorite dyke. Rather, the color shows a gradational variation from dark brown to colourless. Two multiple grain fractions of colourless titanite and three of brown titanite were picked for analysis.

Analytical Results

The four single zircon data points are very discordant and non-colinear (Figure 4.10a). The two monazite analyses are concordant with an average $^{207}Pb/^{206}Pb$ age of 2851 +/-3 Ma. This, coupled with the probable igneous morphology of the monazite, argues against their being inherited from an older source. Two monazite data points and two colinear zircon data points (Z2 and Z3) define a discordia with an upper intercept of 2852 +/-3 Ma and a lower intercept of 690 +/-7 Ma. This corresponds, within uncertainties, to the age determined by monazite alone.

The results of the analyses of the titanites show both colourless and brown populations are colinear and generate data points which define a discordia with an upper intercept of 2587 +3/-2 Ma (Figure 4.10a), a lower intercept of 531 +554/-651 Ma after error expansion. Of the colourless titanites T3 is the most discordant (12%) and T2, though concordant, has a higher proportion of common lead than the other four analyses. When the colourless titanites are excluded from the regression calculation, the upper intercept becomes 2585 +/-1 Ma, the lower intercept 24 +99/-102 Ma with a 77% probability of fit. The colinearity implies a single event is responsible for the crystallization of all the titanite.
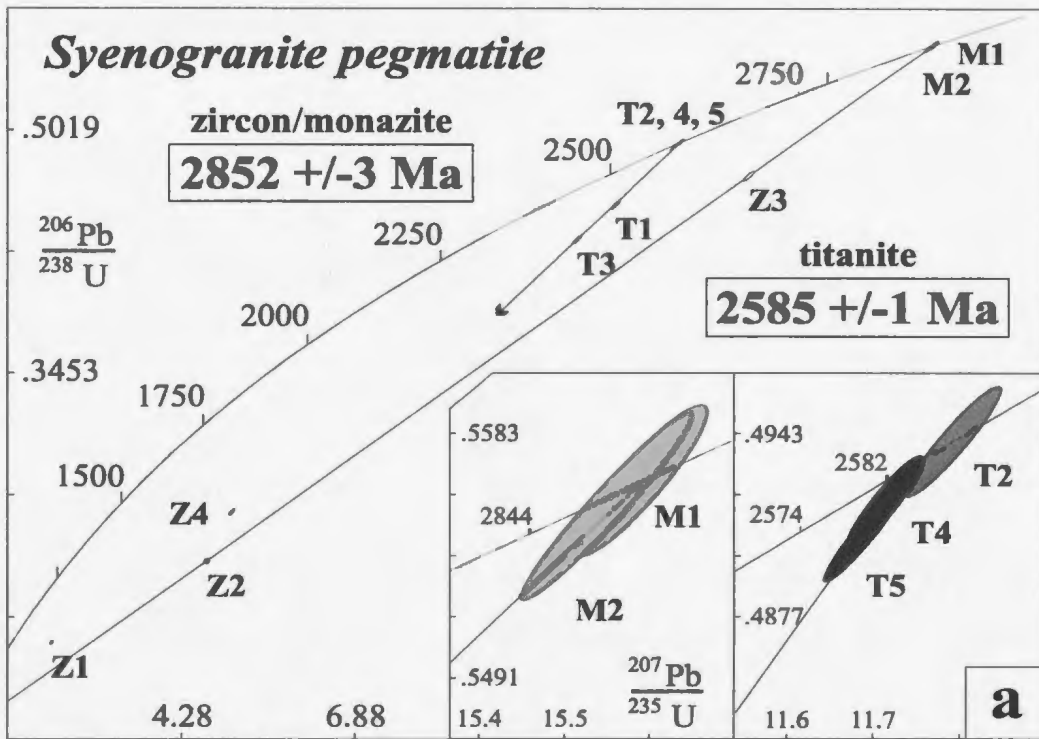
Figure 4.11a: U-Pb concordia diagram of zircon analyses from syenogranite pegmatite. Ellipses are for 2σ uncertainties. Z, zircon; M, monazite; T, titanite. Medium grey ellipses represent colourless titanite, black represents brown titanite analyses.
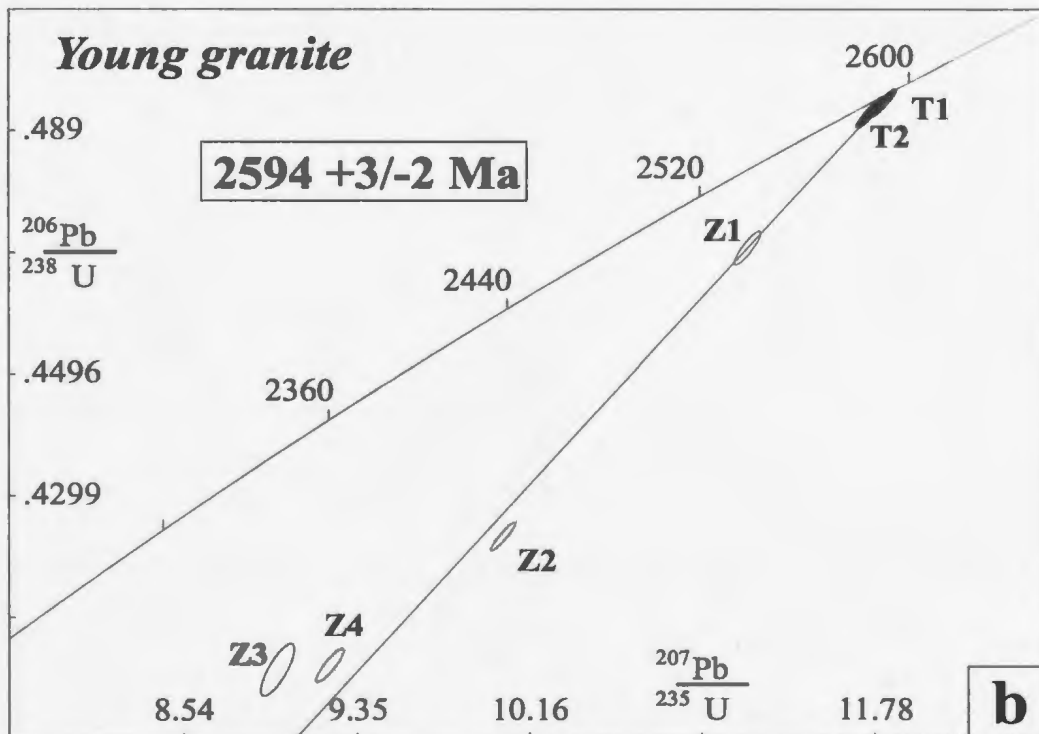
Figure 4.11b: U-Pb concordia diagram of zircon and titanite analyses from the young granite. Ellipses are for 2σ uncertainties. Z, zircon; T, titanite.

4.3.10 Young granite (94VJ253)

A late, cross cutting granite was sampled from near 'Beaver lake' (station 94VJ253) outside the study area (Figure 1.2). Two morphologies of zircon are present in this sample. The most abundant consist of small, needle-like prisms with sharp terminations and aspect ratios between 5:1 and 7:1. They are colourless, clear to slightly turbid and contain opaque, metallic or rust-coloured inclusions. Two multiple grain fractions of the best prisms and prism fragments from the 0^0 non-magnetic separate were picked for dating. The second population consists of large, light brown, equant prisms and prism fragments that make up <<1% of the total population. These zircons have well-developed higher order crystal faces and no visible cores or internal zoning. Two of the best, 0^0 non-magnetic prisms (Z1 and Z4) were picked for dating.

Titanite from this sample occurs as large, dark brown, euhedral to subhedral crystals and crystal fragments, which can be seen in thin section to be igneous in origin (Figure 4.11*b*). They contain opaque inclusions, probably ilmenite, and most are turbid and cracked. Two fractions of the best grains from the 1.7 A separate were picked for dating.

Analytical Results

The zircon analyses are non-colinear and discordant. The two fractions of titanite analyzed are only slightly discordant and have overlapping error ellipses, with $^{207}Pb/^{206}Pb$ ages of 2591 +/-2 and 2594 +/-1 Ma (Figure 4.10*b*). The titanite data points, combined with those produced for the two least discordant zircon analyses (Z1 and Z2), define a discordia line with an upper intercept age of 2594 +3/-2 Ma and a lower intercept of 456 +455/-521 Ma, after error expansion. This age is interpreted as the age of the granite

4.4 Discussion of Results

With the exception of the young granite, all zircon ages from the study area fall within the pre 2.8 Ga age range for rocks classified as basement in the Slave Province. In addition, monazite and titanite ages reveal several episodes of mid-to-lower amphibolite and greenschist facies metamorphism. The age ranges of the zircons and other accessory minerals are shown in Figure 4.12.

4.4.1 Zircon ages

The non-colinear array of zircon data points from the tonalite gneiss suggests they may lie on a shallow lead-loss line to a later metamorphic event, possibly the intrusion of the megacrystic granites at ca. 2880 Ma. Further lead loss during still later metamorphic events (i.e. the 1.9-1.8 Ga Wopmay Orogen or the intrusion of the 723 Ma Franklin diabase sills) could have resulted in the evolution of points off of the initial lead-loss line to produce the scattered pattern seen in the concordia diagram (Figure 4.3a). Zircon data from the granite gneiss, though slightly non-colinear, is consistent with the crystallization of this gneiss at ca. 3200 Ma.

The distribution of zircon analyses from the monzogranite gneiss, as well as their igneous habit (Figure 4.2c) suggests two possible interpretations. In the first interpretation, the monzogranite gneiss may be one of the older gneiss units. In this case, the older zircons may be part of an early (i.e. pre-3100 Ma) igneous population which has suffered polyphase lead loss subsequent to emplacement, resulting in the non-colinear
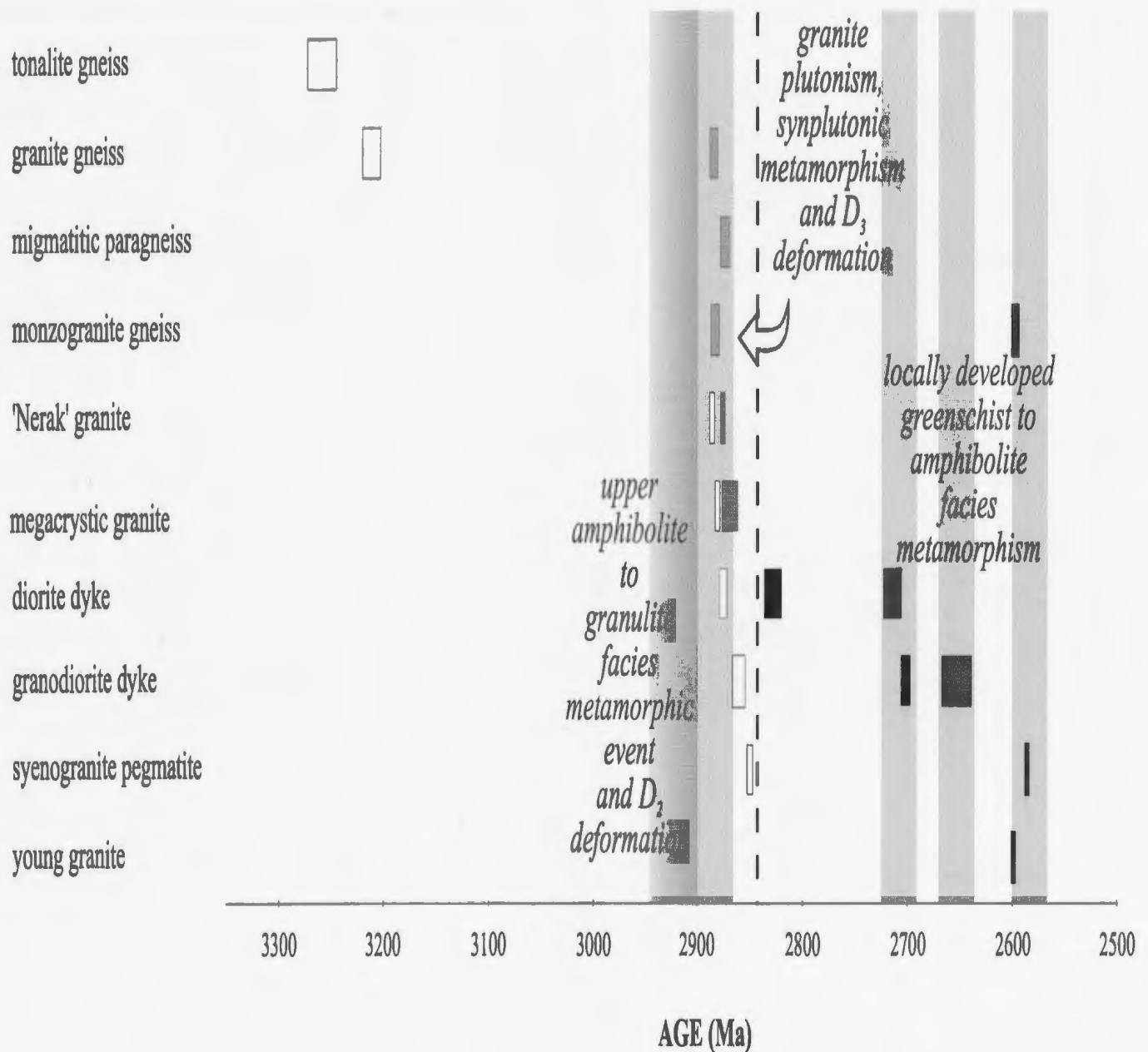
Figure 4.12: Summary of U-Pb ages for the Eokuk Uplift. The two-sigma uncertainties reported for analyses define the width of the box representing each rock. White boxes, zircon; light grey boxes, monazite; dark grey, colourless titanite; black, brown titanite. Shaded areas represent various tectonic and plutonic events within the Eokuk Uplift . Dotted line represents approximate end of deformation in the Uplift. Granite plutonism was synchronous with the last greenschist facies metamorphic episode at ca. 2600.

pattern of data points. In this case, the zircons colinear with the monazite analyses would have formed during a later thermal event. Alternatively, the two analyses colinear with the monazite ages could represent the crystallization age of the rock, and the data points further to the right contain cryptic, xenocrystic cores. If this is the case, the monzogranite gneiss may be a more highly deformed phase of the 'Nerak granite'.

Zircon ages from both the 'Nerak granite' (2887 +/-2 Ma) and the pegmatitic granite (2881 +4/-3 Ma) are within uncertainty of each other, suggesting a single magmatic event is responsible for both. The apparent gradational contact between these two granites strengthens the interpretation that they are two different phases of the same pluton.

Zircon upper intercept ages for the minor intrusive rocks, taken in conjunction with the decrease in strain state from the boudinaged diorite dyke to the undeformed syenogranite pegmatite, effectively constrain the end of deformation in the study area to between 2860-2855 Ma.

The combined zircon/titanite age of the young granite places it within the age range for the Slave Province-wide 2.62-2.58 Ga plutonic event.

4.4.2 Monazite ages

Monazite ages from the older gneiss package show a remarkable consistency, with upper intercept ages ranging from 2889 to 2874 Ma. These ages are similar to the crystallization ages for the 'Nerak granite' and the pegmatitic granite (see Figure 4.12), and suggest that the intrusion of the fluid-rich granites at ca.2880 Ma may have resulted in the crystallization of monazite in the older gneisses.

In the case of the migmatitic paragneiss, the one, younger analysis (M2) may fall on a lead loss line to a later metamorphic event (see discussion of titanite ages, below) or it may represent crystallization of new monazite at 2814 Ma.

Monazite grains with apparent cores and overgrowths are present in both the pegmatitic granite and the migmatitic paragneiss. In the pegmatitic granite, one monazite analysis (M3) plots to the right of the discordia lines formed by both monazite and zircon, with a $^{207}Pb/^{206}Pb$ age of 2880 at 2.4% discordance. In the migmatitic paragneiss, one monazite is 0.32% discordant with a $^{207}Pb/^{206}Pb$ age of 2879 +/- 2 Ma. The presence of these older monazite grains suggests that older populations of monazite exist in some of the gneissic rocks.

4.4.3 Titanite Ages

With the exception of the late granite, and possibly the diorite dyke, all of the titanite in the rocks dated appears to be the result of metamorphic reactions. The titanite analyses from the monzogranite gneiss and the various dykes and pegmatites reveal a number of lower amphibolite to greenschist facies metamorphic events. Titanite from the diorite dyke shows two distinct clusters of data points. The data points produced by brown titanite, which are only slightly discordant and whose error ellipses do not overlap, give ages very close to the crystallization age of the dyke as defined by the zircon analyses. These titanites may represent an original igneous population that has suffered minor lead loss causing them to be displaced slightly down concordia. Data points from the colourless titanite, on the other hand, appear to define a distinct lead loss line, suggesting

they formed during a separate, younger titanite crystallization event. The one concordant colourless titanite data point (T1) has a $^{207}Pb/^{206}Pb$ age of 2715 +/-10 Ma and is taken as the crystallization age for this population. The presence of titanite intergrown with blue-green hornblende and actinolite in fractures in the diorite dyke (Figure 4.9a) would indicate they crystallized during a lower amphibolite to upper greenschist facies thermal event.

Titanite data points from the granodiorite dyke also fall into two distinct clusters, representing analyses of brown and colourless titanite. In contrast to the titanites from the diorite dyke, evidence from thin sections, combined with the overlapping cluster of age data, suggests the brown titanites from the granodiorite dyke are metamorphic rather than igneous in origin. The $^{207}Pb/^{206}Pb$ age for the concordant brown titanite analysis (T3) from this sample is 2703 +/-4 Ma and is taken to be the crystallization age for this population. This age is also the same, within uncertainty, as the crystallization age for the colourless titanite from the diorite dyke. The difference in colour for the two populations is likely a function of the lower uranium content of the diorite dyke. The analyses for the colourless titanites from the granodiorite define a discordia line with an upper intercept age of 2651 Ma. This is similar to ages obtained for the peak of metamorphism and deformation in the nearby Kangguyak gneiss and the western Anialik greenstone belt, and is discussed in more detail in Chapter 6. The middle Proterozoic lower intercept suggests that events connected with the Wopmay Orogen may be responsible for the lead loss seen in some samples.

Both brown and colourless titanite from the monozogranite gneiss and the syenogranite pegmatite are metamorphic, and associated with the breakdown of biotite to

chlorite (Figure 4.11*a*). Both populations define discordia with upper intercept ages similar to zircon crystallization age for the young granite. This implies that the young granite was responsible for at least one of the greenschist grade metamorphic events in the study area.

Chapter 5: Laser Ablation Microprobe-ICP-MS U-Pb Geochronology

5.1 Introduction

Zircons from the assemblage of old gneissic and granitic rocks in the study area exhibit complex internal structures in the form of apparent xenocrystic cores and metamorphic or magmatic overgrowths. It therefore becomes important to obtain radiometric ages *in situ*, so that this data can be related to the various features within individual zircon grains. As well, the migmatitic paragneisses potentially contain detrital zircons with a wide range of ages, which would necessitate a large number of analyses to determine a meaningful population distribution. The recently developed Laser Ablation Microprobe Inductively Coupled Plasma Mass Spectrometer (LAM-ICP-MS) allows U-Pb analyses of single zircon grains. It is capable of ablating pits as small as 20 μm across, and can therefore analyze, *in situ*, the different zones in zircons with cores and overgrowths. Provided the zircons are large enough, the laser is capable of ablating multiple pits in a single zircon crystal, and these analyses may be used to create a discordia line for each grain. The LAM-ICP-MS is also capable of a high throughput (ca.

fifty analyses per day) after relatively simple sample preparation. This ability to do U-Pb analyses, with some loss of precision, more quickly than the conventional isotope dilution TIMS method makes it a valuable tool for the analysis of large numbers of detrital zircons or zircons with complex overgrowths.

5.2 Analytical Methods

5.2.1 Instrumentation and Data Acquisition

An abbreviated description of the instrumentation and analytical procedures for the U-Pb analysis of zircon grains is presented below. A more detailed description of instrumentation and methodology is presented in Appendix II. Zircon analyses were done using the Laser Ablation Microprobe-Inductively Coupled Plasma-Mass Spectrometer (LAM-ICP-MS) at Memorial University. The laser apparatus consists of a frequency quadrupled Nd: YAG laser operating in the ultraviolet at a 266 nm wavelength. The laser is routed by the use of three dielectric mirrors into the phototube of a petrographic microscope. It is then focussed onto the sample through a silica window in the ablation cell. The microscope allows the viewing and selection of sample sites in the grain mounts in the ablation cell. In order to reduce element fractionation, an ablation spot cooling jet has been incorporated into the ablation cell. Ablated material is entrained in a flow of Argon gas through polyurethane tubing to the ICP torch. The ICP-MS instrument is a FISONS Plasmaquad PQII + "S", which can detect U and Pb isotopes in low parts per billion concentrations. ICP-MS operating conditions were optimized by continuous

ablation of the NIST 612 standard, for maximum sensitivity in the heavy mass range (Lu-U). Sample ablations were done in blocks of twenty analyses. Each sample run began with the measurement of four standards (three of an in-house zircon standard and one of the NBS 612 spiked glass standard) followed by twelve sample measurements and finished with the four standards. Analysis time for each ablation pit was 120 seconds, including a 60-second background measurement prior to ablation, and a single ablation was done per sample spot. Ablation pit sizes ranged from 20-40µm. For grains with apparent cores and overgrowths, pits were ablated in both core and rim. Cathodoluminescence photographs of the various zircons were used to pinpoint internal structures for ablation. Data were acquired on five selected isotopes of Th, U and Pb (^{232}Th, ^{238}U, ^{206}Pb, ^{207}Pb and ^{208}Pb). Initial data acquisition is done using the mass spectrometer's software in the time-resolved acquisition mode, which reports signal intensity data in counts per second for each isotope. Raw counts-per-second were converted to background corrected isotopic ratios using an in-house, LOTUS-based trace element program (LAM-TRACE version 1.57). By using time-resolved acquisition, it was possible to examine the signal and integrate the most appropriate signal intervals for the background and sample measurements. It was also possible to integrate more than one signal interval from a single ablation. If a signal acquisition is long enough, it is possible to create three point discordia line from a single sample ablation. The graphic presentation of the signal data allows easy visualization of the change in isotope ratios with depth, which is especially useful when analyzing zircons with cores and rims.

5.2.2 Sample selection and preparation

For each sample, 10-30 zircon grains larger than 100 μm were handpicked for analysis. Grains were selected on the basis of clarity, and lack of alteration, inclusions and cracks. In samples with more than one population of zircon, representative samples of each type were analyzed. The grains were mounted in epoxy resin and polished. The grain mounts were placed in nanopure water in an ultrasonic to remove any residual polishing grit. The samples were then placed in a bath of 2N HNO_3 for 20 minutes to remove any surface Pb contamination.

5.3 U-Pb Results

U-Pb data for zircons from 4 samples are presented in Table 5.1. Concordia diagrams for the samples are presented in Figures 5.1, 5.2, 5.4 and 5.5. Linear regressions were done using the method of Davis (1982). Age uncertainties, errors on regression calculations and error ellipses on concordia plots are given at a 2σ confidence limit. The percent discordance of analyses was calculated by comparing $^{206}Pb/^{238}U$ and $^{207}Pb/^{206}Pb$ ages. Concentrations of U and U/Th ratios were approximated using background corrected counts-per-second. Both of these methods are described in Appendix II.

5.3.1 Tonalite gneiss (94KE241GD)

As described in Chapter 4, one population of zircon is present in the tonalite gneiss. These are medium sized, brown prisms with square cross sections and pointed to slightly

Table 5.1: LAM-ICP-MS U-Pb Analytical Results

Fraction	Counts/Sec			Atomic Ratios						Age (Ma) +/- 2σ					
	^{238}U (ppm)	^{238}U	^{232}Th	$\frac{^{206}Pb}{^{238}U}$	2σ	$\frac{^{207}Pb}{^{235}U}$	2σ	$\frac{^{207}Pb}{^{206}Pb}$	2σ	$\frac{^{206}Pb}{^{238}U}$		$\frac{^{207}Pb}{^{235}U}$		$\frac{^{207}Pb}{^{206}Pb}$	
Tonalite gneiss (94KE241GD): zoned zircon															
Z1 brn prism	416	551650	122233	0.4845	102	16.0730	4018	0.24058	217	2547	42	2881	24	3122	14
Z2 brn prism	124	165166	73386	0.5888	80	19.9173	3227	0.24532	236	2985	32	3087	16	3154	16
Z3 brn prism	105	138956	68896	0.6250	65	22.6761	2676	0.26312	242	3130	26	3213	11	3264	14
Z4 brn prism	293	322556	101164	0.5440	53	18.4186	2394	0.24555	192	2800	22	3012	13	3156	12
Z5 brn prism	151	166343	61181	0.5567	55	18.4709	2253	0.24064	366	2853	23	3015	12	3124	24
Z6 brn prism	394	433027	131579	0.5254	49	17.0409	1840	0.23521	132	2722	21	2937	10	3086	10
Z7 brn prism	154	168999	74636	0.5788	59	19.8696	2782	0.24895	289	2944	24	3085	14	3178	18
Z8 brn prism	227	249313	109368	0.5373	39	18.1286	1813	0.24469	186	2772	16	2997	10	3150	12
Z9 brn prism	94	102809	40408	0.5916	83	20.9854	3316	0.25726	566	2996	34	3138	15	3230	34
Z10 brn prism	586	766227	130230	0.4814	60	15.8371	1964	0.23860	110	2533	26	2867	12	3110	8
Z11 brn prism	92	119763	43565	0.6180	37	21.3003	2428	0.24997	280	3102	15	3152	11	3184	18
Z12 brn prism	98	128571	49091	0.5652	80	18.9920	3912	0.24371	258	2888	33	3041	20	3144	18
Z13 brn prism	287	375344	236571	0.5686	84	18.7941	2782	0.23972	163	2902	35	3031	14	3118	10
Z14 brn prism	103	134129	51184	0.5514	72	18.3455	2789	0.24131	386	2831	30	3008	15	3128	26
Z15 brn prism	288	375766	240412	0.5371	70	17.8917	2505	0.24157	155	2771	29	2984	14	3130	10
Z16 brn prism	122	159337	50388	0.5605	73	19.4446	2295	0.25159	332	2869	30	3064	11	3194	20
Tonalite gneiss (94KE241GD): unzoned zircon															
Z1 brn prism	73	96987	35235	0.5989	66	21.5822	2504	0.26137	324	3025	27	3165	11	3254	20
Z2 brn prism	116	153330	70805	0.6001	41	21.5082	2151	0.25994	229	3030	16	3162	10	3246	14
Z3 brn prism	98	130617	36635	0.5957	70	20.7264	3482	0.25234	270	3012	28	3126	16	3198	18
Z4 brn prism	105	139790	51876	0.5503	43	18.7816	2404	0.24753	297	2826	18	3031	12	3168	20
Z5 zoned prism	288	382485	263246	0.5914	41	19.5477	1486	0.23974	201	2995	17	3069	7	3118	14

Fraction	Counts/Sec			Atomic Ratios						Age (Ma) +/- 2σ					
	^{238}U (ppm)	^{238}U	^{232}Th	$\frac{^{206}Pb}{^{238}U}$	2σ	$\frac{^{207}Pb}{^{235}U}$	2σ	$\frac{^{207}Pb}{^{206}Pb}$	2σ	$\frac{^{206}Pb}{^{238}U}$		$\frac{^{207}Pb}{^{235}U}$		$\frac{^{207}Pb}{^{206}Pb}$	
Z6 brn prism	91	120572	55862	0.6206	63	22.3971	2553	0.26174	361	3112	25	3201	11	3256	22
Z7 brn prism	115	126800	69447	0.6158	43	22.1318	2036	0.26064	229	3093	17	3190	9	3250	14
Z8 brn prism	134	147553	55125	0.5675	30	19.3301	1933	0.24703	262	2898	12	3058	10	3164	18
Z9 brn prism	125	136951	54843	0.5943	50	21.3755	2779	0.26085	292	3007	20	3156	13	3250	18
Z10 brn prism	141	154600	89543	0.5902	72	21.2683	2552	0.26135	277	2990	29	3151	12	3254	16
Z11 brn prism	296	325831	277441	0.5981	44	19.3110	1390	0.23418	155	3022	18	3057	7	3080	12
Z12 zoned prism	377	415190	302136	0.5391	47	17.9557	1580	0.24154	145	2780	20	2987	9	3130	10

Granite gneiss (94KE241)

Fraction															
Z1 lbrn prism (c)	707	760205	214156	0.4902	77	15.7008	3957	0.23240	307	2571	34	2859	24	3068	22
Z2 lbrn prism (c)	640	688661	194755	0.5802	233	18.8910	8652	0.23622	222	2950	95	3036	44	3094	16
Z3 lbrn prism (c)	1163	1251604	248288	0.4817	339	15.3199	17832	0.23074	1094	2535	147	2835	111	3056	76
Z4 lbrn prism (c)	448	481815	229609	0.6563	145	22.6774	11792	0.25071	737	3253	57	3213	50	3188	48
Z5 lbrn prism (r)	442	475407	288013	0.7080	61	25.2523	7071	0.25877	750	3451	23	3318	27	3238	44
Z6 lbrn prism (c)	556	598663	193554	0.5750	90	19.0100	3004	0.23985	225	2928	37	3042	15	3118	16
Z7 lbrn prism (r)	722	776979	293027	0.5292	131	17.2079	5094	0.23588	311	2738	56	2946	28	3092	22
Z8 lbrn prism (r)	1462	1572804	260440	0.4365	191	12.9858	9584	0.21584	850	2335	86	2679	70	2948	64

Migmatitic paragneiss (94KE240M)

Fraction															
Z1 brn prism	430	420190	137496	0.3670	68	10.2142	1593	0.20186	202	2015	32	2454	15	2840	16
Z2 brn prism	365	356316	109413	0.4833	248	13.5118	6972	0.20276	239	2542	108	2716	49	2848	20
Z3 brn prism	528	515198	215378	0.4209	54	11.7785	1790	0.20296	211	2265	25	2587	14	2850	18
Z4 brn prism	766	748284	15108	0.4074	44	11.3843	1571	0.20268	149	2203	20	2555	13	2846	12
Z5 brn prism	842	821861	50734	0.4382	278	12.2425	7492	0.20261	142	2343	125	2623	57	2846	12
Z6 rnd detr	169	165487	62006	0.5225	190	16.4843	5770	0.22879	444	2710	80	2905	33	3042	32
Z7 rnd anh	531	518322	128748	0.2159	181	6.1313	5224	0.20596	251	1260	96	1995	74	2874	20

Fraction	^{238}U (ppm)	^{238}U	^{232}Th	$\frac{^{206}Pb}{^{238}U}$	2σ	$\frac{^{207}Pb}{^{235}U}$	2σ	$\frac{^{207}Pb}{^{206}Pb}$	2σ	$\frac{^{206}Pb}{^{238}U}$		$\frac{^{207}Pb}{^{235}U}$		$\frac{^{207}Pb}{^{206}Pb}$	
		Counts/Sec				*Atomic Ratios*						*Age (Ma) +/- 2σ*			
Z8 rnd anh	1416	1382978	183460	0.2696	245	6.8842	6981	0.18519	200	1539	124	2097	90	2698	18
Z9 rnd anh	1671	1631875	942247	0.2581	435	6.5764	12969	0.18480	347	1480	223	2056	174	2696	30
Z10 rnd anh	1284	1253706	162595	0.3831	388	10.7834	11258	0.20412	155	2091	181	2505	97	2858	12
Z11 rnd detr*	NA	NA	NA	0.6322	149	19.1664	5635	0.21987	405	3158	59	3050	28	2978	30
'Nerak granite' (94KE223)															
Z1 pink bpy prism	169	217965	99615	0.5997	73	21.0738	4046	0.25468	387	3029	29	3142	19	3214	22
Z2 pink bpy prism	187	240190	47336	0.5304	69	16.9865	2616	0.23209	334	2743	29	2934	15	3066	22
Z3 pink bpy prism	471	606190	144095	0.4257	83	12.0888	3191	0.20576	251	2286	38	2611	25	2872	20
Z4 pink prism	88	113699	63647	0.6211	77	20.8020	3744	0.24265	422	3114	30	3129	17	3136	28
Z5 pink prism	104	133217	53521	0.5975	69	20.2679	4256	0.24574	555	3020	28	3104	20	3156	36
Z6 brn prism	144	185387	123528	0.5010	109	14.4232	3548	0.20852	284	2618	47	2778	23	2894	22
Z7 brn prism	441	567127	319907	0.5518	50	15.7360	1668	0.20657	285	2833	21	2861	10	2878	22
Z8 brn prism	255	328456	144141	0.4407	152	12.4451	5103	0.20453	479	2354	68	2639	39	2862	38
Z9 brn prism	76	98315	59164	0.5304	84	15.0202	3755	0.20510	336	2743	35	2817	24	2866	28
Z10 brn prism	187	240856	138624	0.5743	67	16.3109	2316	0.20571	214	2926	27	2895	14	2872	18
Z11 pnk sq prism	235	302782	137613	0.5355	145	17.0571	6141	0.23072	332	2765	61	2938	35	3056	24
Z12 pnk bpy prism	588	756088	260725	0.3927	160	10.8792	5113	0.19844	238	2156	74	2513	44	2812	20
Z13 pnk bpy prism*	NA	NA	NA	0.4956	100	16.2376	4514	0.23746	399	2595	43	2891	27	3102	28
Z14 pnk bpy prism*	NA	NA	NA	0.4615	101	14.0745	4251	0.22098	331	2446	44	2755	29	2986	24

Notes: [a]Z, zircon; anh, anhedral; bpy, bipyramidal; brn, brown; detr, detrital; lbrn, light brown; pnk, pink; rnd, round; (c), core analysis; (r) rim analysis; * refers to second signal increment from one ablation.

[b] Uncertainties on isotope ratios refer to the final digits. Ages calculated using the method of Davis (1982).

resorbed terminations. Internal zoning is present in some grains. Two fractions of the best, large (>150 μm) zircon prisms were picked from the 1^0 nonmagnetic and magnetic mineral separates. Analyses were done on 10 zircons with internal zoning and 10 unzoned zircons. For both the zoned and unzoned zircons, analyses were taken from both cores and rim, to rule out the presence of possible cryptic cores.

Analytical Results

Sixteen zircon analyses from the zoned population and 12 analyses from the unzoned population are shown in Figures 5.1a and 5.1b respectively. For the unzoned zircon, a discordia line through the five least discordant data points farthest to the right gives an upper intercept age of 3259 +77/-28 Ma, and a lower intercept of 275 +1175/-1489 Ma at an 85% probability of fit (Figure 5.1a). A discordia through the five data points from the zoned zircon population which plot farthest to the right provides an older upper intercept age of 3291 +23/-20 Ma and a lower intercept of 1114 +108/-101 Ma at a 73% probability of fit (Figure 5.1b). Both samples show the same scatter of data points, with no apparent age differences between core and rim analyses.

5.3.2 Granite gneiss (94KE241)

Zircons from the granite gneiss consist of one population of medium sized, light brown prisms with rounded, resorbed terminations (see Figure 4.1b). These zircons display dark central zones that were interpreted as being potential xenocrystic cores. Five large (>100 μm) zircon prisms were mounted, polished and analyzed by laser ablation.

Figure 5.1a: U-Pb concordia diagram of zoned zircon LAM-ICP-MS analyses from tonalite gneiss (94KE241GD). Ellipses are for 2σ uncertainties. Grey ellipses represent core analyses, colourless ellipses represent rim analyses. Dotted line represents discordia determined by TIMS analysis.
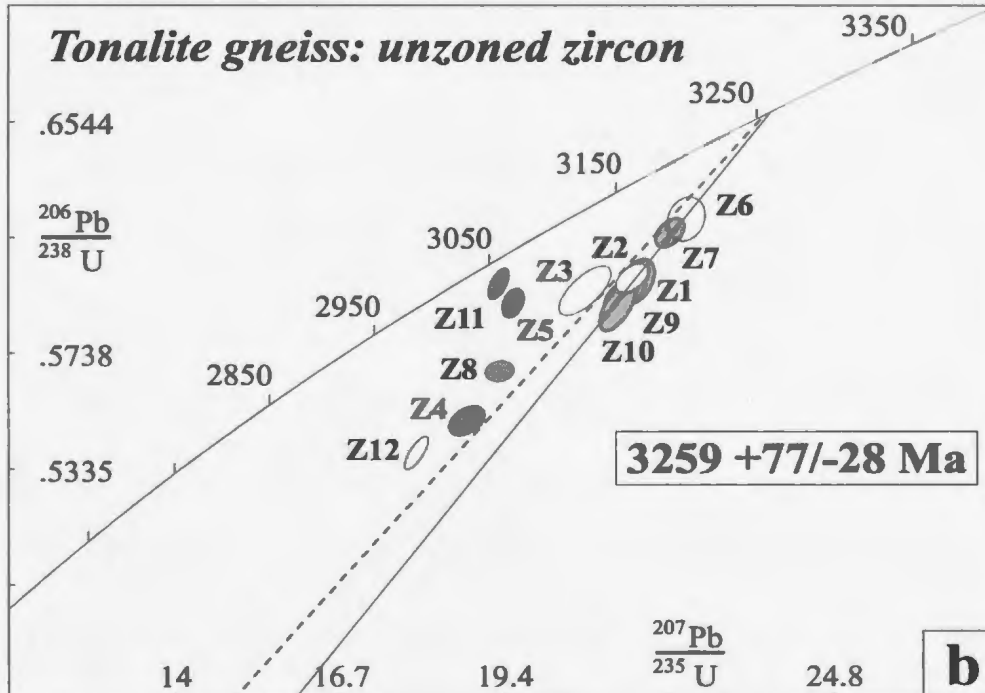
Figure 5.1b: U-Pb concordia diagram of unzoned zircon LAM-ICP-MS analyses from tonalite gneiss (94KE241GD). Ellipses are for 2σ uncertainties. Grey ellipses represent core analyses, colourless ellipses represent rim analyses. Dotted line represents discordia determined by TIMS analysis.

Analytical Results

The analysis of five large, zoned zircons yielded eight data points, five from cores and three from rims (Figure 5.2*a*). All of the data points are roughly colinear, and generate a discordia line with an upper intercept of 3169 +32/-25 Ma and a lower intercept of 1105 +/-260 Ma using the error expansion routine of Davis (1982). By excluding Z2 and Z8, which plot slightly to the left of the linear array of points, the upper intercept becomes 3168 +28/-22 Ma, with a lower intercept of 925 +215/-205 Ma and a 45% probability of fit (Figure 5.2*a*). Both of these ages are younger than the 3216 +14/-13 TIMS U-Pb, upper intercept age for this unit (see Figure 4.3*b*). The colinear nature of the data, and the absence of a pattern of old cores vs. young overgrowths, suggests that the zoning in these zircons is due to igneous growth and is not a function of inheritance.

5.3.3 Migmatitic paragneiss (94KE240M)

Two zircon populations are present in the paragneiss. The first consist of small (<75 μm), round to flattened oval grains which are colourless to turbid, and have many opaque inclusions. Zircon from this population appears strongly resorbed, and some have recrystallized to form framboidal aggregates. Zircon from the second population consists of small, light brown prisms with square cross-sections and rounded terminations. Many of these contain round, colourless to white, turbid cores, suggesting they may be later euhedral overgrowths on original detrital zircons. Twenty-nine zircons were chosen for analysis, 22 from the round, anhedral population, and seven prisms with cores. Analyses using 20 μm ablation pits were done on both core and rims of zoned prisms and cores
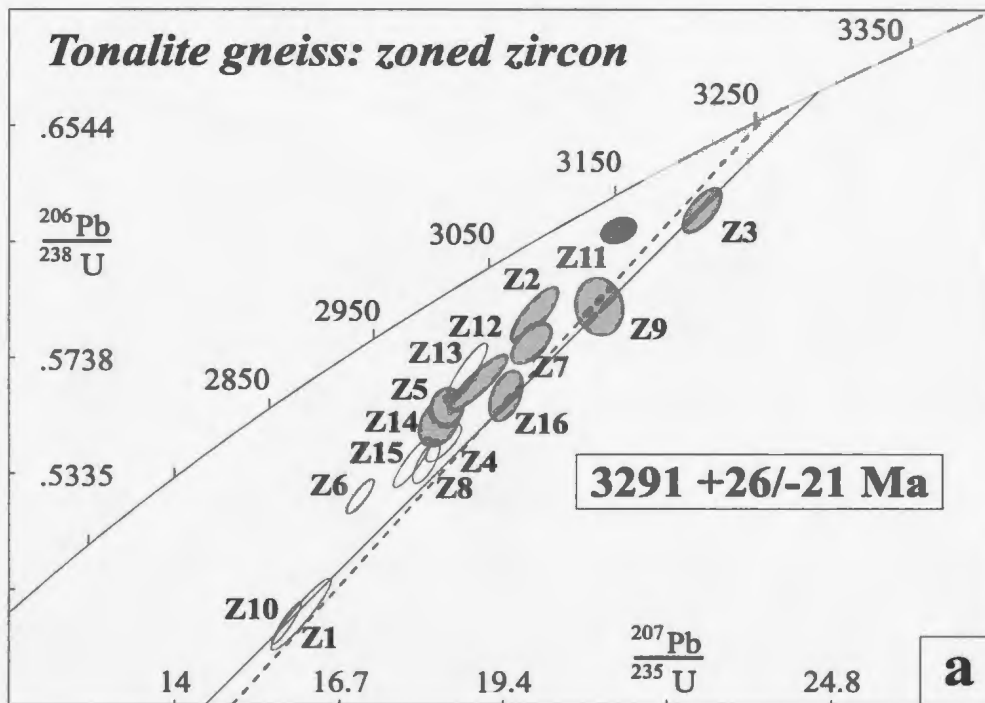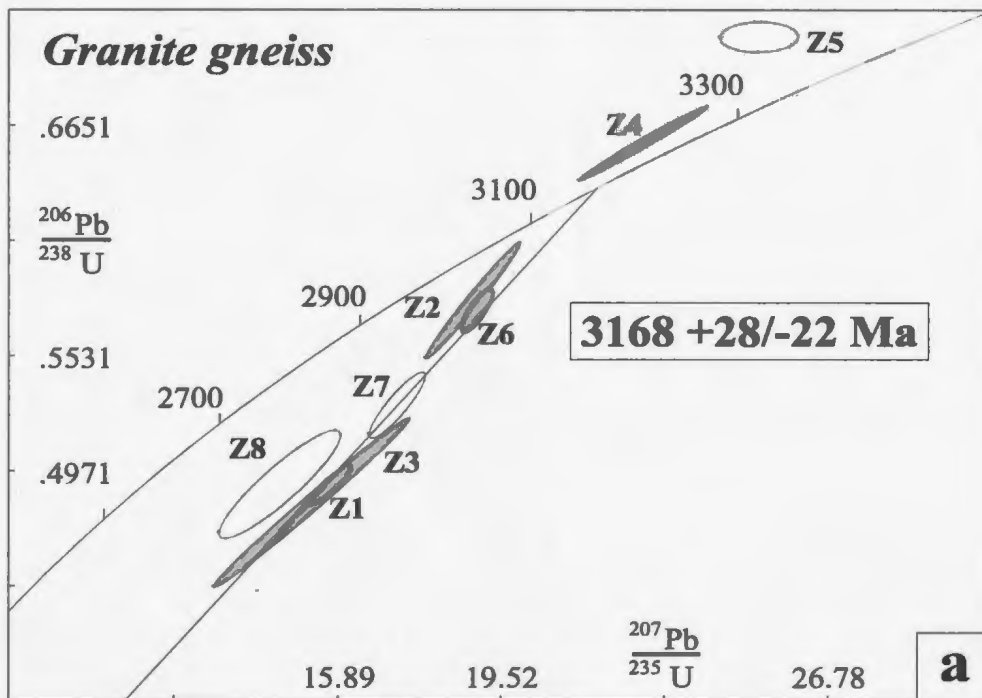
Figure 5.2a: U-Pb concordia diagram of zircon analyses from granite gneiss (94KE2411). Ellipses are for 2σ uncertainties. Grey ellipses represent core analyses, colourless ellipses represent rim analyses.
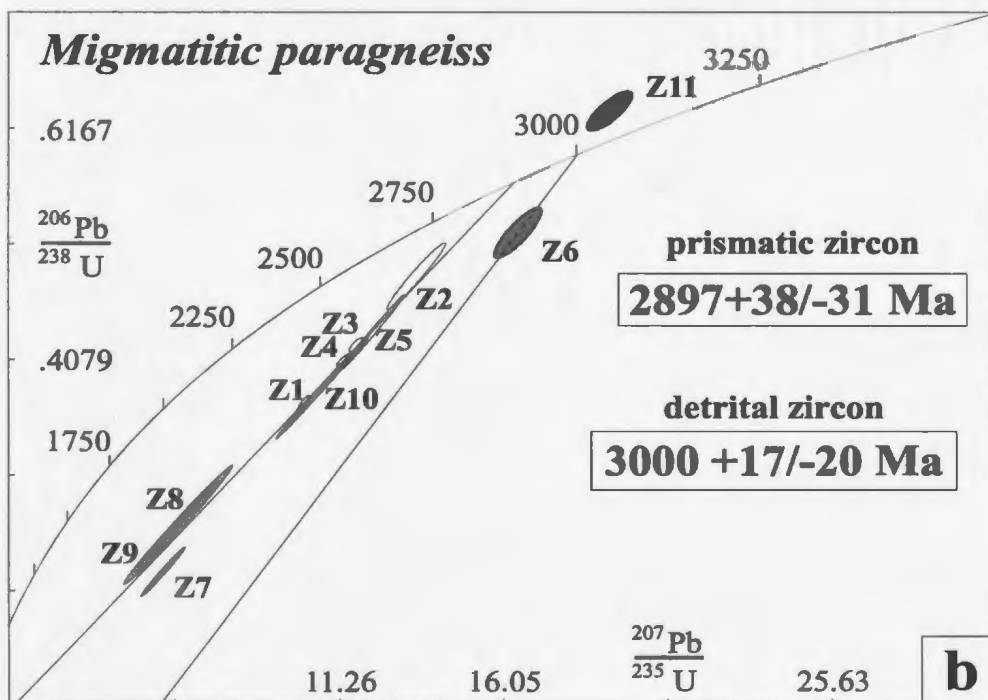
Figure 5.2b: U-Pb concordia diagram of LAM-ICP-MS zircon analyses from migmatitic paragneiss (94KE240M). Ellipses are for 2σ uncertainties. Light grey ellipses represent core analyses, colourless represents rim analyses. Dark grey ellipses are analyses from the same grain of inferred detrital origin.

Figure 5.3

Figure 5.3:   (*a*) anhedral, inclusion-rich zircon grain from the migmatitic paragneiss (94KE240M). Zircon is 100 μm in diameter.
(*b*) subhedral zircon from the migmatitic paragneiss. Note the inclusion-rich core with faint laminar zoning in the surrounding rim. Zircon is 120 μm long.
(*c*) round, possibly detrital zircon from the migmatitic paragneiss. Note growth zoning truncated by rounded grain surface. The black hole in the lower left of the photo is a laser ablation pit. Zircon is 150 μm long.
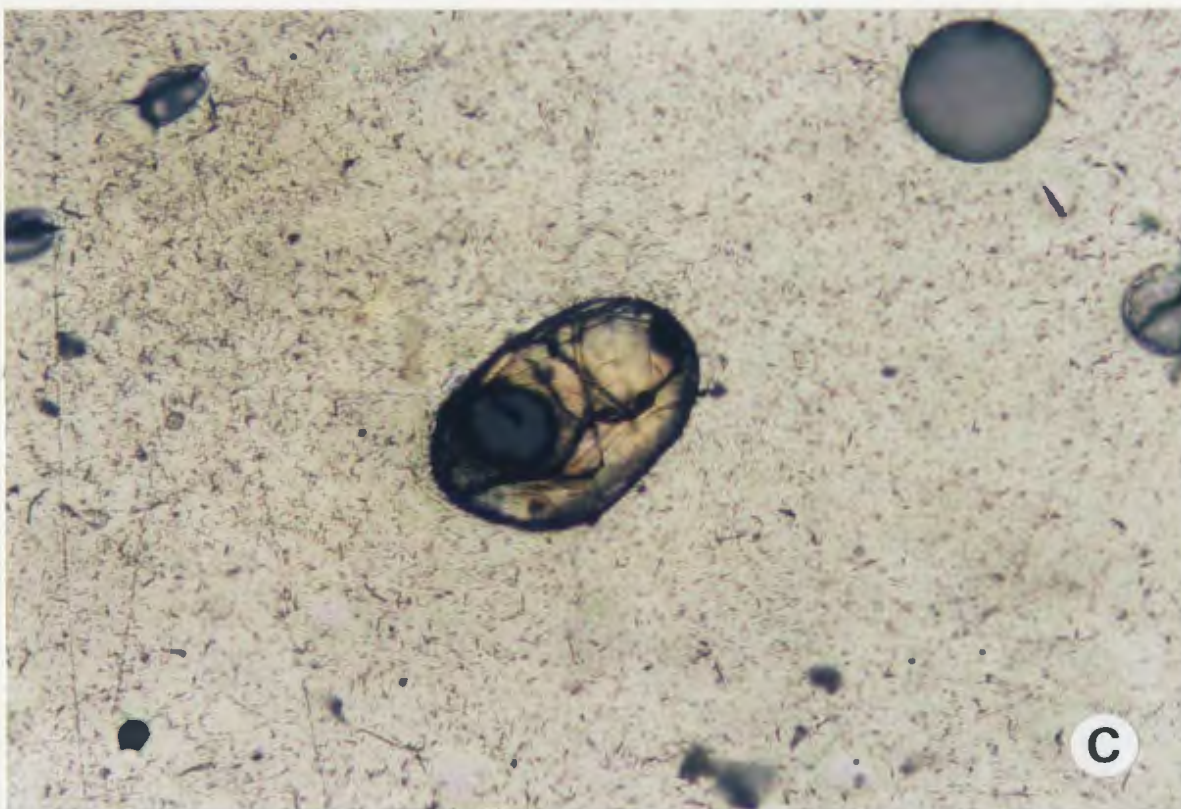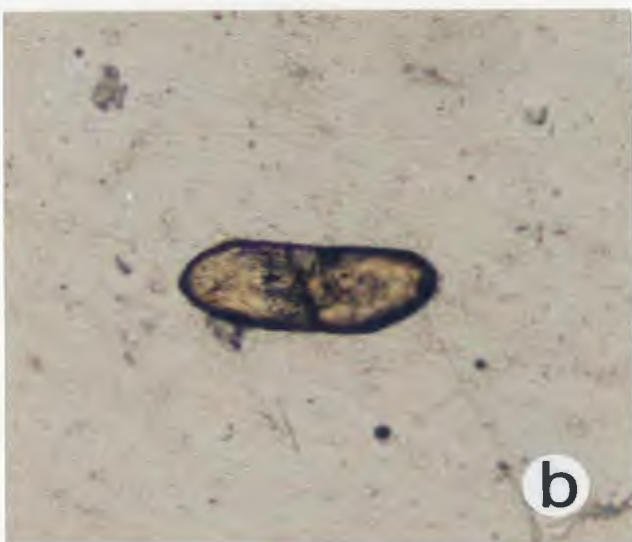
only of round grains. Due to the small size of the grains and their fractured, inclusion-rich nature (Figure 5.3 *a, b*), 12 grains shattered during ablation and only 10 viable analyses were obtained.

Analytical Results

Analyses from both round and prismatic zircon grains give data points which generate a discordia line with an upper intercept of 2853 +19/-18 Ma and a lower intercept of -15 +131/-140 Ma after error expansion. Data points from the rounded grains tend to be very discordant or have large error ellipses. When only the data points from analyses of prismatic zircon (Z1-Z5) are included, a discordia line is produced with an upper intercept of 2897 +38/-31 Ma and a lower intercept of 293 +196/-200 Ma with a 29% probability of fit (Figure 5.2*b*). One data point (Z6), a 20-second signal from a round, anhedral zircon, falls to the right of this discordia line. By taking the next 12 seconds of the acquired signal for this grain, a second data point (Z11) from a deeper level in the same grain is generated. Z6 has a ^{207}Pb/^{206}Pb age of 3042 Ma and is 11% discordant while Z11 has a ^{207}Pb/^{206}Pb age of 2978 Ma and is -6% discordant. When a discordia line is calculated for these two analyses, an upper intercept age of 3000 +17/-20 Ma is obtained. Microscopic examination of this grain reveals oscillatory growth zoning truncated by the rounded surface of the zircon (Figure 5.3*c*), implying this is one of a population of detrital zircons.

5.3.4 'Nerak granite' (94KE223)

Single grains from two populations of zircon from the 'Nerak granite' were analyzed. Four grains were medium-sized, brown, rectangular to equant prisms and four other grains were medium-sized, pink, bipyramidal prisms. When examined using cathodoluminescence, the brown zircon showed evidence only of igneous growth zoning, while the pink zircon has obvious luminous cores and dark overgrowths (see Figures 5.4 and 5.5). Laser ablation analyses were done on the cores and overgrowths in the pink zircon and in the cores only of the brown zircon.

Analytical Results

The data points from the brown zircon population generate a discordia line with an upper intercept age of 2878 +12/-11 Ma and a lower intercept age of -38 +317/-346 Ma with a 28% probability of fit (Figures 5.4c and 5.5c). Data points from the pink population of zircon appear to fall along two discrete discordia lines representing ages of older xenocrystic zircon. In Figure 5.4c, Z4 and Z5 are core and overgrowth analyses from the zircon shown in Figure 5.4a; Z11 is core analysis from another zircon. A discordia line through these three data points has an upper intercept age of 3165 +57/-34 Ma. The error ellipse for the Z4 analysis overlaps concordia, while the data point for Z5 plots only slightly below it. This suggests that, in spite of obvious internal zoning, the zircon in Figure 5.4b is all one age. In Figure 5.5c, analyses Z1, Z2, Z3 and Z12 are from the core and rim of the zircon in Figure 5.5a, Z13 and Z14 were generated by integrating data from a second 20 second signal increment for Z1 and Z2 respectively. A discordia

Figure 5.4
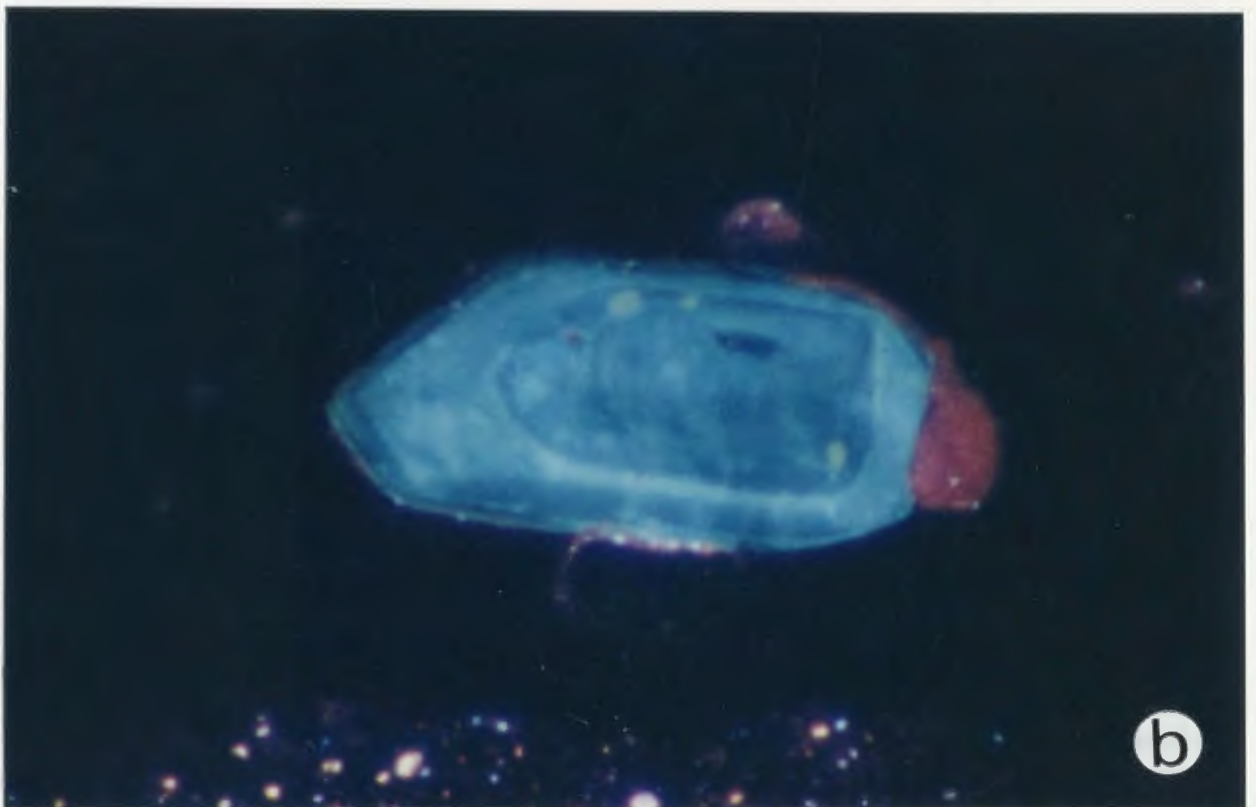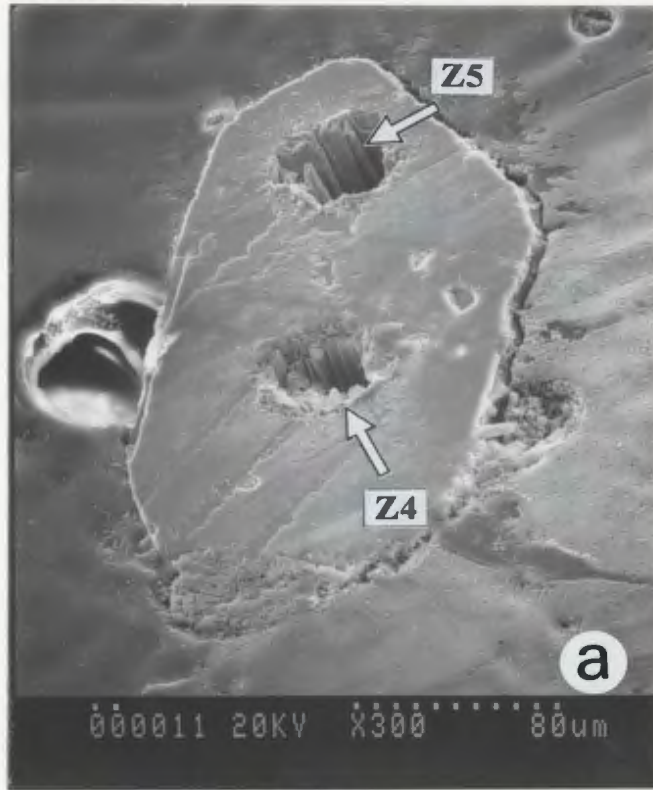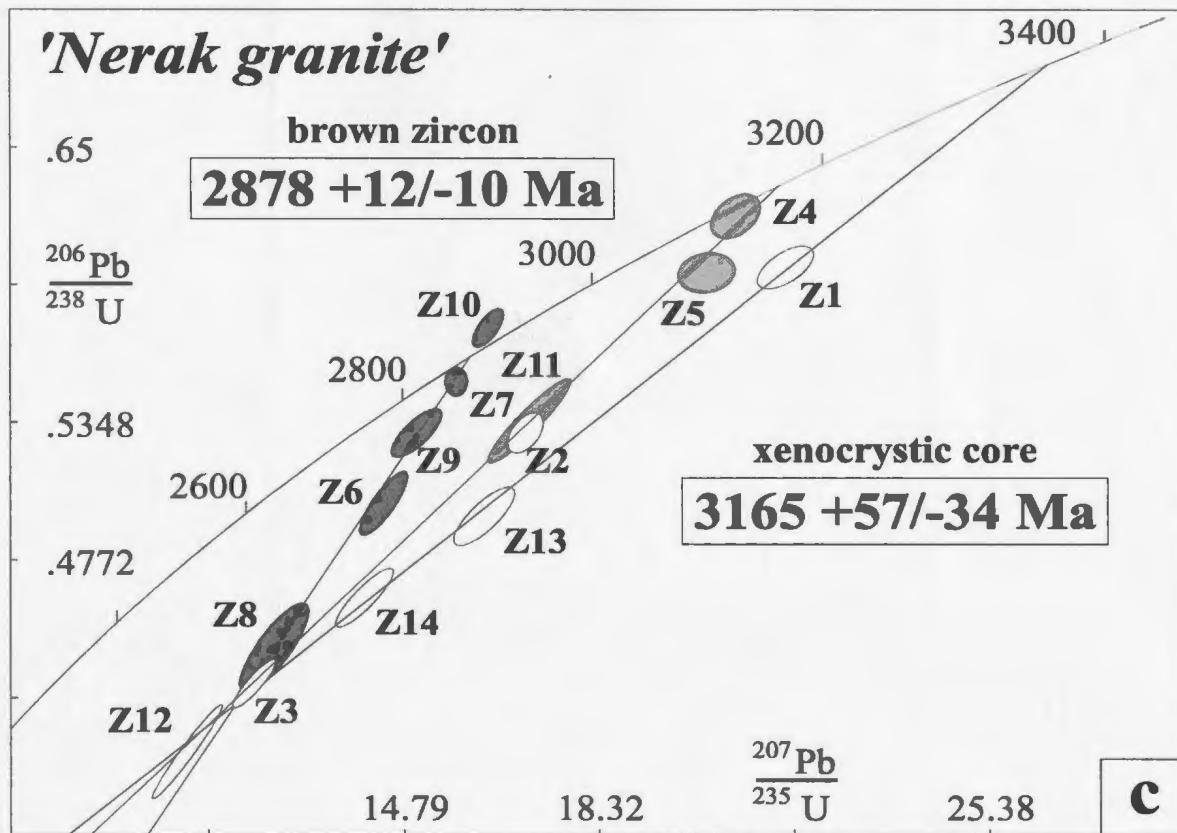
Figure 5.4: (a) Scanning electron microscope photo of zoned pink zircon from the 'Nerak granite'. Holes in zircon are ablation pits from LAM-ICP-MS analyses. Labels indicate data points seen in 5.4*c*.
(b) Cathodoluminescence micrograph of the zircon in 5.4*a*. Zircon grain is 290 μm long. Note the apparent internal zoning within the zircon: a central, core surrounded by a lighter, euhedral overgrowth with oscillatory zoning.
(c) U-Pb concordia diagram of LAM-ICP-MS zircon analyses from 'Nerak granite'. Ellipses are for 2σ uncertainties. Medium grey ellipses represent analyses from the zircon in Figure 5.4*b*. Dark grey ellipses are analyses of brown zircon

Figure 5.5
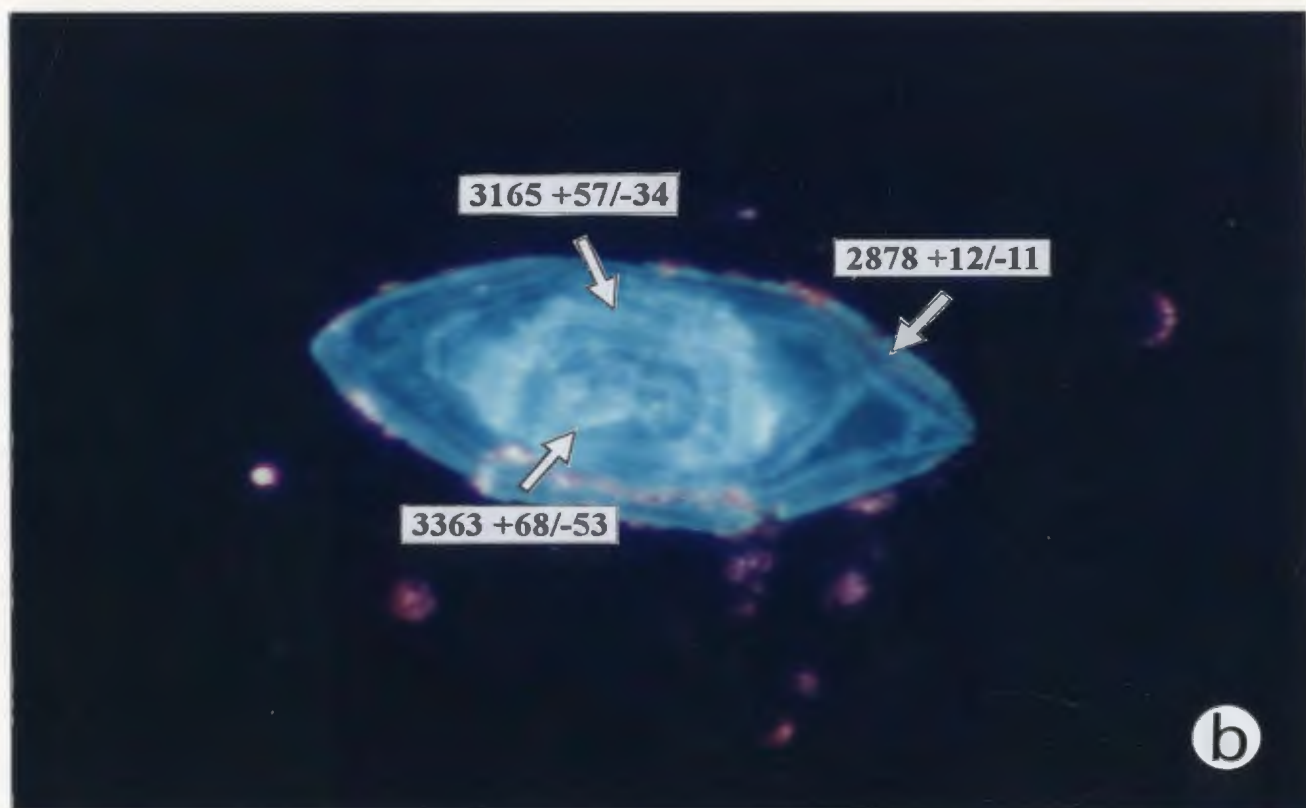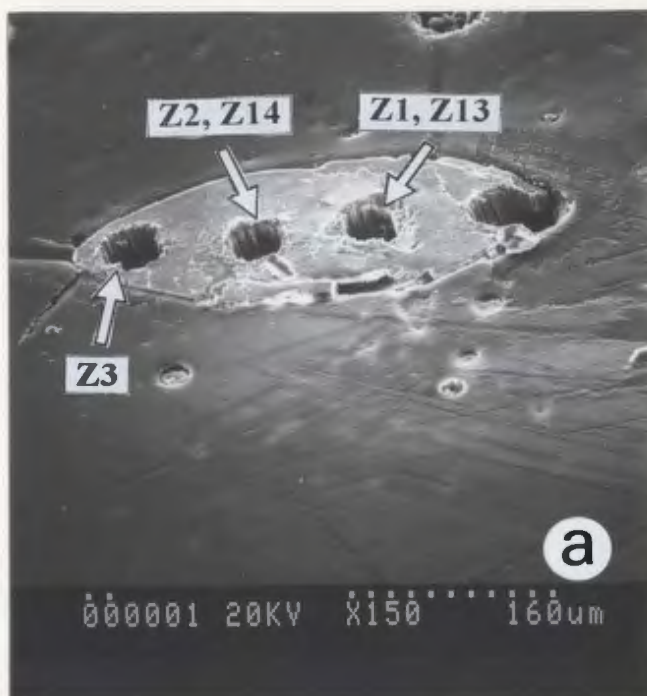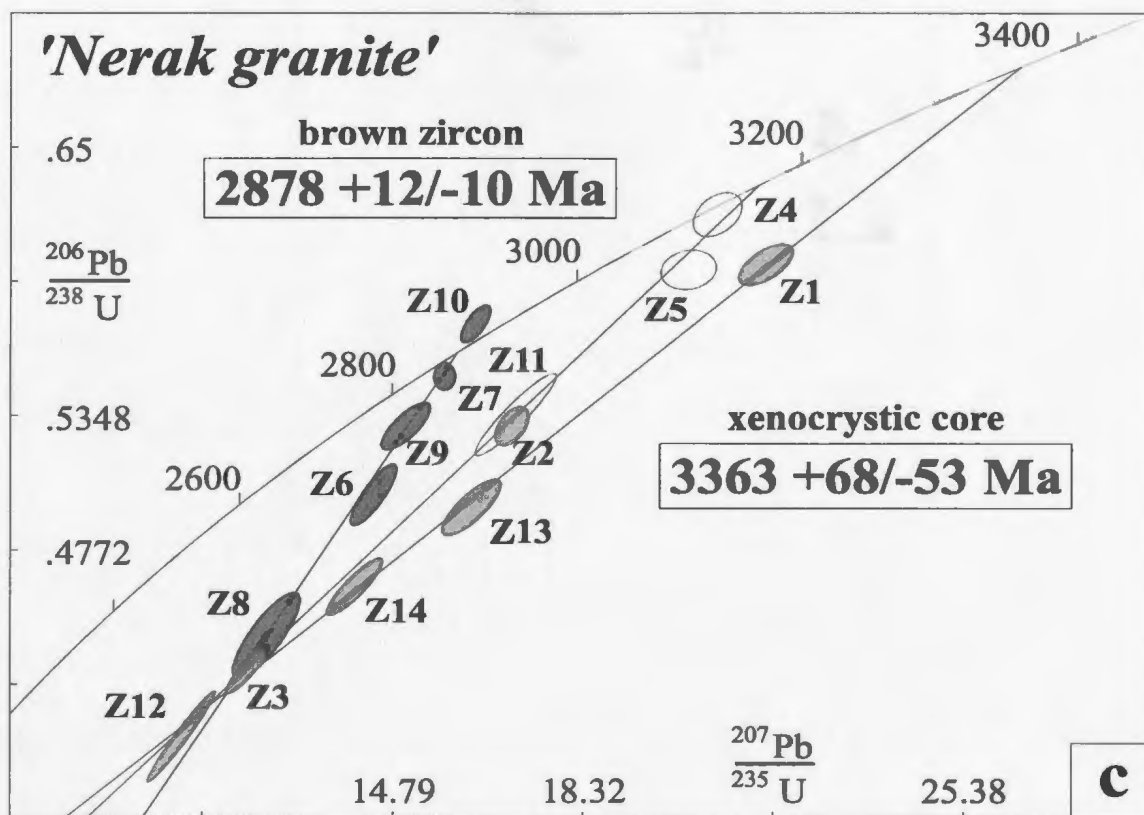
Figure 5.5: (a) Scanning electron microscope photo of zoned pink zircon from the 'Nerak granite'. Holes in zircon are ablation pits from LAM-ICP-MS analyses. Labels indicate data points seen in 5.5c.
(b) Cathodoluminescence micrograph of the zircon in 5.5a. Zircon is 370μm long. Note the three distinct zones within the zircon: a central, dark, oval core surrounded by a lighter overgrowth and finally a darker, zoned, euhedral overgrowth. Ages for each phase are indicated with arrows.
(c) U-Pb concordia diagram of LAM-ICP-MS zircon analyses from 'Nerak granite'. Ellipses are for 2σ uncertainties. Medium grey ellipses represent analyses from the zircon in Figure 5.5b. Dark grey ellipses are analyses of brown zircon

line generated by Z1, Z13 and Z14 yields an upper intercept age of 3363 +68/-53 Ma and a lower intercept of 1520 +165/-162 Ma with a 31% probability of fit. It is interesting to note that Z2 overlaps the error ellipse of data point Z11. This implies two generations of overgrowth may be present on the core of the zircon in Figure 5.5*b*.

5.4 Discussion of Results

When compared with the 3254 +13/-6 Ma age for the tonalite gneiss produced by the TIMS U-Pb analysis (Figure 4.3*a*), the ages as determined by LAM-ICP-MS (3259 +77/-28 and 3291 +26/-21 Ma) are slightly older. In both cases, the data produced shows the same distribution of points as seen in the TIMS data. The scatter of data points to the left of the discordia line is interpreted as being the result of radiogenic Pb loss from a single igneous population of zircon. This pattern does not appear to be due to analytical mixing of older inherited and younger igneous zircon since no difference in age is apparent between data points from core analyses and those from the apparent overgrowths. Concentrations of uranium and uranium/thorium ratios, calculated from the background corrected counts-per-second calibrated on the in-house zircon standard, indicate no difference between the two populations. Two mechanisms for producing the apparent cores and rims would be a hiatus in zircon growth or injection of new magma during crystallization of the tonalite. This could result in resorption of zircon, creating apparent oval 'cores'.

Data points from the granite gneiss yield a discordia with a younger upper intercept age (3168 +28/-22 Ma) than the 3216 Ma age derived from TIMS U-Pb analysis. This

young age could be a result of low ^{207}Pb counts on the standard used. The zircon used as the standard is 295 +/-1 Ma old and does not contain high concentrations of ^{207}Pb. Combined with the small ablation pit size used for most samples, this would result in low counts-per-second of ^{207}Pb from the standard, creating larger uncertainties in the ^{207}Pb/^{235}U ratios. For these analyses, the ^{207}Pb/^{235}U ratios were calibrated indirectly using the ^{206}Pb/^{238}U ratios (see Appendix II). Whether this calibration adequately reflects the actual ^{207}Pb count rates, or whether the larger uncertainties could conceivably systematically shift data points to the left on the concordia diagram is unknown. Conversely, 3168 Ma could represent the true age of this gneiss. It should be noted that the three least discordant data points for this gneiss, as determined by TIMS methods, yield a discordia with an upper intercept age of 3200 +58/-40 Ma. This is well within the uncertainty for the LAM-ICP-MS age. It is also interesting to note that one xenocrystic zircon core from the 'Nerak granite' has an age of 3165 Ma.

The zircon data points from the migmatitic paragneiss fall along a discordia to 2897 +38/-31 Ma. The colinear distribution of data points for both rounded and prismatic zircon suggests that both populations formed during the same event. The inclusion-rich nature of these zircons, coupled with low Th/U ratios in some grains (0.02-0.12) argues that part of this population is metamorphic. It is possible that these zircons represent a population formed in partial melts in the metasediments during the granulite facies metamorphic event. If so, this would put the age of high-grade metamorphism at ca. 2900 Ma. However, the LAM-ICP-MS zircon age is also within uncertainty of the zircon age generated by TIMS U-Pb analysis for the pegmatitic granite (2881 +4/-3 Ma). Since the pegmatitic granite intrudes the migmatitic paragneiss at the sample location, it is the

conceivable that heat and rare earth element-rich fluids derived from this granite might cause the crystallization new metamorphic zircon. The two data points that fall to the right of this discordia likely represent the age from an actual detrital grain. The photomicrograph showing truncated growth zoning in this grain tends to support this interpretation (Figure 5.3c). A discordia forced through these two points gives an upper intercept of 3000 +17/-20 Ma. If this is the actual age then the metasedimentary rocks must be younger than ca. 3000 Ma. Since granulite metamorphism predates the intrusion of the megacrystic granites at ca. 2880 Ma, this leaves a roughly 120 Ma 'window' for the high-grade event to take place.

Data points from the two zircon morphologies in the 'Nerak granite' reveal a population of magmatic zircon as well as least two distinct ages of xenocrystic zircon. Data points from the brown zircon have a discordia with an upper intercept of 2878 +12/-11 Ma. This agrees, within uncertainty, with the 2887 +/-2 Ma age determined by TIMS U-Pb analysis (Figure 4.7a). The absence of xenocrystic cores in this population suggests that these are magmatic zircons. The population of pink zircons has a more complex history. The zircon in Figure 5.4b is morphologically more like a square igneous prism than the multifaceted bipyramidal prisms typical of the pink population. The Th/U ratios for this zircon are between 0.40-0.56, values associated with igneous rather than metamorphic zircon. The zircon shown in Figure 5.5b appears to have two generations of overgrowth. One data point (Z3) is colinear with the discordia produced by the brown, igneous zircon. A second data point (Z2) overlaps with a point (Z11) on the 3165 Ma discordia. Data points from the core of this zircon form a colinear array with an upper intercept of 3368 Ma. This suggests that the 'Nerak granite' sampled at least two older

phases of crustal rocks prior to crystallization. What this pattern of overgrowths also seems to suggest is a possible magmatic event at ca. 3165 Ma, crystallizing new zircon on ca. 3363 Ma grains.

It is interesting to note that none of these data points indicative of possible inheritance were present in the data from the TIMS analyses of this same rock. This may be due to several factors, such as old, fragile, radiation-damaged cores being lost during aggressive abrasion to remove the more robust, lower uranium overgrowths. Also, bias may be introduced during the selection of grains for analysis. If only the best grains are picked, the relatively turbid, inclusion-rich cores may be excluded.

Chapter 6: Discussion and Conclusions

6.1 U-Pb Results from the Eokuk Uplift

The combination of detailed lithological and structural mapping (Jackson, 1996), petrographic study and U-Pb geochronology of igneous and metamorphic minerals in key rock units permits the deciphering of much of the tectonic history of the Eokuk Uplift. The evolution of rocks in the study area appears to have taken place over ~650 Ma. This time span can be subdivided into 5 different periods, during which the main depositional, plutonic and metamorphic events occurred (Figure 6.1). Each period is discussed as a separate section below. Radiometric age data from rocks in the northern parts of the main body of the Slave Province show several points of similarity compared to age data from the Eokuk Uplift. However, the southern part of the Slave Province shows a different pattern of dates from those found in the north and in the Eokuk Uplift. This suggests that the old gneissic rocks in the Slave Province may be composed of two different basement blocks, each with its own lithotectonic history.

6.1.1 3.25-2.90 Ga: Early crustal formation and evolution

Early crustal formation in the study area spanned over 200 Ma, from >3254 to ~2880 Ma. Included in this period are at least one episode of deposition of supracrustal rocks, an upper amphibolite to granulite grade metamorphic event and the deformation event (F_2) that deformed the metamorphic fabric. The ages of high-grade metamorphism and supracrustal deposition in the study area have not been directly dated, but the megacrystic granites, which contain xenoliths of mafic gneiss and paragneiss that retain relict granulite mineral assemblages and textures, are dated at ca. 2880 Ma. They also cut the shallowly plunging F_2 folds associated with the older gneiss assemblage. Though locally deformed, the granites do not display the degree of structural complexity, recrystallization or migmatization seen in the gneisses, indicating that they were emplaced after peak metamorphism and F_2 folding. Thus, the supracrustal gneisses, the high grade metamorphic event and F_2 folding must pre-date 2880 Ma. The results from the LAM-ICP-MS analyses, though not conclusive, tend to support this interpretation. In particular, the ca. 2900 Ma old metamorphic zircons from the migmatitic paragneiss may have formed as a result of partial melting in the metasediments and thus may roughly date the high grade metamorphic event. The LAM-ICP-MS data also suggest the presence of crust older than 3250 Ma in the area. The 3363 Ma old xenocrystic core in the zircon from the 'Nerak granite' suggests this pluton was sampling, if not derived from the melting of, still older basement rocks.
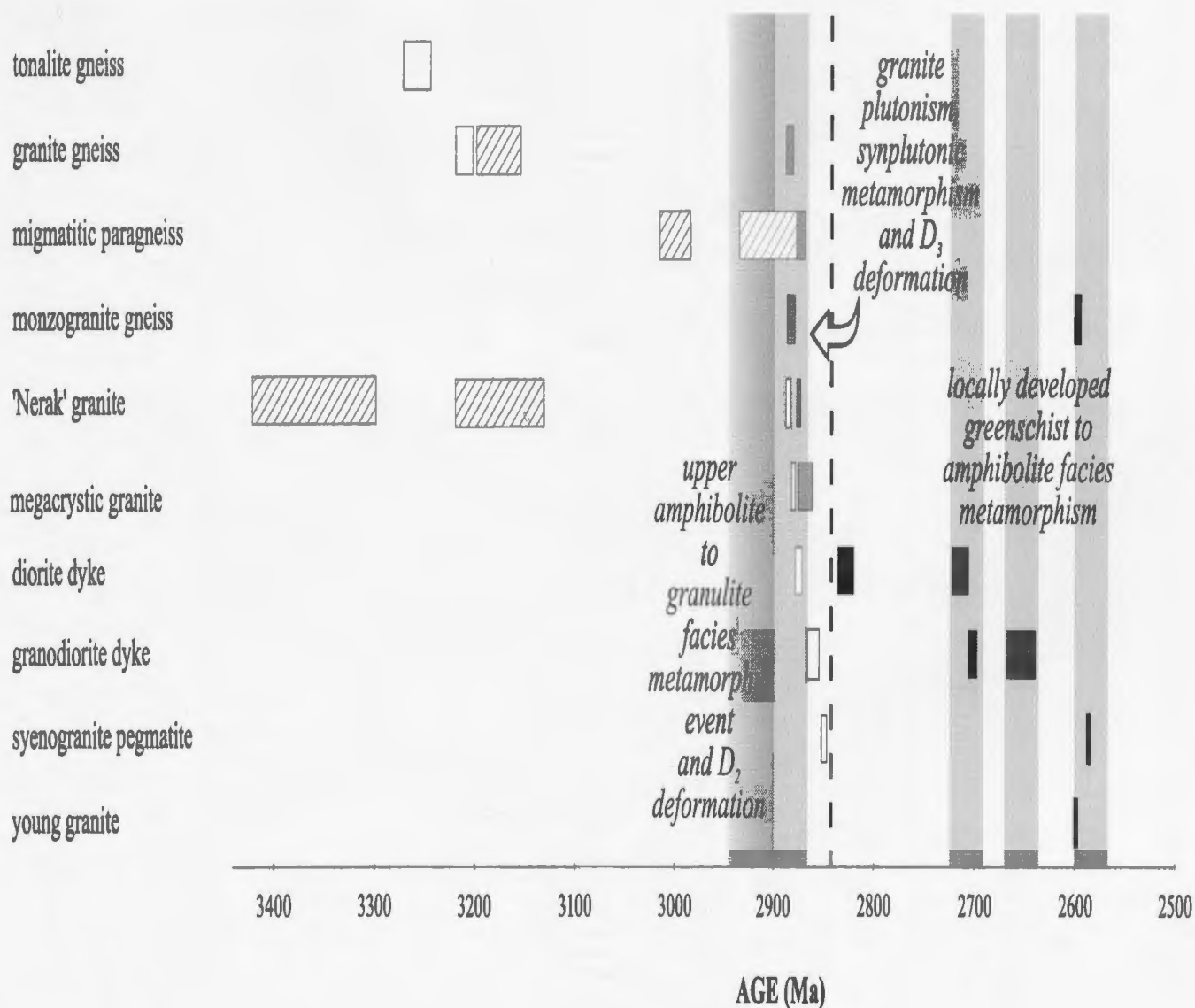
Figure 6.1: Summary of U-Pb ages for the Eokuk Uplift. The two-sigma uncertainties reported for analyses define the width of the box representing each rock. White boxes, zircon; diagonally hatched boxes, LAM zircon; light grey boxes, monazite; dark grey, colourless titanite; black, brown titanite. Shaded areas represent various tectonic and plutonic event within the Eokuk Uplift. Dotted line represents approximate end of deformation in the Uplift. Granite plutonism was synchronous with the last greenschist facies metamorphic episode at ca. 2600.

6.1.2 2.90-2.88 Ga: Plutonic event and amphibolite facies metamorphism

The two bodies of ca. 2880 Ma megacrystic biotite granite, possibly phases of the same pluton, exhibit no clear evidence of S_2-related deformation and field evidence suggests that they were emplaced pre- to syn-S_3. Penecontemporaneous granite plutonism and an amphibolite-grade metamorphic overprint on the mafic granulites is documented by the replacement of ortho- and clinopyroxene by hornblende along intrusive contacts and fractures in the gneiss. The concordant to near-concordant analyses of metamorphic monazite from three of the four high grade gneiss units give ages roughly corresponding to the crystallization ages of the granite (Figure 6.1). The subhedral nature of monazite grains may suggest that they are metamorphic (Parrish, 1990), and further points to synplutonic metamorphism as a controlling factor in their evolution. Intrusion of the granite and associated hydrothermal fluids would have resulted in the crystallization of new monazite or the partial to complete resetting of original monazite in the gneissic rocks. The presence of monazite grains with cores in the migmatitic paragneiss argues that an older population of monazite was present in the gneissic rocks.

6.1.3 2.88-2.85 Ga: Minor intrusive rocks and the end of deformation

The three dykes dated in this study provide evidence for the continuation of mafic to felsic intrusive activity during the waning stages of D_3, and constrain the end of the main phase of deformation in this part of the Eokuk uplift to ca. 2850 Ma. It should be noted that, with the exception of late granite plutonism at ca. 2.59 Ga, U-Pb age data from the

Eokuk Uplift do not record the ca. 2.62-2.59 Ga tectonothermal events recorded elsewhere in the Slave Province (Card and King, 1992; Isachsen and Bowring, 1994). Lack of evidence for significant post-2.8 Ga deformation suggests that the rocks in the study area were tectonically decoupled from the rest of the Slave craton for 200 Ma before Archean tectonism ceased in the Slave Province.

6.1.4 2.72-2.64 Ga: Lower amphibolite to greenschist facies metamorphism

Titanite ages from the diorite and granodiorite dykes document two episodes of lower amphibolite to greenschist facies metamorphism. In the diorite dyke, the brown titanite is thought to represent a partially reset, igneous population. In contrast, the colourless titanite is metamorphic in origin, and is concentrated in fractures with lower amphibolite facies minerals such as blue-green hornblende and actinolite. The discordia line produced for these titanites has an upper intercept age of 2715 +/-10 Ma.

In the granodiorite dyke, all of the titanite appears to be subhedral and metamorphic in origin. The dyke appears to have undergone a pervasive greenschist grade alteration, with retrograde chlorite replacing biotite and extensive sericitization of plagioclase. Two populations of titanite are present, and the age distribution of older brown grains and younger colourless grains suggests two discrete episodes of titanite growth at 2703 +/-4 Ma and 2646 +/-18 Ma, respectively. The 2703 Ma age for the brown titanite is the same, within uncertainty, as that for the colourless titanite from the diorite dyke, suggesting that the two populations are the result of the same event. A possible cause for the crystallization of these metamorphic titanites is discussed more fully in section 6.2.

6.1.5 2.60-2.59 Ga: Plutonic event and greenschist facies metamorphism

The 2595 Ma age for the young granite corresponds well with the ages for other late Archean granitoid rocks in the Slave Province (van Breemen et al., 1992). More than 80% of the granitoid rocks in the Slave were intruded between 2625 and 2580 Ma (van Breemen et al., 1992).

Evidence exists for the involvement of the young granite in greenschist grade metamorphism. Titanite from the monzogranite gneiss and the syenogranite pegmatite yield ages of 2593 and 2589 Ma respectively. In thin section, titanite in these samples occurs as anhedral masses, associated with ilmenite that has grown in the mineral cleavages of biotite that has undergone alteration to chlorite. This petrographic relationship implies that the titanite formed during greenschist grade alteration. In the retrograde reaction of biotite to chlorite, Ti and Fe are released from the crystal lattice. If any Ca (or CO_2) is present in the environment during alteration, both titanite and ilmenite can crystallize titanite at greenschist facies (Deer, Howie and Zussman, 1992). This suggests that hydrothermal fluids derived from the young granite may be responsible for the pervasive greenschist overprint seen in the other rocks along the coast.

6.2 Comparison of U-Pb Results from the Eokuk Uplift with Geochronological Data from the Slave Province

Published geochronological data from other basement occurrences in the northern Slave Province have outlined plutonic and depositional events roughly contemporaneous

with similar events in the Eokuk Uplift. These ages may be used to construct a geochronological context for the Eokuk Uplift.

Pre-2.8 Ga gneissic and supracrustal rocks with ages contemporaneous to those from the Eokuk Uplift occur in the main body of the Slave Province. Thirty kilometres to the east of the Eokuk Uplift, the Kangguyak gneiss belt (Figure 6.2), consists of upper amphibolite grade mixed gneisses and migmatites, in faulted contact with the western side of the Anialik River volcanic belt (Relf, 1995). The tonalite to granite orthogneisses which form the bulk of the Kangguyak gneiss belt have produced ages quoted as 3.3 to 2.95 Ga (Isachsen and Bowring, 1994; Villeneuve, et al., 1997).

At Point Lake, to the south to southwest of the Eokuk Uplift (see Figure 6.2), the Augustus granite has a zircon crystallization age of 3155 +/-3 Ma, with possible inheritance from a 3225 Ma old source (Villeneuve and van Breeman, 1994). Sensitive High Resolution Ion Microprobe (SHRIMP) analyses have been carried out on zircons from tonalite cobbles in a late Archean conglomerate from the Keskarrah Formation at Point Lake. These cobbles, thought to be Augustus granite, have yielded ages of 3240 +/-6 Ma (Padgham, 1996). At Hanikahimajuk Lake, a northeast-trending portion of the Point Lake volcanic belt that is dominated by felsic volcanic rocks is structurally juxtaposed against a foliated tonalite which has been dated at ca. 3379 Ma (Gebert, 1994; Yamashita et al., 1997).

Zircons from a tonalitic component of a layered orthogneiss from the Acasta Gneiss Complex have cores with prismatic metamorphic overgrowths. Analyses of these overgrowths using the SHRIMP yield an age of 3356 +/-14 Ma, which is interpreted by Stern and Bleeker (1998) to be the age of the dominant period of high grade
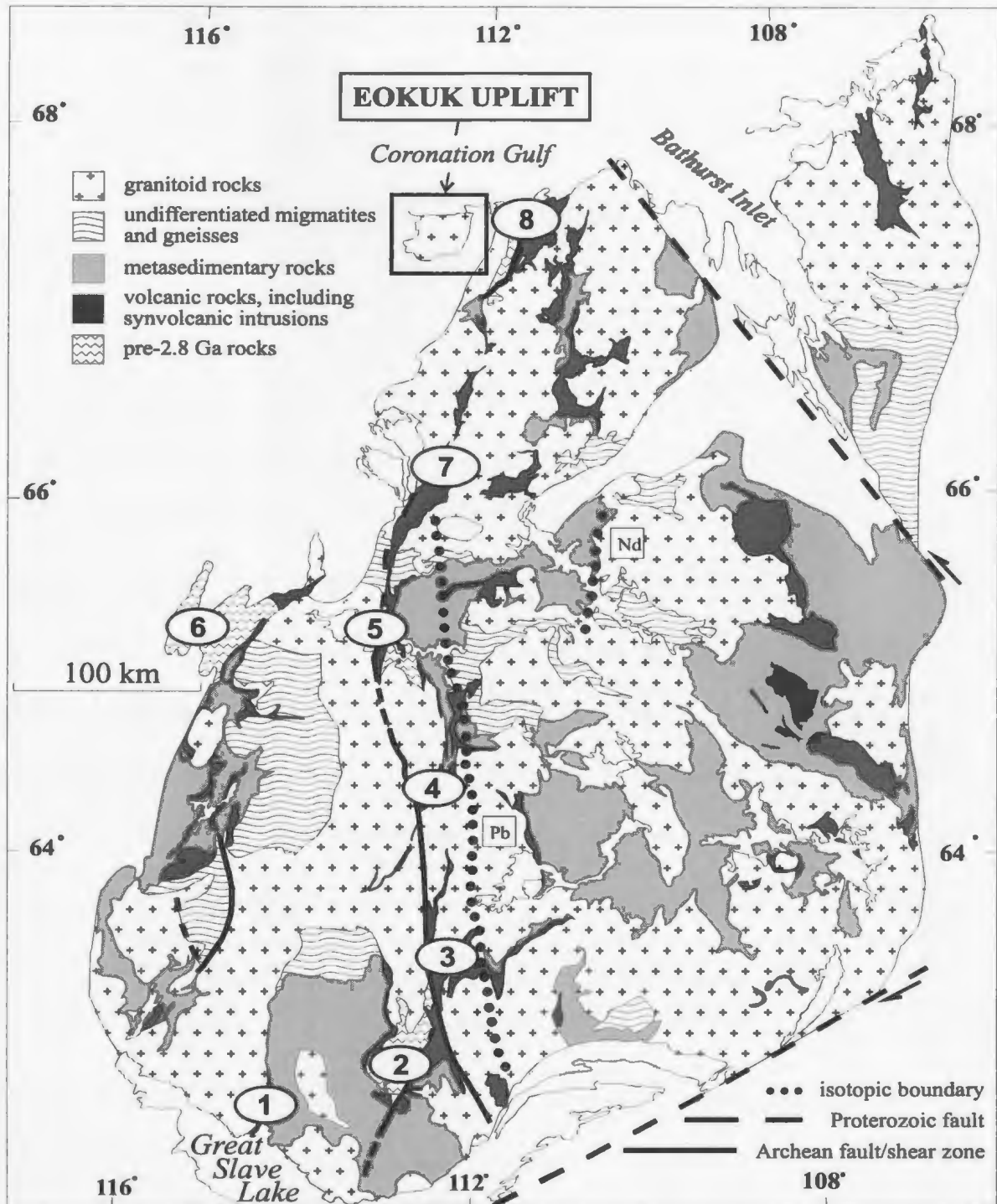
Figure 6.2: Geology map of the Slave Structural Province showing the location of the Eokuk Uplift. Pre-2.8 Ga rocks are shown in zig-zag pattern. Isotopic age boundaries for Nd and Pb are shown with black dots (Nd: Davis and Hegner, 1992; Pb: Thorpe et al., 1992). Numbered ovals show locations discussed in the text: (1) Yellowknife; (2) Sleepy Dragon Complex; (3) Beniah Lake; (4) Winter Lake; (5) Point Lake; (6) Acasta River; (7) Napaktulik Lake; (8) Anialik River.

metamorphism in the gneiss complex. Foliated and lineated, but unmigmatized, granite from the same area has a SHRIMP zircon age of 3348 +43/-34 Ma (Bleeker and Stern, 1997). It is interesting to note the correspondence of the ages from Point Lake, Hanikahimajuk Lake and Acasta, within uncertainty, to the LAM-ICP-MS age of 3363 Ma and 3165 Ma for the xenocrystic zircon cores from the 'Nerak granite', indicating the possible presence of similar aged rocks underlying the Eokuk Uplift.

Evidence for pre-2.8 Ga supracrustal successions in the northern Slave Province is widespread. Detrital zircons from a quartzite in the paragneiss package of the Kangguyak gneisses have ages between 3.13 and 3.27 Ga (Relf et al., 1994; Relf 1995). A conglomerate from the same area yields detrital zircons with $^{207}Pb/^{206}Pb$ ages ranging from ca 3450 to 2881 Ma, and has a maximum deposition age of 2881 +/-2 Ma (Villeneuve and van Breemen, 1994, Villeneuve et al., 1997). As the degree of discordance of the various dated detrital zircons is not provided, the ages cannot be assumed to represent the actual ages of source rocks, especially considering the complicated Pb-loss history evident in the data set for single grains from the Eokuk gneisses. It can only be stated that there appears to be an old source for the sediment-forming detritus.

U-Pb age data also exists for felsic rocks from a north-northeast trending supracrustal belt east of Napaktulik Lake (Figure 6.2). The belt consists predominantly of low to medium metamorphic grade volcanic, volcaniclastic and sedimentary rocks. A quartz eye rhyolite to dacite porphyry from within this supracrustal belt has yielded a U-Pb zircon upper intercept age of 3142 +/-1 Ma, and a second, more intensely deformed rhyolite has a zircon age of 3134±1 Ma (Villeneuve et al., 1993). In the same age range is a rhyolite

from Winter Lake that has a U-Pb zircon age of 3118 +11/-8 Ma. A quartz arenite unit overlying the felsic volcanic rocks contains detrital zircons with a narrow range in ages from 3.14-3.16 Ga (Villeneuve et al., 1993).

In contrast, the ages of pre-2.8 Ga plutonic, gneissic and supracrustal rocks in the southern part of the Slave Province show a different age distribution. On the eastern margin of the Sleepy Dragon Complex, Lambert and van Breemen (1991) obtained an age of 2936 +17/-14 Ma for a granodiorite gneiss. A cataclasic granitoid gneiss from the southwestern part of the Sleepy Dragon Complex yields a zircon age of 2819 +40/-31 Ma (Henderson et al., 1987). Tonalite gneisses from the western margin of the Sleepy Dragon Complex have zircon ages of 2910 +17/-12 Ma (Patterson Lake) and 2935 +9/-8 Ma (Webb Lake) (Ketchum and Bleeker, 1998). Farther to the west, north of Yellowknife, a granodiorite gneiss from the Anton Complex at Dwyer Lake yielded a U-Pb zircon age of 2929 +/-1 Ma (Isachsen and Bowring, 1997). A granite mylonite from the same complex, but farther to the north at Bell Lake, gives a U-Pb zircon age of 2945 +/-1 Ma. Other samples from the same area reveal complex U-Pb systematics and inheritance of zircon from > 3.0 Ga sources (Isachsen and Bowring, 1997).

Pre-2.8 Ga supracrustal rocks in the southern Slave Province comprise a uniform sequence of quartz arenite, rhyolite, iron formation, and related sedimentary rocks along with mafic to ultramafic volcanic rocks that are interpreted as a locally developed authochthonous cover sequence on basement gneisses from Yellowknife north to Winter Lake (Bleeker and Ketchum, 1998). Age data from these rocks is sparse but a chromite-bearing quartzite at Dwyer Lake has yielded detrital zircon ages that indicate a depositional age of younger than 2924 Ma (Isachsen and Bowring, 1997). An overlying

rhyolite ash flow tuff is dated at 2835 +/-4 Ma (*ibid.*) but the scatter among the individual data points suggests there may be zircon inheritance. An arkosic metasediment at the top of the Patterson Lake formation contains detrital zircons with $^{207}Pb/^{206}Pb$ ages between 2943 and 3147 Ma (Bleeker and Ketchum, 1998). Ages from supracrustal rocks in the southern Slave Province, as well as their underlying basement, overlap with, but are generally younger than, ages from the pre-2.8 Ga rocks in the northern Slave.

Several plutons with ca. 2880 Ma ages occur in the northern Slave Province. SHRIMP analyses of zircon from granite sheets that have intruded a dioritic 'banded gneiss' in the Acasta River area yielded ages of 2875 +39/-16 Ma (Bleeker and Stern, 1997). A rhyolite from an island on the south shore of Point Lake has a minimum zircon age of 2827 Ma (Mortensen, et al., 1988), and may therefore be an extrusive equivalent of the ca. 2.88 Ga granites. A granodiorite clast from the Keskarrah Formation conglomerates at Point Lake yielded a zircon age of 2874 +/-7 Ma (Krogh and Gibbons, 1978). It is interesting to note that preliminary $^{40}Ar-^{39}Ar$ results for hornblende from a tonalitic member of the Kangguyak gneiss gives an age of 2853 +/-6 Ma (H. Sandeman, unpub. data in Relf, 1995), i.e.: 20-30 Ma younger than the U-Pb zircon and monazite ages from the Eokuk Uplift. U-Pb data from this study suggest a thermal event coincident with the $^{40}Ar-^{39}Ar$ cooling age in the Kangguyak gneisses.

Post-2.8 Ga events in the Eokuk Uplift are reflected by the ages of titanite from the diorite and granodiorite dykes. These correspond roughly to the age of emplacement of the Yellowknife Supergroup (ca. 2.72-2.65 Ga; Card and King, 1992) and the age of earliest deformation in the Anialik River volcanic belt (ca. 2.65 Ga; Relf, 1995). While no crystallization ages in this range have been identified in rocks from the Eokuk Uplift,

Figure 6.3

Figure 6.3:   Comparison of U-Pb ages for the Eokuk Uplift with U-Pb ages for the Slave Province. Dotted line represents range of detrital zircon ages from a conglomerate in the Kangguyak gneiss belt. Data for: Kangguyak gneiss (Villeneuve and van Breemen, 1994; Relf, 1995); Point Lake (Krogh and Gibbins, 1978; Villenueve and van Breemen, 1994; Padgham, 1996); Acasta River (Bleeker and Stern, 1997; Stern and Bleeker, 1998); Napaktulik Lake (Villeneuve et al., 1993); Sleepy Dragon Complex (Ketchum and Bleeker, 1998); Anton Complex (Isachsen and Bowring, 1997). Dates for Yellowknife Supergroup deposition and Slave Province-wide deformation and metamorphism are taken from Card and King (1992) and Isachsen and Bowring (1994).

Eokuk Uplift

Synplutonic greenschist facies metamorphism

Lower amphibolite to greenschist facies metamorphism

End of deformation

Granite plutonism and amphibolite-facies metamorphism

Granulite facies metamorphism

Age (Ma)

2500
2600
2700
2800
2900
3000
3100
3200
3300
3400

Slave Province

Slave province-wide greenschist to amphibolite-grade metamorphism andconcurrent granitoid plutonism

Formation of volcanic-turbidite sequence supracrustal and associated intrusive rocks.

Kangguyak Gneiss   Point Lake   Acasta River   Napatulik Lake   Sleepy Dragon Complex   Anton Complex

Northwestern Slave Province   **Southern Slave Province**

☐ Xenocrystic zircons   ▽ Felsic volcanic rocks

◯ Granitoid plutons or gneisses   ◆ Tonalitic plutons or gneisses

▼ Detrital zircons   ◆ Granitoid cobbles in conglomerate

dates from both the Kangguyak gneisses and the Anialik River volcanic belt correspond to ages from titanite analyses of the diorite and granodiorite dykes. The concordant brown titanite from the granodiorite dyke (2703 +/-4 Ma) and the concordant clear titanite from the diorite dyke (2715 +/-10 Ma) have ages which correspond, within uncertainty, to the 2705-2703 Ma ages given for the emplacement of mafic phases of the Anialik River igneous complex (Abraham et al., 1994). The time of amphibolite facies metamorphic conditions in both the Kangguyak gneiss and the western Anialik River igneous complex has been constrained by U-Pb analysis of titanite and $^{40}Ar/^{39}Ar$ analysis of hornblende from igneous plutons. This event occurred at 2.65-2.64 Ga (Abraham et al., 1994; Villeneuve and van Breeman, 1994; Relf et al. 1994, H. Sandeman, unpub. data in Relf, 1995), which is also interpreted to be the age of collision between the gneiss belt and the volcanic belt. Clear titanite from the granodiorite dyke has an age of 2646 +/-18 Ma, suggesting metamorphic effects from this event may have reached the Eokuk Uplift.

Finally, the age of the 'young granite' is coeval with granitoid plutons from the Slave province with ages in the time bracket 2625-2580 Ma. These have been subdivided into syn-deformational plutons, mainly diorite to tonalite, intruded from 2625 to 2595, and late- to post deformational granitoids range from megacrystic biotite granodiorite to two-mica granite, with ages from 2605 to 2580 Ma (van Breeman et al., 1992). The peraluminous composition and lack of penetrative deformational fabrics in the 'young granite' pluton suggest that it is one of the latter.

6.3 Conclusions

Based on the geological, structural, petrological and U-Pb geochronological data presented above, the following tectonic history for the Eokuk Uplift is proposed:

(1) Formation of granodiorite-tonalite and granitic basement during at least two intrusive events from 3250 to ca. 3200 Ma. The absence of supracrustal xenoliths in these rocks suggests they formed the basement for the deposition of the supracrustal sequence.

(2) The deposition of a supracrustal sequence including mafic volcanic and sedimentary rocks. This can be tentatively dated to post-3.0 Ga on the basis of the one detrital LAM-ICP-MS analysis.

(3) An upper amphibolite to granulite facies metamorphic event ca. 2.9 Ga (?), possibly associated with D_2 deformation.

(4) The emplacement of megacrystic granite plutons at ca. 2880 Ma, coincident with D_3 deformation and synplutonic, amphibolite facies metamorphism.

(5) The end of deformation by ca. 2855 Ma, as constrained by the age of the cross cutting syenogranite pegmatite dyke.

(6) Two episodes of lower amphibolite to greenschist facies metamorphism at ca 2705 Ma and ca. 2650 Ma respectively. These events are coeval with, and may be related to, the emplacement of the Anialik River volcanic belt (Abraham et al., 1994; Villeneuve et al., 1997) and collision of the volcanic belt with the Kangguyak gneisses (Relf, 1995).

(7) A locally developed greenschist facies metamorphic event at ca. 2600 Ma, possibly

related to the emplacement of the young granite.

The Eokuk Uplift contains rocks with ages similar to those in previously identified

basement gneiss terranes in the northern Slave Province such as those at Point Lake,

Arcadia Bay and the Acasta River. No evidence has been found to date of rocks with

ages coeval with the 3.6 Ga and older Acasta gneisses. However, xenocrystic zircons

from the 'Nerak granite' yield an age of ca. 3363 Ma, which is similar to the 3379 Ma age

derived from tonalitic gneisses at Hanikahimajuk Lake (Yamashita et al., 1997) and the

3348 Ma age of the granite from the Acasta gneisses (Bleeker and Stern, 1997). This

implies that the rocks of the Eokuk Uplift may have been intruded into, and possibly

derived from, older underlying crustal material that is similar in age to rocks from Acasta

and Hanikahimajuk Lake. The similarities in these ages suggest that the Eokuk may be

part of a larger basement block that encompasses the northwestern part of the Slave

Province.

In relation to the pre-2.8 Ga gneissic and supracrustal successions in the southern

Slave Province, rocks of the Eokuk Uplift do not share lithological and age similarities.

Granitoid gneisses of the Sleepy Dragon and Anton Basement Complexes have ages

ranging from roughly 2900-2950 Ma. Rocks of the Central Slave Basement Cover

succession of Bleeker and Ketchum (1998) unconformably overlie the older gneissic

rocks and must therefore post-date ca. 2900 Ma. This contrasts with the rocks from both

the Eokuk Uplift and the northern part of the Slave Province, which appear to have a

longer, more complex history. The granitoid plutons and gneisses show a range of ages

from 4.0 Ga for the oldest Acasta gneiss to ca 2.88 Ga for 'young' granitic intrusions.

Supracrustal rocks from the north have ages that cluster around ca. 3100 Ma and do not display the distinctive quartzite/iron formation/ mafic to ultramafic volcanic sequence that characterizes supracrustals from the southern half of the Slave Province. In the Eokuk Uplift, the supracrustals are dominated by pelitic to psammitic bulk composition metasediments, with local mafic and sulphide-bearing units that may have been mafic volcanic rocks and iron-formation respectively. The deposition of these supracrustal rocks pre-dates granite plutonism at 2880 Ma. It should also be noted that the bulk compositions of the supracrustal gneisses in the Eokuk are very similar to the supracrustal gneisses in the Kangguyak gneiss belt.

In light of the differences in the pre-2.8 Ga rocks in the northern and southern parts of the Slave Province, it has been suggested (Bleeker et al., 1999) that existing basement rocks may be divisible into two discrete terranes, each with its own lithotectonic history. The results of the present study tend to support this interpretation.

While granulite facies rocks from the Eokuk Uplift display many of the structural and metamorphic characteristics of high-grade rocks in the southern part of the Slave Province, U-Pb dating suggests that granulites in the south are roughly 400 Ma younger than those exposed in the Eokuk Uplift. In fact, the Eokuk Uplift represents the first well-preserved occurrence of pre-2.8 Ga granulite facies rocks in the Slave Province. It is interesting to note that zircons from the Acasta gneisses display overgrowths that show evidence for high-grade events in these rocks at 3350 Ma and possibly at ca. 3100 Ma (Bleeker and Stern, 1997). The existence of early granulite facies rocks causes speculation that some form of collisional or extensional tectonic event is responsible. More work is needed to resolve this question.

The similarities in U-Pb titanite and monazite ages from the Eokuk Uplift and U-Pb titanite and ^{40}Ar-^{39}Ar hornblende ages from the Kangguyak gneiss belt and Anialik River igneous complex suggest the two areas may have a shared history in regard to younger (2.7-2.65 Ga) metamorphic events. This would imply that the two areas may be part of a continuous basement terrane extending under Coronation Supergroup rocks.

The data presented in this thesis confirms the complex early history of the coastal section of the Eokuk Uplift and suggests contemporaneous early histories for the Uplift and other pre-2.8 Ga domains in the northern Slave Province. As well, the differences in ages and lithologies between basement occurrences in the northern and southern parts of the Slave Province suggest that there may in fact be two juxtaposed basement blocks as opposed to a simple, continuous basement terrane west of 112^0 longitude, as proposed by Kusky (1989).

References

Abraham, A.P.G., Davis, D.W., Kamo, S.L., and Spooner, E.T.C., 1994.
Geochronological constraints on late Archean magmatism, deformation and
gold-quartz vein mineralization in the northwestern Anialik River greenstone
belt and igneous complex, Slave Province, NWT. Canadian Journal of Earth
Sciences, **31**: 1365-1383.

Bethune, K.M., and Carmichael, D.M., 1998. Metamorphism along the Slave portion of
the SNORCLE transect. *In* Slave-Northern Cordillera Lithospheric Evolution
(SNORCLE) Transect and Cordilleran Tectonics Workshop Meeting (March 6-
8). *Compiled by* F. Cook and P. Erdmer. Simon Fraser University, Lithoprobe
Report No. 64, p. 17-24.

Bleeker, W., and Stern, R., 1997. The Acasta gneisses: an imperfect sample of the
earth's oldest crust. *In* Slave-Northern Cordillera Lithospheric Evolution
(SNORCLE) Transect and Cordilleran Tectonics Workshop Meeting (March 7-
9). *Compiled by* F. Cook and P. Erdmer. University of Calgary, Lithoprobe
Report No. 56, p. 32-35.

Bleeker, W., and Ketchum, J., 1998. Central Slave Basement Complex, Northwest
Territories: its autochthonous cover, decollement, and structural topology. *In*
Current Research 1998-C, Geological Survey of Canada, p. 9-19.

Bleeker, W., Davis, B., and Ketchum, J., 1999. Crustal architecture of the Slave Craton.
    In Slave-Northern Cordillera Lithospheric Evolution (SNORCLE) Transect and
    Cordilleran Tectonics Workshop Meeting (March 5-7). *Compiled by* F. Cook
    and P. Erdmer. University of Calgary, Lithoprobe Report No. 69, p. 32-33.

Bowring, S.A., Williams, I.S. and Compston, W., 1989. 3.96 Ga gneisses from the Slave
    Province, Northwest Territories, Canada. Geology, **17**: 971-975.

Card, K.D. and King, J.E., 1992. The tectonic evolution of the Superior and Slave
    Provinces of the Canadian Shield: Introduction. Canadian Journal of Earth
    Sciences, **29**: 2059-2065.

Carmichael, D.M., Hemlstaedt, H.H., and Thomas, N., 1987. A field trip in the Frontenac
    Arch with emphasis on stratigraphy, structure and matamorphism. Friends of the
    Grenville, Field Trip Guidebook.

Corfu, F., and Stott, G.M., 1986. U-Pb ages for late magmatism and regional deformation
    in the Shebandowan belt, Superior Province, Canada. Canadian Journal of Earth
    Sciences, **23**: 1075-1082.

Covello, L., Roscoe, S.M., Donaldson J.A., Roach, D., and Fyson, W.K., 1988. Archean quartz arenite and ultramafic rocks at Beniah Lake, N.W.T. *In* Current Research, part C. Geological Survey of Canada, Paper 88-1C, pp. 223-232.

Craig, B.G., Davison, W.L., Fraser, J.A., Fulton, R.J., Heywood, W.W., and Irvine, T.N., 1960. Geology north-central District of Mackenzie, Northwest Territories. Geological Survey of Canada, Map 18-1960.

Davis, D.W., 1982. Optimum linear regression and error estimation applied to U-Pb data. Canadian Journal of Earth Sciences, **19**: 2141-2149.

Davis, W.J. and Hegner, E., 1992. Neodymium isotopic evidence for the tectonic assembly of late Archean crust in the Slave Province, northwest Canada. Contributions to Mineralogy and Petrology, **111**: 493-504.

Davis, W.J., Fryer, B.J., and King, J.E., 1994. Geochemistry and evolution of Late Archean plutonism and its significance to the tectonic development of the Slave craton. Precambrian Research, **67**: 207-241.

Deer, W.A., Howie, R.A., and Zussman, J., 1992. An Introduction to the Rock-Forming Minerals, 2nd edition. Longmans Scientific and Technical, London.

Easton, R.M., 1985. The nature and significance of pre-Yellowknife Supergroup rocks in the Point Lake area, Slave Structural Province, Canada. *In* L.D. Ayers, P.C. Thurston, K.D.Card and W. Weber (eds.), Evolution of Archean Supracrustal Sequences, Geological Association of Canada, Special Paper 28, pp. 153-167.

Frith, R.A., Loveridge, W.D., and van Beemen, O., 1986. U-Pb ages on zircon from basement granitoids of the western Slave Structural Province, northwestern Canadian Shield. *In* Current Research, Part A, Geological Survey of Canada, Paper 86-1A, pp. 113-119.

Fyson, W.K. and Helmstaedt, H., 1988. Structural patterns and tectonic evolution of the supracrustal domains in the Archean Slave Province, Canada. Canadian Journal of Earth Sciences, **25**: 301-315.

Gebert, J., 1994. Final Summary of mapping in the Hanikahimajuk Lake area, a portion of the Point Lake Volcanic Belt, west-central Slave Province. *In* Kusick, R., and Goff, S.P.(eds.), Exploration Overview 1994: Yellowknife, Northwest Territories Geology Division, Northern Affairs Program, p.35.

Gunther, D., Longerich, H.P., and Jackson, S.E., 1995. A new enhanced sensitivity quadrupole inductively coupled plasma-mass spectrometer (ICP-MS). Canadian Journal of Applied Spectroscopy, **40**: 111-116.

Harley, S.L., 1989. The origin of granulites: a metamorphic perspective. Geological Magazine, **126**: 215-247.

Heaman, L.M., LeCheminant, A.N., and Rainbird, R.H., 1992. Nature and timing of Franklin igneous events, Canada: Implications for a Late Proterozoic mantle plume and the breakup of Laurentia. Earth and Planetary Science Letters, **109**: 117-131.

Henderson, J.B., 1981. Archean Basin evolution in the Slave Province, Canada. *In* Kroner, A., (ed.), Precambrian Plate Tectonics, Elsevier, Amsterdam, p. 213-235.

Henderson, J.B., van Breemen, O., and Loveridge, W.D., 1987. Some U-Pb zircon ages from Archean basement, supracrustal and intrusive rocks, Yellowknife-Hearne Lake area, District of Mackenzie. *In* Radiogenic Age and Isotope Studies: Report 1, Geological Survey of Canada, Paper 87-2, p. 111-121.

Henderson, J.B. and Schaan, S.E., 1993. Geology of the Wijinnedi Lake area: a transect into mid-crustal levels in the western Slave Province, District of Makenzie, Northwest Territiories. *In* Current Research, 1997-C, Geological Survey of Canada, p. 83-91.

Henderson, J.B., and Chacko, T., 1995. A reconnaissance of the high grade metamorphic terrane south of Ghost Lake, southwestern Slave Province, Northwest Territories. *In* Current Research, 1995-C, Geological Survey of Canada, p. 77-85.

Hoffman, P.F., 1986. Crustal accretion in a 2.7-2.5 Ga. 'granite-greenstone' terrane, Slave Province, N.W.T.: a prograding trench-arc system? Geological Association of Canada, Program with Abstracts, **11**, A82.

Hoffman, P.F., Tirrul, R., Grotzinger, J.P., Lucas, S.B., and Erikson, K.A., 1984. The externides of the Wopmay orogen, Takijuq Lake and Kikerk Lake map areas, District of Mackenzie. *In* Current Research, Part A. Geological Survey of Canada, Paper 84-1A, p. 383-395.

Hoffman, P.F. and Bowring, S.A., 1984. Short-lived 1.9 Ga continental margin and its destruction, Wopmay orogen, northwest Canada. Geology, **12**: 68-72.

Holdaway, M.J. and Lee, S.M., 1977. Fe-Mg cordierite stability in high grade pelitic rocks based on experimental, theoretical and natural observations. Contributions to Mineralogy and Petrology, **63**: 175-198.

Isachsen, C.E. and Bowring, S.A, 1994. Evolution of the Slave craton. Geology, **22**: 917-920.

Isachsen, C.E. and Bowring, S.A., 1997. The Bell Lake group and Anton Complex: a
   basement-cover sequence beneath the Archean Yellowknife greenstone belt
   revealed and implicated in greenstone belt formation. Canadian Journal of Earth
   Sciences, **34**: 169-189.

Jackson, V.A., 1984. Structure and metamorphism of the Keskarrah Bay area, Point
   Lake, N.W.T. Second preliminary report. *In* Contributions to the geology of the
   Northwest Territories. Vol. 1. J.A. Brophy (ed.). Department of Indian
   Affairs and Northern Development, Yellowknife, NWT, EGS 1984-6, p. 47-54.

Jackson, V.A., 1994. Geology of Eokuk Uplift. *In* Kusick, R., and Goff, S.P.(eds.),
   Exploration Overview 1994: Yellowknife, Northwest Territories Geology
   Division, Northern Affairs Program, pp.39-43.

Jackson, V.A., 1996. Preliminary geology of the Archean Eokuk Uplift; part of NTS
   areas 86 P/6-11. Indian and Northern Affairs, NWT Geology Division,
   Yellowknife, NWT, EGS 1996-9, 12 p.

Jaffey, A.H., Flynn, K.F., Glendenin, L.E., Bentley, W.C. and Essling, A.M., 1971.
   Precision measurements of half-lives and specific activities of ^{235}U and ^{238}U.
   Physical Reviews C: Nuclear Physics, **4**: 1889-1906.

Jenner, G.A., Foley, S.F., Jackson, S.E., Green, T.H., Fryer, B.J. and Longerich, H.P., 1993. Determination of partition coefficients for trace elements in high pressure-temperature experimental run products by laser ablation microprobe-inductively coupled plasma-mass spectrometry (LAM-ICP-MS). Geochemica et Cosmochemica Acta, **57**: 5099-5103.

Kelly, J.A., 1984. Summary report on the GS 1-5, Green 1-2, Fraz 1, Mike 1-2, Con 1-4, Chuk 1, Hill 1-2, Coast 1, Fit 1 and West 2 Mineral Claims, Coronation Gulf area, Mackenzie Mining District, Northwest Territories Canada, NTS 86P-7, P-9, P-10 and P-11. Westsun Petroleum and Minerals Ltd., Indian and Northern Affairs Canada Assessment Report 062186.

Ketchum, J., and Bleeker, W. 1998. U-Pb geochronology of the Sleepy Dragon Complex in the Morose-Patterson Lakes area, with tectonic implications. *In* Slave-Northern Cordillera Lithospheric Evolution (SNORCLE) Transect and Cordilleran Tectonics Workshop Meeting (March 6-8). *Compiled by* F. Cook and P. Erdmer. Simon Fraser University, Lithoprobe Report No. 64, pp. 25-30.

King, J.E., Davis, W.J. and Relf, C., 1992. Late Archean tectono-magmatic evolution of the central Slave Province, Northwest Territories. Canadian Journal of Earth Sciences, **29**: 2156-2170.

King, J.E., Stubley, M., Hrabi, B., Villeneuve, M. and Peshko, M., 1994. Extent, tectonic significance and implications for regional mineral potential of a major fault belt, southern Slave Province, Northwest Territories. *In* Geological Survey Of Canada Mineral Colloquium, Program with Abstracts, p. 24.

Kretz, R., 1983. Symbols for rock-forming minerals. American Mineralogist, **68**: 277-279.

Krogh, T.E., 1973. A low-contamination method for hydrothermal decomposition of zircon and extraction of U and Pb for isotopic age determinations. Geochimica et Cosmochimica Acta, **37**: 485-494.

Krogh, T.E., 1982. Improved accuracy of U-Pb ages by the creation of more concordant systems using an air abrasion technique. Geochemica et Cosmochemica Acta, **46**: 637-649.

Krogh, T.E., and Gibbons, W.A., 1978. U-Pb isotopic ages of basement and supracrustal rocks in the Point Lake area of the Slave Province, Canada. Geological Association of Canada/Mineralogical Association of Canada, Program with Abstracts, **3**: 438.

Kusky, T.M., 1989. Accretion of the Archean Slave Province. Geology, **17**: 63-67.

Kusky, T.M., 1990. Evidence for Archean ocean opening and closing in the southern Slave Structural Province. Tectonics, **9**: 1533-1563.

Lambert, M.L. and van Breemen, O., 1991. U-Pb zircon ages from the Sleepy Dragon Complex and a new occurrence of basement rocks within the Meander Lake Plutonic Suite, Slave Province, N.W.T. *In* Radiogenic Age and Isotope Studies: Report 4, Geological Survey of Canada, Paper 90-2, p. 79-84.

LeCheminant, A.N. and Heaman, L.M., 1989. Mackenzie igneous events, Canada; middle Proterozoic hotspot magmatism associated with ocean opening. Earth and Planetary Science Letters, **96**: 38-48.

Mortensen, J.K., Thorpe, R.I., Padgham, W.A., King, J.E., and Davis, W.J., 1988. U-Pb zircon ages for felsic volcanism in the Slave Province, N.W.T. *In* Radiogenic Age and Isotope Studies: Report 2, Geological Survey of Canada, Paper 88-2, p. 85-95.

Padgham, W.A., 1996. Slave conglomerate dating. Indian and Northern Affairs, NWT Geology Division, Yellowknife, NWT., EGS 1996-12, 85 p.

Padgham, W.A., and Fyson, W.K., 1992. The Slave Province: a distinct Archean craton Canadian Journal of Earth Sciences, **29**: 2072-2086.

Parrish, R.R., 1990. U-Pb dating of monazite and its application to geological problems. Canadian Journal of Earth Sciences, **27**: 1431-1450.

Pehrsson, S.J., and Chacko, T., 1997a. Contrasting styles of deformation and metamorphism between mid and upper crustal rocks of the western Slave Province, Northwest Territories. *In* Current Research 1997-C, Geological Survey of Canada, p. 15-25.

Pehrsson S.J., and Chacko, T., 1997b. Geology of the Snare Lake-Winter Lake area, a new low pressure granulite domain in the western Slave Province: implications for ca. 2.6 Ga mid-crustal uplift and magmatism. Geological Association of Canada/ Mineralogical Association of Canada, Program with Abstracts, **22**, A114.

Perks, M, and Chacko, T, 1997. The deep crust of the western Slave Province-geological mapping and U-Pb geochronology of the Forked Lake area. Geological Association of Canada/ Mineralogical Association of Canada, Program with Abstracts, **22**, A115.

Rainbird, R.H., and Jefferson, C.W., 1993. Geology and resource potential of the Neoproterozoic Minto Inlier, Victoria Island, NWT. *In* Exploration Overview 1993, NWT Geology Division, pp. 48.

Relf, C., 1992. Two distinct shortening events during the late Archean orogeny in the west-central Slave Province, Northwest Territories, Canada. Canadian Journal of Earth Sciences, **29**: 2104-2117.

Relf, C., 1995. Geology, mineral potential, and tectonic setting of the Anialik River volcanic belt and the Kangguyak gneiss belt, northwestern Slave Province, NWT. Canada-NWT Mineral Initiatives Office, Report EGS 1995-7, Yellowknife, NWT, 113 p.

Relf, C., Chouinard, A., Sandeman, H., and Villeneuve, M., 1994. Contact relationships between the Anialik River volcanic belt and the Kangguyak gneiss belt, northwestern Slave Province, Northwest Territories. *In* Current Research 1994-C, Geological Survey of Canada, p. 49-59.

Roscoe, S.M., Stubley, M., and Roach, D., 1989. Archean quartz arenites and pyritic paleoplacers in the Beaulieu River supracrustal belt, Slave Structural Province, N.W.T. *In* Current research, Part C, Geological Survey of Canada, Paper 89-1C, p. 199-214.

Spear, F.S., 1993. Metamorphic Phase Equilibria and Pressure-Temperature-Time Paths. Mineralogical Society of America, Monograph, Washington D.C., 799 p.

Stacey, J.S., and Kramers, J.D., 1975. Approximation of terrestrial lead isotope evolution by a two-stage model. Earth and Planetary Science Letters, **26**: 207-221.

Stern, R., and Bleeker, W., 1998. Age of the world's oldest rocks refined using Canada's SHRIMP: the Acasta gneiss complex, Northwest Territories, Canada. Geoscience Canada, **25**:27-31.

Stubley, M., Jaegli, K., Bilben, S., and Tyler, T., 1995. Geology of the Nardin Lake area, south-central Slave Province, Parts of NTS 85P5, 12; 85O8, 9. Geological Mapping Division, Indian Affairs and Northern Development, EGS-1995-04.

Thompson, P.H., 1978. Archean regional metamorphism in the Slave Structural Province- a new perspective on some old rocks. *In* Metamorphism in the Canadian Shield. Fraser, J.A., and Heywood, W.W. (eds.), Geological Survey of Canada Paper 78-10, p. 85-102.

Thompson, P.H., 1989. An empirical model for metamorphic evolution of the Archean Slave Province and adjacent Thelon Tectonic Zone, northwestern Canadian Shield. In Evolution of metamorphic belts. Daly, J.S., Cliff, R.A. and Yardley B.W.D., (eds.). Geological Society Special Publication (London) no. 43, pp. 245-263.

Thorpe, R.I., Cumming, G.L., and Mortensen, J.K., 1992. A significant Pb isotope boundary in the Slave Province and its probable relation to ancient basement in the western Slave Province. *In* Richardson, D.G and Irving, M. (eds.), Summaries, Canada-Northwest Territories Mineral Development Subsidy Agreement 1987-1991. Geological Survey of Canada, Open File 2484, p. 179-184.

van Breemen, O., Davis, W.J., and King J.E., 1992. Temporal distribution of granitoid plutonic rocks in the Archean Slave Province, Northwest Canadian Shield. Canadian Journal of Earth Sciences, **29**: 2186-2199.

van Breemen, O., Henderson, J.R., Jefferson, C.W., Johnstone, R.M., and Stern, R., 1994. U-Pb age and Sm-Nd isotopic studies in Archean Hood River and Torp Lake supracrustal belts, northern Slave Province, Northwest Territories. *In* Radiogenic Age and Isotope Studies: Report 8, Geological Survey of Canada, Current research 1994-F, p. 21-36.

Villeneuve, M., Hrabi, B., Jackson, V., and Relf, C., 1993. Geochronology of supracrustal sequences in the central and northern Slave Province. *In* Goff, S.P., (ed)., Exploration Overview 1993: Yellowknife, Northwest Territories Geology Division, Northern Affairs Program, p.53.

Villeneuve, M.E., and van Breeman, O., 1994. A compilation of U-Pb age data from the Slave Province, Northwest Territories. Geological Survey of Canada, Open File 2972, 53 p.

Villeneuve, M.E., Henderson, J.R., Hrabi, R.B., Jackson, V.A. and Relf, C., 1997. 2.70-2.58 Ga plutonism and volcanism in the Slave Province, District of Mackenzie, Northwest Territories. *In* Radiogenic Age and Isotope Studies: Report 10. Geological Survey of Canada, Current Research 1997-F, p. 37-60.

Vogg, G., 1984. Geology of the Nerak vein, Coronation Gulf, NWT. Echo Bay Mines Ltd, Indian and Northern Affairs Canada, Assessment Report 081837.

Yamashita, K., Creaser, R.A., and Heaman, L.M., 1997. Geochemical and isotopic study of western Slave Province crust. *In* Slave-Northern Cordillera Lithospheric Evolution (SNORCLE) Transect and Cordilleran Tectonics Workshop Meeting (March 7-9). *Compiled by* F. Cook and P. Erdmer. University of Calgary, Lithoprobe Report No. 56, p 18-19.

Yardley, B.W.D., 1981. A note on the composition and stability of Fe-staurolite. Nueus Jahrbuch fur Mineralogie Monatschafte Jg 1981, pp. 127-132.

Appendix I: Sample Preparation for Isotope Dilution U-Pb Analysis

Sample preparation and processing were done according to procedures developed at the Royal Ontario Museum.

Sample Preparation

Initial preparation involved washing the sample to remove dirt and lichen and then breaking it into fist-sized chunks. The chunks were reduced to 5-10 mm chips in a jaw crusher. The rock chips were then reduced to a fine sand sized (<1mm) powder in a disk mill. The initial heavy mineral concentration was done by passing the rock powder over a Whiffley table. The recovered heavy minerals were then washed with alcohol, dried and sieved through disposable 70 mesh. The −70 fraction was then allowed to fall vertically in front of a large magnet to remove any minerals with high magnetic susceptibility or steel chips from the milling process. The nonmagnetic fraction is removed for heavy liquid separation

Heavy liquid separation, using methyl iodide, removes quartz, feldspar and apatite. The sample was poured into a separating funnel ¾ full of methyl iodide, which was then agitated. The heavy mineral fraction sink to the bottom where it was decanted into a filter paper lined funnel. This fraction was then rinsed with acetone and dried.

The initial magnetic heavy mineral separation of the dried sample was done on a Franz isodynamic separator with a 10^0 tilt. Magnetic fractions were collected at amperages of 0.25, 0.5, 1.0 and 1.7 A. The final magnetic separation took place with the amperage of

the magnet held constant at 1.7A and the tilt of the instrument progressively decreased through 5, 3, 1 and finally 0^0.

Selection of Zircon

Zircons from the sample were hand picked from the least magnetic fraction, usually the 0^0 nonmagnetic fraction. Grains were picked on the basis of clarity and the absence of inclusions, cracks and visible cores and overgrowths. Samples were then air abraded according to the method described in Krogh (1982). Zircons were abraded until crystal faces were rounded off, to remove any outer surfaces that may have lost Pb.

Sample Dissolution and Chemistry

Abraded samples were cleaned in a solution of 4N HNO_3, to remove any surface common lead. For zircons, the samples were then weighed and loaded into Teflon dissolution capsules. Samples were spiked with $^{205}Pb/^{235}U$, after estimating the amount of radiogenic Pb in the zircon. 10 drops of conc. HF and one of 8N HNO_3 are added to the dissolution capsule. Samples in capsules were placed in steel jackets and heated in an oven at 220^0 C. After one week, the bombs were removed from the oven, cooled to room temperature. Sample conversion consisted of removing the Teflon capsules to a hot plate and drying the dissolved zircon to solid precipitate. The capsules were cooled to room temperature and 10 drops of 3.1 N HCl were added. The capsules were sealed again and placed in an oven at 220^0 C for 12-24 hours.

Column chemistry on the zircon samples was done using small anion exchange resin columns using the method described in Krogh (1973). The size of the columns and the amounts of reagents used are one tenth the volume reported in Krogh (1973).

Monazite and titanite dissolution and chemistry were carried out somewhat differently. Dissolution was carried out in 7ml Savillex containers using 30 drops of conc. HF and one drop of 8N HNO3 for titanite and 30 drops of 6.2 N HCl for monazite. Samples were placed on a hot plate for a week. Sample conversion is the same as for zircon except that 30 drops of 3.1 N HCl are used. Extraction of U and Pb was by HBr column chemistry (Corfu and Stott, 1986) with an additional purification of U.

Data Acquisition and Reduction

Isotopic measurements for zircon, monazite and titanite were carried out on a Finnigan-Mat 262 mass spectrometer with four Faraday detectors in multicollection mode and ^{204}Pb measured in the SEM-ion counter. Small samples were measured entirely on the SEM-ion counter in peak jumping mode. Measured Pb and U atomic ratios are corrected for fractionation as determined by repeated measurement of the NBS 981 standard.

Data reduction and analysis were carried out using an in-house written geochronology program. Stacey and Kramers (1975) model Pb isotopic compositions were used to correct for common lead in excess of the laboratory blank. Linear regressions were done using the method of Davis (1982). Decay constants used were those of Jaffey et al. (1971).

Appendix II: LAM-ICP-MS U-Pb Analytical Methods

The Laser

The laser was built at the LAM-ICP-MS facility at Memorial University. It consists of a Q-switched, Nd:YAG 320 mJ pulsed laser operating at a fundamental wavelength of 1064 nm. The LAM has been modified by the installation of frequency quadrupling hardware enabling the laser to operate at 266 nm in the ultraviolet (Jenner et al., 1993). The laser is also equipped with wavelength separation elements to provide an output of 20 mJ/pulse at a repetition rate of 10 Hz. Beam intensity is controlled with a polarizing optical attenuation system consisting of a rotatable crystal quartz half-wave plate and a Glan laser polarizer. The half-wave plate allows the plane of polarization of the linearly polarized UV beam to be adjusted. The Glan polarizer allows transmission of radiation polarized in one direction only. Used in combination, the half-wave plate and polarizer allow the attenuation and adjustment of the laser beam for optimum ablation. Pulse energies used during sample ablation in this study range from 0.15-0.25 mJ. The laser is routed, by the use of three dielectric mirrors, into the photo tube of a petrographic microscope. It is then focussed using a UV achromatic 10 x lens onto the sample through a silica window in the ablation cell. The microscope allows the viewing and selection of sample sites in the grain mounts in the ablation cell. The sample cell itself sits on a manual X-Y-Z mechanical stage to allow movement between samples and reference material. Ablated material is entrained in a flow of Argon gas through polyurethane tubing to the ICP torch.

Table 3: LAM-ICP-MS Operating Conditions

LAM

Wavelength	266nm
Repetition Rate	10 Hz
Pulse Duration (FWHM)	9 ns
Focusing objective achromat,	10x fused silica/Ca/F2 UV laser
	f.l.=20mm
Incident pulse energy	0.15-0.25 mJ

ICP-MS

Model	FISONS PQII+ "S"
Forward power	1350 kW
Gas Flows	
Plasma	14 L/min
Auxiliary	1 L/min
Carrier	ca. 1.1 L/min
Sampler cone	Custom made, 0.5 mm aperture
Expansion chamber pressure	4.5×10^{-1} Torr

Data acquisition parameters

Data acquisition protocol	Time Resolved Analysis
Scanning mode	Peak hopping, 1 point per peak
Isotopes determined	^{238}U, ^{232}Th, ^{206}Pb, ^{207}Pb, ^{208}Pb
Dwell time per isotope	8.485 ms
Quad. settling time	0.05 ms
Time/scan	300 ms
Number of scans	2400
Analysis time	120 seconds
Pre-integration	15 scans/replicate

LASER ABLATION MICROPROBE

SHG, FHG = 2nd and 4th harmonic generators
A = aperture
HWP = half wave plate
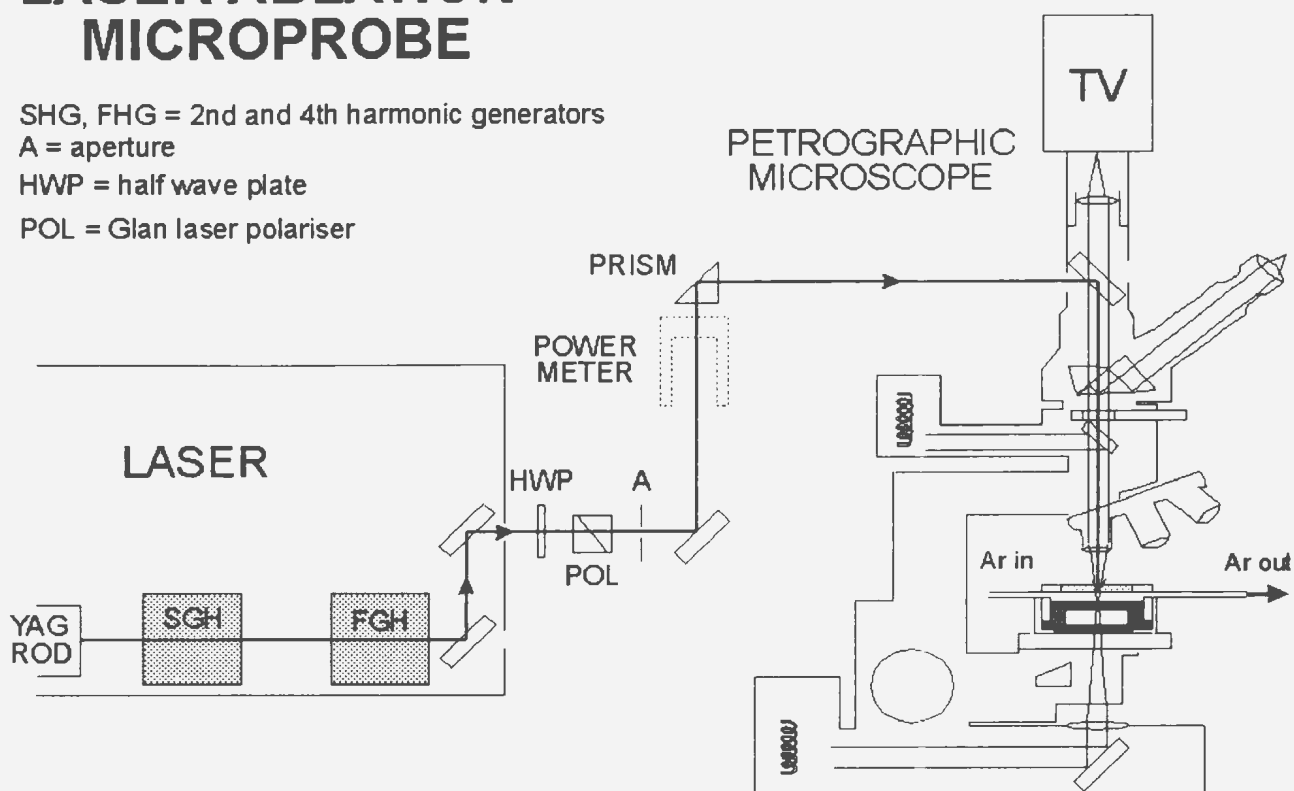POL = Glan laser polariser

Figure 1: Schematic diagram of the laser ablation microprobe (LAM) at Memorial University.

The ICP-MS

The ICP-MS used in this study is a Fisons-VG PQII+"S" with an enhanced sensitivity quadropole. A custom built sampler cone (0.5mm orifice as opposed to the factory delivered 0.7mm) enables reduction of background signals without loss of sensitivity (Gunther et al., 1995). The detection limits for high mass elements (atomic mass > 85) are in the low parts per billion range for 20 μm ablation pit sizes. The instrument was

tuned on ^{232}Th by ablating NBS 612 glass standard at 10 Hz using a pulse energy of 0.15-0.25 mJ.

Fractionation and Interferences

Typically during ablation and transport of the sample to the ICP-MS there is a very large elemental fractionation of U with respect to Pb. Several procedures have been used to reduce this fractionation and ensure precise U/Pb elemental ratios:

(1) By using a 266 nm laser wavelength. Most minerals absorb radiation better in the UV wavelengths and therefore will ablate more efficiently, reducing fractionation.

(2) Incorporating a spot cooling jet in the ablation cell reduces fractionation by lowering the temperature of the ablation.

(3) By reducing the temperature, ablation takes place in a more controlled manner and only completely ablated material is entrained to the ICP-MS.

(4) Fractionation was also reduced by defocusing the beam before commencing ablation. If a laser beam is focused at the beginning of ablation, as it drills into the sample it becomes defocused and loses power. Defocusing the beam 120 μm provides a wider surface for ablation and a more constant energy to the sample surface.

(5) Fractionation effects can also be reduced by integrating data for the same time interval on each run, ensuring consistency across a series of runs.

^{204}Pb suffers from the interferences of instrumental ^{204}Hg background. For this reason, accurate measurement of common Pb was not possible. ^{204}Pb in the system was reduced

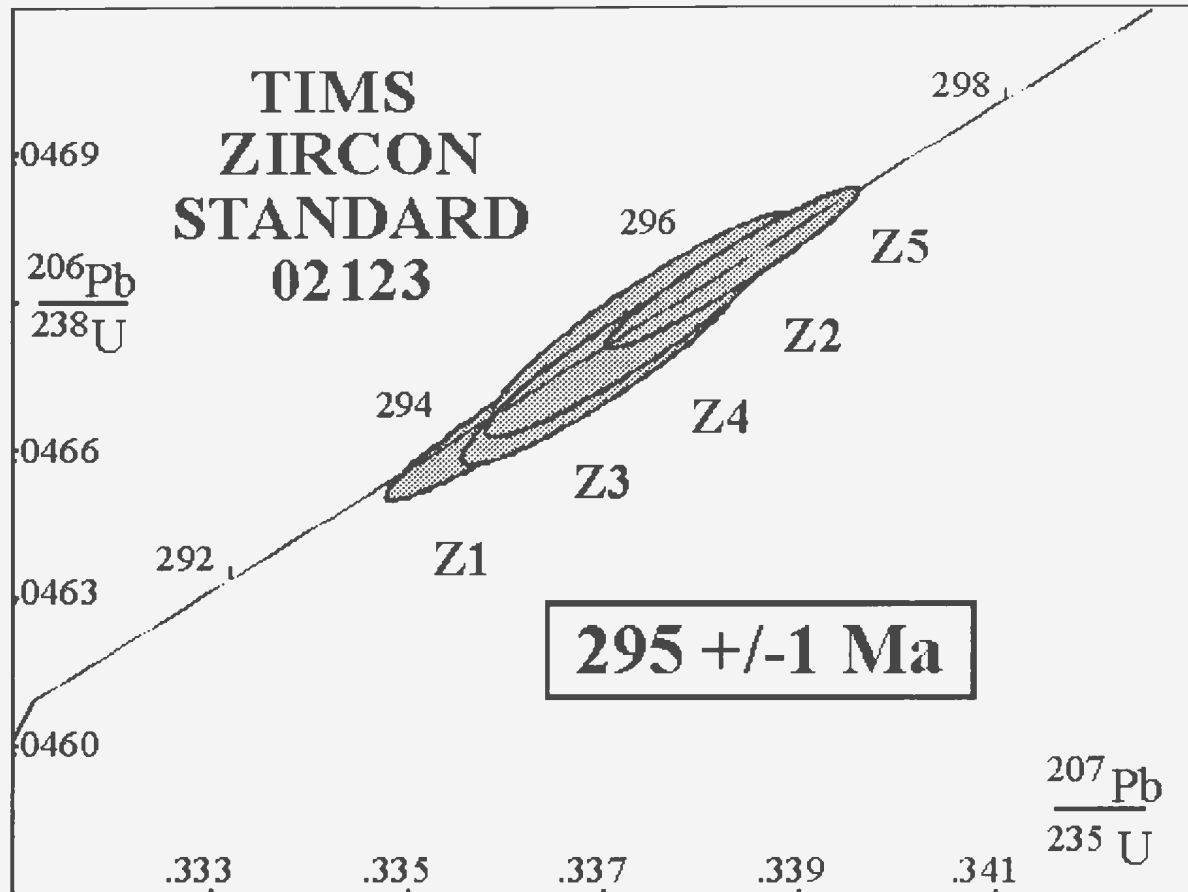by filtration of the argon carrier gas through activated charcoal and by careful attention to system cleanliness.

Figure 2: Results of TIMS analyses for zircon standard 02123 from Norwegian syenogranite pegmatite

Data Acquisition

Analyses for this study were done using a laser wavelength of 266 nm and a repetition rate of 10 Hz. Pulse energies were adjusted according to the ablation pit size: 0.15 mJ for 20 μm pits and 0.25 mJ for 40 μm pits. Standards were analysed using the same pluse

energies as sample analyses. Two standards were used during this study. The first was a spiked silicate glass NBS (or NIST) standard reference material 612. This standard was ablated at the beginning and end of sample runs to optimize ICP-MS operating conditions for the heavy mass range (Lu-U). The second was an in house zircon standard consisting of crystals from a Carboniferous syenogranite pegmatite from Norway. This was used as the calibration standard during sample analyses. The age of this standard was determined by conventional isotope dilution TIMS U-Pb analysis. A series of five concordant grains gave an age of 295+/-1 Ma (Figure 1). Standards were analysed as the first three or four samples of a twenty sample run. Typically, three of the zircon standard and one of the NBS 612 glass would be analysed. Data was acquired in peak jumping mode for five isotopes: ^{238}U, ^{232}Th, ^{206}Pb, ^{207}Pb and ^{208}Pb. Dwell time for each element was 8.485 ms. Samples were analysed in blocks of twenty individual ablation runs. The first four runs were of the standard, followed by twelve sample runs and finishing with four standard analyses. Analysis time for both standards and sample was 120 seconds. Background levels of isotopes in the dry carrier gas were measured for 60 seconds before commencing ablation. During data processing, count rates were pre-integrated by averaging consecutive groups of 15 mass sweeps into single readings. The time resolved signals were then downloaded to a PC where they were integrated using an in-house written LOTUS-based program (LAMTRACE) to determine isotope ratios. $^{207}Pb/^{206}Pb$, $^{208}Pb/^{206}Pb$, $^{208}Pb/^{232}Th$, $^{206}Pb/^{238}U$ and $^{207}Pb/^{235}U$ ratios were calculated for each analysis. The time resolved signals for each run were examined and the most appropriate signal intervals for background and ablation were chosen for integration and matched with

similar intervals for the standards. Background corrected count rates for each isotope were used to calculate sample ages.

Ratios of $^{207}Pb/^{235}U$ were calculated using analyses of the 02123 zircon standard to correct for the effects of U/Pb fractionation and mass discrimination in the mass spectrometer. Since the standard is relatively young, it has low count rates on ^{207}Pb, making it difficult to derive a precise calibration of $^{207}Pb/^{235}U$ and $^{206}Pb/^{207}Pb$. However, since the standard is concordant and has the same fractionation correction for $^{206}Pb/^{238}U$ as $^{207}Pb/^{235}U$, the $^{206}Pb/^{238}U$ ratio can be used to directly calibrate the $^{207}Pb/^{235}U$ ratio. This was done using a mass discrimination correction for the $^{207}Pb/^{235}U$ ratio that is derived from the $^{206}Pb/^{238}U$ ratio and assumes that mass discrimination is linear over the mass range 206 to 238. The 2σ errors on the ratios were calculated from integrated repeats. Corrected ratios and 2σ errors were calculated and ploted using the method of Davis (1982). The uranium decay constants used were those of Jaffey et al. (1971). U/Th ratios, used to determine metamorphic vs. igneous origin for various samples, were calculated using the raw counts-per-second of U and Th derived from measurments calibrated using the 02123 zircon standard. Element concentrations were not calculated.

Sample Preparation

For zircon analysis, grains were picked from the two diamagnetic fractions from final magnetic separation (see Appendix I). Grains chosen had to be relatively alteration, crack and inclusion free, and representative of the population being dated. Where possible, large zircons (>150 μm) were chosen. Zircons were then mounted in epoxy resin and

polished until a cross-section of the grain was uncovered for analysis. The polished grain mounts were placed in a beaker of nanopure water in an ultrasonic for 1 minute, to remove any residual polishing grit. The grain mount was then placed in a bath of 2N HNO_3 for 20 minutes, to remove any surface contamination.

Calculation of Th/U concentration ratios

Th/U concentration ratios in the sample zircons were calculated using the known [238]U and [232]Th concentrations of the 02123 zircon standard averaged from 6 previous TIMS analyses. These standard concentration values were used to determine sensitivity (cps/ppm) for U and Th derived from the standard during data acquisition by laser ablation. Since the same operating conditions were used for both the 02123 zircon standard and the unknown sample zircons, it was possible to estimate the concentrations of U and Th for the unknown sample by dividing the unknown counts-per-second by the sensitivity (cps/ppm) determined for the standard. These estimated concentrations were then used to calculate Th/U ratios. These steps were repeated for each sample run.